

**Novel Technologies and Optimised Formulations for Delivery of Solid
Dispersions of BCS Class II Drugs**

being a thesis submitted for the degree of

Master of Science

by

Dean T. Hurley, BSc (Hons) in Pharmaceutical Sciences



Based on the research carried out under the supervision

of

Prof. Clement L. Higginbotham

Dr. Sean Lyons

Dr. Luke Geever

Materials Research Institute,
Technological University of the Shannon,
Dublin Road,
Athlone, Co. Westmeath
Ireland

June 2023

Declaration

I hereby declare that this thesis submitted to the Technological University of the Shannon: Midlands Midwest for the degree of Master of Science, is a result of my own work and has not in the same or altered form, been presented to this institute or any other institute in support for any degree other than for which I am now a candidate.

Dean Hurley

(Date)

“If we knew what it was we were doing,
it would not be called research, would it?”

Albert Einstein *1879-1955*

Acknowledgements

Firstly, and most importantly, I would like to take this opportunity to thank Prof. Clement Higginbotham and Dr. Sean Lyons for stepping in and acting as my supervisors. Sean's and Clem's expertise, advice and technical know-how were invaluable and very much appreciated (and I think he took up the hill walking to get away from me). I would like to thank Clem and Sean for their friendship and leadership while I completed this thesis. I would never have got this far without them, and I can only hope this experience hasn't put him off supervising postgraduate students for life!

I would like to thank Dr. Catherine Potter and Professor, Dr. Mark Davis and Gavin Walker in UL for helping me with hyper DSC, XRPD and accelerated stability testing and I want to thank them for their time, effort and knowledge for helping me with this thesis.

Thank you to the technicians and support staff throughout the college, but particularly Mary McGee for her help and guidance.

I would like to thank all the postgrad students at A.I.T., who have helped or encouraged me throughout my (extended) stay in the college. I would especially like to thank my colleagues, Shane Halligan, Gavin Burke, Luke Geever, Martin Forde, Alan Murphy and Declan Devine, who have made my time here both enjoyable and at times excruciating. Their humour, camaraderie and friendship made the time I spent in Athlone pass quickly and enjoyably, cheers lads!

I would like to thank my best friend Olivia Whaley for her unconditional support, and kindness (and for not having me committed despite the many provocations I have given her over the past few years). You are amazing, Thank You.

I would like to thank all my family, especially my mam Phil for helping me through college and for all their encouragement, and of course my friends for their help (financial and otherwise!!!) throughout my time in college.

Table of Contents

Declaration.....	2
Acknowledgements.....	4
Table of Contents.....	5
Abstract.....	7
Abbreviations.....	8
List of Figures.....	10
List of Tables.....	15
1.0 Introduction.....	19
2.0 Literature Review.....	23
2.1 BCS class II drugs and factors solubility of BCS class II drugs.....	23
2.2 Solid dispersions.....	26
2.3 Factors that affect the physical and chemical stability of solid dispersions.....	29
2.3.1 Polymeric carriers used.....	29
2.3.2 Amorphous state.....	30
2.3.3 Intermolecular interactions.....	32
2.3.4 Recrystallization.....	34
2.6 A review of the current state of hot melt extrusion used to prepare amorphous SDs....	37
2.7 Materials used in this study.....	45
2.7.1 Indomethacin.....	45
2.7.2 PVP VA64/Plasdone S-630.....	48
2.7.3 Poloxamer 407.....	49
2.8 Aim and objectives of this study.....	51
3.0 Materials & Methods.....	54
3.1 Materials.....	54
3.2 Preparation of physical mixtures.....	56
3.3 Hot-melt extrusion conditions.....	56
3.3.1 Compounding of materials.....	59
3.4 Cooling Process.....	63
3.5 Pre-Formulation; calculation of solubility parameters (δ), glass transition temperature (T_g) and drug-polymer interaction factor (χ).....	63
3.6 ATR-FTIR spectroscopy.....	64

3.7	Raman Spectroscopy.....	65
3.8	X-ray powder diffraction (XRPD).....	65
3.9	Scanning electron microscopy (SEM).....	66
3.10	Phase solubility studies.....	67
3.11	<i>In-Vitro</i> dissolution studies.....	68
3.12	Statistical analysis.....	69
3.13	Accelerated amorphous stability studies.....	69
4.0	Results and Discussion.....	71
4.1	Introduction.....	71
4.1.1	Drug-polymer miscibility Studies.....	72
4.1.2	XRPD studies of extruded solid dispersions.....	76
4.1.3	ATR-FTIR and Raman Spectroscopic studies.....	81
4.1.4	SEM studies.....	95
4.1.5	Phase solubility studies.....	98
4.1.6	<i>In-vitro</i> dissolution studies.....	105
4.1.7	Accelerated stability studies.....	120
5.0	Conclusion & future work.....	124
5.1	Conclusion.....	124
5.2	Future work.....	125
	References.....	127
	<i>Relevant Publications</i>	138

Abstract

The optimal design of amorphous solid dispersion (SD) formulations require the use of excipients to maintain supersaturation and improve physical stability in order to ensure shelf-life stability and better absorption during intestinal transit, respectively. Previous research has focused on spray dried and supercritical fluid quaternary mixtures which due to the addition of a surfactant affected the physical stability and amorphous stability of selected model drugs. Very little research has focused on how inter-molecular interactions play a role in the successful formulation of hot-melt extruded quaternary amorphous blends and how they affect physical stability and solubility of amorphous SDs using semi-crystalline polymers. Also, the effect of cooling on the degree of crystallinity, solid-state and dissolution properties of multi-component hot-melt extruded SDs is of great interest for the successful formulation of amorphous SDs and is an area that is unreported, especially in the context of improving the stability of these specific systems. Therefore, the main objectives of this study are to prepare SDs via hot melt extrusion (HME) using a semi-crystalline polymer to overcome the dissolution and physical stability barriers compared to previous methods and finally investigate the role of inter-molecular interactions and cooling and their effect on the solid-state and dissolution properties of mixed copovidone amorphous solid dispersions. The solubility parameters, drug-polymer interactions, solubility and amorphous stability over time were investigated. X-ray powder diffraction (XRPD) confirmed that indomethacin (INM) was converted to the amorphous state, however the addition of poloxamer 407 (P407) had a significant effect on the amorphous nature and solubility of the SD formulations. Spectroscopy studies using infrared and Raman spectroscopy identified the mechanism of interaction and solubility studies showing a higher dissolution rate compared to amorphous and pure INM in pH 1.2 with a kinetic solubility of 20.63 $\mu\text{g/ml}$ and 34.7 $\mu\text{g/ml}$ after 3 and 24 hours. XRPD confirmed that INM remained amorphous after 5 months stability testing in solid solutions with Poly (vinylpyrrolidone-co-vinyl acetate) (PVP VA64) and Plasdone S-630 (PL-S630). Although cooling had a significant effect on the P407 crystallinity & solubility of INM, the cooling method used did not have any significant effect on the amorphous stability of INM over time.

Abbreviations

δ	Solubility parameter
δ_{total}	Total solubility parameter
$\Delta\delta$	Change in solubility parameter
ΔH	Heat of fusion
AFM	Atomic force microscopy
aINM	Amorphous indomethacin
APIs	Active pharmaceutical ingredients.
ASDs	Amorphous solid dispersions.
ATR	Attenuated total reflectance
BASF	Badische Anilin- und soda-fabrik
BCS	Biopharmaceutical Classification System.
β -CD	β -Cyclodextrin
CBZ	Carbamazepine
CDs	Cyclodextrins.
CED	Cohesive energy density
CGT	Cyclodextrin-glycosyltransferase
DSC	Differential scanning calorimetry
DVS	Dynamic vapor sorption
E_v	Energy of vaporisation
FH	Flory-Huggins
FT-IR	Fourier-transform Infrared Spectroscopy
GFA	Glass forming ability
GI	Gastrointestinal
GMP	Good manufacturing practice
HCl	Hydrochloric acid
HME	Hot melt extrusion
HPCD	2-hydropropyl- β -Cyclodextrin

HPMC	Hydroxypropyl methylcellulose
HSPs	Hansen solubility parameters
INM	Indomethacin
MMC	Myoelectric complex
NSAIDs	Non-steroidal anti-inflammatory drugs
P407	Poloxamer 407
PDF	Pair-wise distribution function
PEG	Poly (ethylene glycol)
PEO	Poly (ethylene oxide)
PM	Physical mixture
PPO	Propylene oxide
PRP	Propranolol HCL
PSAD's	Polymeric amorphous solid dispersions
PVP	Poly (vinylpyrrolidone)
PVP-VA	Poly (vinylpyrrolidone-co-vinyl acetate)
QbD	Quality by design
SBCD	Sulfobutyl- β -cyclodextrin
SCF	Supercritical fluids
SD	Spray drying
SEM	Scanning electron microscopy
T_c	Critical temperature
T_g	Glass transition temperature
T_p	Critical pressure
T_m	Melting temperature
USFDA	US Food and drug administration
V_m	Molar volume
VT	Variable temperature
XRPD	X-Ray powder diffraction
ZM	Ziprasidone mesylate

List of Figures

Chapter 2: Literature Review

Figure 1. Biopharmaceutics classification system (BCS) and formulation approaches for various classes of drugs.

Figure 2. Currently marketed solid dispersion (SD) formulations (drug, indication, polymer (HPMC is hydroxypropyl methyl cellulose; HPMCAS is hydroxypropyl methyl cellulose acetate succinate; PVP-VA is poly (vinyl pyrrolidinone-*co*-vinyl acetate)), and processing method (SD is spray-drying; HME is hot-melt extrusion)) (adapted from (Liu *et al.*, 2013)).

Figure 3. Enthalpy and volume of various state of crystalline drugs as a function of temperature; glass transition temperature (T_g) and melting temperature (T_m) are glass transition temperature and melting temperature respectively (reproduced from (Baghel, Redington & O'Reilly, 2016)).

Figure 4. Drug profile based on the aqueous solubility of amorphous and crystalline drug (reproduced from (Handa, Malik & Guarve, 2022)).

Figure 5. Diagram detailing terms used in relation to screw dimensions (adapted from (Lyons, Higginbotham & Blackie, 2007)).

Figure 6. Illustration of various extruder types.

Figure 7. Types of Twin –screw extrusion compounding systems.

Figure 8. Transporting and kneading elements in the co-rotating twin screw extruder, number of kneading elements: 8, upper image: front view, lower image: side view.

Figure 9. 'Ternary phase diagrams' (experimental not theoretical) of one amorphous polymer, one crystalline excipient and a poorly soluble drug (adopted from (Gumaste, Gupta & Serajuddin, 2016)).

Figure 10. Chemical Structure of the BCS class II drug indomethacin (INM).

Figure 11. Chemical Structure of Poly (Vinylpyrrolidone-vinyl acetate copolymer) (PVP VA64).

Figure 12. Chemical Structure of Plasdane S-630 (PL-S630).

Figure 13. Chemical Structure of Poloxamer 407 (P407) (Ethylene oxide and propylene glycol copolymer) (P407).

Chapter 2: Experimental Details

Figure 14. Chemical Structure of the BCS class II drug INM.

Figure 15. Chemical Structure of PVP VA64/PL-S630.

Figure 16. Chemical Structure of P407.

Figure 17. The Prism™ twin screw 25:1 length to diameter (L/D) ratio extruder used in this study.

Figure 18. Schematic representation of Prism™ twin screw 25:1 L/D extruder barrel and screw configuration used to compound materials for trials to investigate the drug-polymer miscibility and drug-polymer intermolecular interactions using PVP VA64 as the matrix forming material adapted by (Lyons, Higginbotham and Blackie, 2007).

Figure 19. The Prism™ twin screw 15:1 L/D ratio extruder used in this study.

Figure 20. Perkin Elmer Spectrum One (attenuated total reflectance-fourier-transform infrared) ATR-FTIR spectrometer (left hand side) and schematic diagram of fourier-transform infrared FTIR spectrometer (right hand side).

Figure 21. Renishaw inVia Raman confocal microscope attached to a motorized stage.

Figure 22. Philips PANalytical X'Pert MPD Pro X-ray powder diffractometer (XRPD) with PW3064 sample spinner used in this work.

Figure 23. Mira scanning electron microscope (SEM) (left hand side) and Bal-Tec SCD005 sputter coater (right hand side).

Figure 24. Distek 50947 dissolution apparatus (left hand side) and ultraviolet (UV)-1280 UV-Vis (UV) Spectrophotometer (Right hand side).

Chapter 3: Results & Discussion

Figure 25. XRPD diffractograms of selected formulations indicating that the INM is present in the amorphous form but the P407 is not solubilised and exists in its crystalline form.

Figure 26. a) XRPD diffractograms of the pure components and (b) XRPD diffractograms of selected SD formulations indicating that the INM is present in the amorphous form, but the P407 is not solubilized and due to its semi-crystalline nature exists in its semi-crystalline form. The 70% INM ASD formulations remained crystalline.

Figure 27. XRPD diffractograms of the pure components. INM is transformed to the amorphous form.

Figure 28. XRPD diffractograms of SD formulations and XRPD diffractograms of the SD formulation used to investigate the effect of cooling. P407 was still present in its crystalline form in all formulations (AC= Air cooled, NT= Normal room temperature and Liq N₂ = Liquid Nitrogen).

Figure 29. (Top) FTIR spectra of selected 25% SD formulations and pure components indicating a broadening of the amide carbonyl peak of PVP VA64 for both extruded dispersions. Figure 29 (b): (Bottom) SD formulations with 0% P407 loading and Figure 29 (c): (Bottom) SD formulations with 20% P407 loading.

Figure 30. Full Raman spectra of pure components and selected SD formulations (30% INM), indicating potential hydrogen bonding due to the shift in the amide carbonyl of both PVP VA64 and PL-S630 from 1673 cm⁻¹ to 1680 cm⁻¹. The vinyl acetate carbonyl peak appears at a low intensity at 1732.00 cm⁻¹.

Figure 31. Raman spectra of pure components and selected SD formulations (30% INM), indicating potential hydrogen bonding. There was a shift in the vinyl acetate C=O carbonyl in the all ASD formulations, however they quaternary ASD formulations had the greatest shift.

Figure 32. a) ATR-FTIR Spectra of pure components and selected SD formulations (30% INM). b) ATR-FTIR Spectra of both PVP VA64/PL-S630 and SD1/SD2 indicating potential hydrogen bonding due to the shift in the amide carbonyl of both PVP VA64 and PL-S630 from 1672 cm⁻¹ to 1685 cm⁻¹. There is no shift in the vinyl acetate carbonyl peak as a result of its

weaker hydrogen bond potential. (c) ATR-FTIR spectra of binary SDs of 10 and 30% INM-P407 drug-polymer mixtures.

Figure 33. a) ATR-FTIR Spectra of a selected SD formulation (Quart SD2) illustrating the hydrogen bond between PVP VA64/PL-S630 and INM due to the shift in the amide carbonyl of both PVP VA64 and PL-S630 from 1672 cm^{-1} to 1685 cm^{-1}

Figure 34. ATR-FRIR reference spectrum of amorphous INM (aINM), indicating a shift in the acid-acid dimer C=O stretch (1690 cm^{-1} to 1679 cm^{-1}) and the free carboxylic acid C=O (1714 cm^{-1} to 1707 cm^{-1}).

Figure 35. a) ATR-FTIR Spectra of pure components and selected SD formulations (30% INM) showing a shift in the amide carbonyl C=O from 1672 cm^{-1} to 1680 cm^{-1} . There is no shift in the vinyl acetate carbonyl peak as a result of its weaker hydrogen bond potential. (b) ATR-FTIR spectra of binary SDs (controls) of 10 and 30% INM-P407 drug-polymer mixtures.

Figure 36. ATR-FTIR Spectra of aINM and Physical blend. Crystalline INM is still present in physical blend as expected.

Figure 37. ATR-FTIR Spectrum of crystalline INM.

Figure 38. Raman spectra of crystalline INM, polymeric carriers and chosen SD formulations (30% INM), which shows interaction via hydrogen bonding as a result of the shift in the amide C=O carbonyl stretch of PL-S630 and PVP VA64. The low intense peak at 1732.00 cm^{-1} corresponds to the vinyl acetate C=O carbonyl.

Figure 39. SEM image of Pure PVP VA64 at 100kx magnification.

Figure 40. SEM image of Pure INM at 100kx magnification.

Figure 41. SEM image of Pure P407 at 100kx magnification.

Figure 42. SEM image of physical mixture at 100kx magnification.

Figure 43. SEM image of SD1 (0% P407-10% INM loading) at 100kx magnification.

Figure 44. Solubility of INM ($\mu\text{g/ml}$) in aqueous solutions of PVP VA64 and P407 at 37°C (Each point represents the average \pm SD of three independently prepared samples).

Figure 45. Solubility of INM ($\mu\text{g/ml}$) in aqueous solutions of PL-S630, PVP VA64 and P407 at 37°C (each point represents the average \pm SD of 3 independently prepared ASD samples) with a maximum kinetic solubility of $34 \mu\text{g/ml}$.

Figure 46. Dissolution profile of 25% INM SD formulations in pH buffer 1.2.

Figure 47. Dissolution profile of 20% INM SD formulations in pH buffer 1.2.

Figure 48. Graphical representations of the area under the curve (AUC) for 25% SD formulations in pH 1.2, ** and * represents statistical difference ($p < 0.05$) between SD and pure INM and amorphous INM respectively, for a one way ANOVA and Tukey Kramer post-hoc test.

Figure 49. Graphical representations of AUC for 20% SD formulations in pH 1.2, ** and * represents statistical difference ($p < 0.05$) between ASD and pure INM and amorphous INM respectively, for a one-way ANOVA and Tukey Kramer post-hoc test.

Figure 50. *In-vitro* dissolution profiles of quaternary SDs and graphical representations of AUC of quaternary and ternary SD formulations in pH 1.2. ** and * represents the statistical difference ($p < 0.05$) between SD, amorphous INM and pure INM respectively, for 1-way ANOVA and Tukey Kramer post hoc test.

Figure 51. Illustration of non-sink conditions used in the dissolution test. Dissolution profile 1: dissolution of the crystalline API; profile 2: dissolution of a “spring” effect of the API without the presence of dissolution enhancers profile 3: dissolution of a ‘spring’ and ‘parachute’ form of the API in the presence of dissolution enhancers act as a “parachute.” C_{eq} represents equilibrium solubility.

Figure 52. *In-vitro* dissolution profiles of air-cooled SD formulations performed in buffer of pH 1.2.

Figure 53. *In-vitro* dissolution profiles of quaternary SD formulations performed in buffer of pH 1.2. The maximum aqueous solubility is $20.73 \mu\text{g/ml}$ after 3 hours. (AC= Air cooled, NT= Normal room temperature and Liq N_2 = Liquid Nitrogen).

Figure 54. Graphical representations of AUC of quaternary and ternary SD formulations in pH 1.2. ** and * represents the statistical difference ($p < 0.05$) between ASD, amorphous INM and pure INM respectively, for 1-way ANOVA and Tukey Kramer post hoc test. (AC= Air cooled, NT= Normal room temperature and Liq N₂ = Liquid Nitrogen).

Figure 55. a) XRPD diffractograms of SD formulations and XRPD diffractograms of the SD formulation used to investigate the effect of cooling after 5 months of a stability study under accelerated conditions of 40 °C and 75% RH. P407 was still present in its crystalline form in all formulations (AC= Air cooled, NT= Normal room temperature and Liq N₂ = Liquid Nitrogen).

List of Tables

Chapter 2: Literature Review

Table 1. Examples of various polymers used in the formulation of amorphous solid dispersions (SDs).

Table 2. Different factors affecting the stability of amorphous SDs (adapted from (Baghel *et al.*, 2016)).

Chapter 2: Experimental Details

Table 3. Physicochemical Properties of model drug and polymers.

Table 4. Batch composition used to investigate the effect of Poloxamer 407 (P407) on the dissolution enhancement of hot-melt extruded solid dispersions compounded using 25:1 length to diameter (L/D) ratio extruder (100 grams batch size).

Table 5. Batch composition used to investigate the role of intermolecular interactions, solid-sate and dissolution properties of mixed co-povidone (ternary) hot-melt extruded solid dispersions compounded using the 15: 1 L/D ratio extruder (50 grams batch size).

Table 6. Batch composition used to investigate the role of intermolecular interactions, solid-sate and dissolution properties of mixed co-povidone (ternary) hot-melt extruded solid dispersions compounded using the 15: 1 L/D ratio extruder (50 grams batch size).

Table 7. Batch composition used to investigate the effect of cooling rate on the solid-state and dissolution properties of hot-melt extruded solid dispersions compounded using the 15: 1 and 25:1 L/D ratio extruders (50 grams batch size).

Table 8. Temperature zones of 25:1 L/D ratio extruder used in the hot melt extrusion process.

Table 9. Temperature zones of 15:1 L/D ratio extruder used in the hot melt extrusion process.

Chapter 3: Results & Discussion

Table 10. Calculated solubility parameters using Hansen solubility parameters (HSPs) (δ) and drug-polymer interaction factor (χ).

Table 11. Calculation of HSPs and molar volume for INM according to the Hoftyzer-Van Krevelen method.

Table 12. Calculation of HSPs and molar volume for PVPVA64/PL-S630 according to the Hoftyzer-Van Krevelen method.

Table 13. Calculation of HSPs and molar volume for P407 according to the Hoftyzer-Van Krevelen method.

Table 14. Calculated HSPs and drug-polymer interaction factor for drug and polymers.

Table 15. Interpretation of ATR-FTIR Spectrum of INM.

Table 16. Interpretation of ATR-FTIR Spectrum of Poly (vinylpyrrolidone-co-vinyl acetate) (PVPVA64)/Plasdone-S630 (PL-S630).

Table 17. Interpretation of ATR-FTIR Spectrum of P407.

Table 18. Interpretation of ATR-FTIR Spectrum of SD formulations.

Table 19. Interpretation of Raman Spectrum of INM.

Table 20. Interpretation of Raman Spectrum of PVPVA64/PL-S630.

Table 21. Interpretation of Raman Spectrum of P407.

Table 22. Interpretation of Raman Spectrum of a selected SD formulation (Quart SD4).

Table 23. Gibbs free energy values and apparent stability constants (K_a) of INM-P407, INM-PVP VA64 and INM-P407-PVP VA64 interactions.

Table 24. Gibbs free energy Values and Apparent stability constants (K_a) of ternary and quaternary drug-polymer-surfactant interactions.

Table 25. Comparison of the solubility of INM from various quaternary and ternary ASD formulations and corresponding physical mixtures in pH buffer 1.2 after 3 and 24 hours respectively.

Table 26. Comparison of the aqueous solubility of INM and standard deviation (STD) from various quaternary and ternary SD formulations and physical blends in pH buffer 1.2 after 3 and 24 hours respectively. Physical blends contain crystalline INM.

Table 27. Comparison of the aqueous solubility of INM from various quaternary and ternary SD formulations in pH buffer 1.2 taken at various time intervals over 24 hours.

Table 28. Comparison of the aqueous solubility of INM from various quaternary and ternary SD formulations in pH buffer 1.2 after 3 and 24 hours. Supersaturation parameter (SP) was calculated for SD formulations after 3 hours.

Chapter One

Introduction

1.0 Introduction

Within both the pharmaceutical industry and academia, there is a strong interest in utilizing hot melt extrusion (HME) to prepare amorphous solid dispersions (SDs) which have the potential to significantly improve the kinetic solubility and thus, the bioavailability of biopharmaceutical classification system (BCS) class II drugs which have poor aqueous solubility and high permeability (Alzahrani *et al.*, 2022). The conversion of the active pharmaceutical ingredient (API) to the amorphous state increases dissolution rate and apparent solubility as the penetration of solvents is not prohibited by an endothermic barrier attributed to the disorder of crystalline lattices (Jelić, 2021).

During dissolution the carrier traps the dispersed API in a high energy state, maintaining supersaturation in the medium over time and preventing crystallization (Nair *et al.*, 2020). Simoes *et al.* (2019) reported that hot melt extrusion (HME) has many significant benefits such as the elimination of solvents, good content uniformity due to the low drug loading used, dosage forms of a desired shape, including tablets, pellets and implants can be easily manufactured by this process; HME is also a continuous process and can be scaled up (Simões, Pinto & Simões, 2019) and finally, HME allows conversion of crystalline drugs to amorphous form or dispersion of API into very small particles, enhancing bioavailability and improving patient compliance. However, the application of high shear inherent to the process and high processing temperatures presents a significant challenge when dealing with APIs that are thermo-sensitive.

The inclusion of plasticizers as excipients can lower the processing temperatures associated with HME and can modify the physicochemical and dissolution properties of poorly water-soluble APIs (Hurley *et al.*, 2020). Understanding the physicochemical properties of both the API and polymeric carriers is important when manufacturing SDs as it is the properties of the formulation that is being extruded that dictate the dissolution behaviour. Although the potential of amorphous SDs is enormous, the physicochemical factors of these systems need to be fully understood as they have a significant effect on the dissolution and stability of the amorphous drug. Various factors can affect the solid-state and dissolution properties of these systems and can result in undesirable behaviours, such as nucleation, phase separation and recrystallization during storage (Shi *et al.*, 2020).

Previous studies have focused on using various other methods such as supercritical fluid impregnation and spray drying to overcome the disadvantages associated with HME to significantly improve the dissolution behaviour of BCS Class II drugs (De Mohac *et al.*, 2020). Also, very little research has focused on how inter-molecular interactions and cooling methods play a role in the successful formulation of hot-melt extruded quaternary amorphous blends and how they affect physical stability and solubility of amorphous SDs. Therefore, this study will focus on the use of semi-crystalline polymers to overcome the dissolution barriers associated with hot-melt extruded SDs, the role of inter-molecular interactions will be examined and the effect of various cooling methods (which is vital extrusion parameter) on the solid-state and dissolution properties of mixed copovidone hot-melt extruded quaternary SDs will also be investigated.

For example, Pezzoli *et al.* (2019) performed stability studies of hot-melt extruded ternary solid dispersions of indomethacin (INM) in polyethylene oxide (PEO) SDs, however previous studies haven't looked at the effect of various extrusion parameters (Pezzoli *et al.*, 2019). Therefore, in this study, three process conditions—set mixer temperature, screw speed and residence time—were studied. The results show that the dissolution rate of INM increased with increasing screw rotating speed or the mixer set temperature. Further research was carried out using semi-crystalline polymers such as Poloxamer 407 (P407) to overcome the drawbacks associated with HME such as its high processing temperatures (Hurley *et al.*, 2018), as the processing temperatures can restrict the processing of thermally labile drugs (Davis *et al.*, 2021).

The cooling method used during the extrusion process can also have a significant effect on the crystallization tendency and solubility of the API. Very little has been reported on how various cooling methods effect the degree of crystallinity, solid state properties and dissolution rate of multi-component amorphous SDs. INM will be used as a model drug in this study which is a BCS class II API (low solubility, high permeability). It is well reported in the literature that preparing an SD of INM significantly improved the amorphous stability and solubility of INM (Fael & Demirel, 2021).

Poly (vinylpyrrolidone-co-vinyl acetate) (PVP VA64) and Plasdone-S630 (PL-S630) in terms of monographs, have the same chemical structure; however, they have different solid-state properties and solubilities depending on the manufacturing process used. PVP VA64 and PL-S630 are commonly used carriers for optimizing the solubility of INM, and the effect of these specific carriers will be examined in this study. P407 was chosen as it is reported in literature that P407 cannot only overcome the drawbacks associated with HME, but increase the solubility of INM significantly (Shukla *et al.*, 2023). The relationship between cooling and the physicochemical/dissolution properties of the drug and polymeric carriers is an area that is very important in the manufacture and development of SDs.

It is reported in the literature that slow cooling enhances the physical stability of amorphous INM (Shi *et al.*, 20222), as changes in the cooling rate can have an impact on the crystallinity of the API. This study was, to our knowledge, the first to report how various cooling methods affect the dissolution behaviour of INM using a semi-crystalline surfactant and how it affects the degree of crystallinity of amorphous SDs. Since this study uses a semi-crystalline plasticizer to improve the solubility of INM, the degree of crystallinity of the semi-crystalline polymer in selected SD formulations will be examined as it can affect the processing and physical properties of the API.

Chapter Two

Literature

review

2.0 Literature Review

2.1 BCS class II drugs and factors solubility of BCS class II drugs.

According to Malkawi *et al.* (2022) ASD's have over recent years significantly improved the drawbacks associated with poorly water soluble drugs. They have enhanced the dissolution rate and the bioavailability of poorly water soluble drugs as polymeric carriers have lowered the occurrence of these drawbacks and improved dissolution (Malkawi, Al-Mahmound & Tawalbeh, 2022). Although the oral bioavailability of a drug depends on aqueous solubility, dissolution rate, first-pass metabolism and drug permeability (the ability of a drug to cross biological cell membranes) are also vital parameters that attribute to oral bioavailability. The low aqueous solubility of new chemical entities is now becoming a significant issue within the pharmaceutical industry with recent studies indicating that 90% of active pharmaceutical ingredients (APIs) within pharmaceutical pipelines possess poor aqueous solubility. It is also estimated that 40% of oral drug products currently on the market are considered practically insoluble ($< 100 \mu\text{g/ml}$) (Francisco Javier *et al.*, 2023).

Samineni *et al.* (2021) classifies APIs into four different classes depending on their solubility and permeability which is known as the Biopharmaceutical Classification System (BCS) (as shown in Figure. 1), (Samineni, Chimakurthy & Konidala, 2021). BCS involves mathematical analysis in order to determine experimentally the solubility and permeability of API's under precise conditions (Hurley *et al.*, 2018). This study will primarily be restricted to BCS class II drugs (low solubility and high permeability).

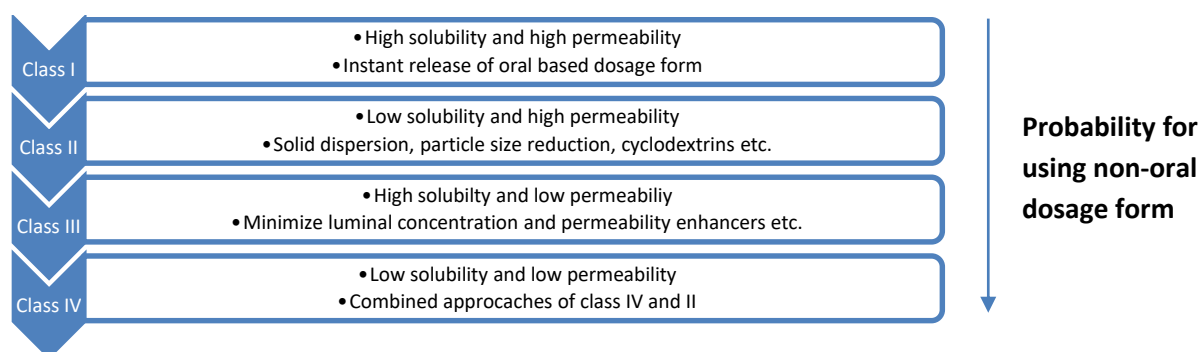


Figure 1. Biopharmaceutics classification system (BCS) and formulation approaches for various classes of drugs.

There are many factors that affect the solubility and dissolution of BCS class II drugs, which is why formulation scientists must use safe, reliable, efficient, inexpensive and effective techniques to enhance the bioavailability and dissolution rate of BCS class II drugs. These factors are as follows;

- Particle size.
- Temperature.
- Nature of solute and solvent.
- Polymorphism.
- Solvent pH and pKa.
- Chemical structure/Polarity.

1/ Particle size: Particle size may influence drug bioavailability, i.e., the smaller the particle size, the larger the surface area of the substance in contact with the dissolution medium, and thus the higher the dissolution rate and the absorption of the drug (Csicsák *et al.*, 2023). Salehi *et al.* (2020) states if particle size is reduced to a minimum level, dissolution is enhanced due to the increase in surface area. However, if particle size is not controlled it will result in variable dissolution rates (Salehi *et al.*, 2020).

2/ Temperature: The solubility of any substance is a function of temperature. Most drugs are endothermic, absorbing heat during the dissolution process. Therefore, an increase in temperature will result in an increase in aqueous solubility. Lu & Murray, (2022) states that as temperature increases, the solubility of a liquid or solid decrease or increases depending on whether the dissolution reaction is endothermic or exothermic.

- In endothermic reactions, the net energy from the bonds breaking and forming results in heat energy being absorbed when the solute dissolves in solution. When the temperature of the system increases this introduces heat into the system (Lu, Tupper & Murray, 2022).
- So according to Le Chatelier's Principle, the system will adjust to this increase in the heat by promoting the dissolution reaction to absorb some of the heat energy. Hence increasing the temperature of the system increases the solubility of the solute (Lu, Tupper & Murray, 2022).

3/ Nature of solvent and solute: The amount of solute that dissolves depends on the type of solute or solvent it is. According to Singh *et al.* (2021) the solubility of any drug is due to the dipole movement and polarity. In addition, hydrogen bonding between the solvent and solute is essential. Therefore, structural features and presence of polar and nonpolar groups in the molecule are vital (Singh, Singh & Singh, 2021).

4/ Solvent pH and pKa: According to Stukeij *et al.* (2020) pKa is used to indicate the strength of an acid, it is the $-\log$ of the Ka value. A lower pKa indicates a stronger acid. According to the Henderson-Hasselbach equation, the relationship between pH, pKa and relative concentrations of a salt and acid is as follows:

$$\text{pH} = \text{pKa} + \log \frac{[\text{A}^-]}{[\text{HA}]}$$

where $[\text{A}^-]$ is the molar concentration of the dissociated species (salt) and $[\text{HA}]$ is the concentration of the undissociated acid. If the concentrations of acid and salt are equal, the pH of the system will equal the pKa of the undissociated acid. If the pH decreases, the concentration of the molecular acid increases and the dissociated species decreases. In the biological acid, the undissociated form is less soluble than the salt, however it is undissociated acid that readily penetrates cell tissues to exert a therapeutic effect in the body (Štukelj *et al.*, 2020). For example, Tres *et al.* (2016) carried out studies using indomethacin (INM) which is a poorly water soluble drug.

According to Tres *et al.* (2016) INM is a weak acid with a pKa of 4.5 and displays pH dependent solubility and dissolution rate. The authors reported that the aqueous solubility of INM has been reported to increase from 1.5 $\mu\text{g}/\text{ml}$ at pH 1.2 to 105.2 $\mu\text{g}/\text{ml}$ at pH 7.4. As INM is a weak acid it will only partially dissociate in water (pH 7). At pH 7 INM completely dissolves due to increasing number of photons and as a result dissociates. At pH 1.2, INM remains undissociated, however it displays poor dissolution within the GI tract, therefore a lot of research has focused on optimizing the solubility of INM at this pH range by altering the polarity of the solute (Tres *et al.*, 2016).

5/ Chemical Structure/Polarity: According to Shi *et al.* (2022) solute molecules are held together by various intra- and intermolecular forces such as dipole-dipole, ion-ion etc. as are molecules of solvent. To enhance dissolution, these cohesive forces must be broken and adhesive forces must be formed between solute and solvent.

Polarity of a solvent plays a significant role in enhancing the solubility of any drug. Solvents can be polar, non-polar or semi-polar (Shi *et al.*, 2022). Polar solvents will dissolve polar and ionic solutes (like dissolves like), non-polar solvents will dissolve molecules that are non-polar, and semi-polar solvents induce a degree of polarity in non-polar molecules and therefore may improve the miscibility of non-polar and polar liquids. In drug delivery, one way of optimizing solubility is altering the polarity of the solute and shifting it between its ionic (dissociated) state and molecular (undissociated) state. A shift towards the molecular state enhances solubility in non-polar solvents, however a shift towards the ionic form enhances solubility within polar solvents such as water.

Other factors include:

- Pressure.
- Surfactants (wetting agents).
- Common ion effect.
- Salting out (electrolytes and non-electrolytes).

2.2 Solid dispersions.

Formulation scientists have often turned their attention in the recent years to polymeric carriers and oligomers to allow formation of systems that can increase aqueous solubility and overcome the disadvantages associated with BCS class II drugs and effectively achieve oral drug administration (Józó *et al.*, 2021). Many of these techniques have given enhanced benefits such as targeted drug release (Ulbrich *et al.*, 2016), or exact control of dissolution rates such as drug release that is zero-order kinetics with respect to time, allowing optimum plasma drug concentration levels within the gastrointestinal fluid.

These added benefits allow for increased patient compliance and convenience due to lower dosage and regularity of medication, especially in the case of drugs with a narrow therapeutic index as they have reduced side effects. Below are several approaches to enhance solubility and dissolution rates (Nair *et al.*, 2020).

- Solubility improvement techniques can be classified into physical modification, chemical modifications of the API, and many other methods.
- Physical modifications: Particle size reduction like sonication and high pressure homogenization, liquid anti-solvent crystallization spray freeze-drying and supercritical carbon dioxide based microionization techniques (Kumar *et al.*, 2021).
- Chemical modifications: Changing the pH, using buffer, derivatization, complexation, and formation of salts.

However, the most frequent method used to improve aqueous solubility and dissolution rate of BCS Class II drugs is by preparation of solid dispersions and the most common way to optimize bioavailability of poorly water-soluble drugs. The term solid dispersion (SD) refers to a group of solid products that consist of solid products that contain at least two different components i.e. a hydrophilic matrix and a hydrophobic drug. The drug is dispersed molecularly as amorphous particles (clusters) or as crystalline products (Malkawi, Al-Mahmound & Tawalbeh, 2022). Pharmaceutical based polymers are used to synthesize this matrix and their selection is based on the following, physiochemical properties (e.g. drug-polymer miscibility and stability), pharmacokinetic (e.g. rate of absorption) (Pires *et al.*, 2023). and pharmacodynamic (effect of the drug on the biological system) properties.

The SD consists of API's, polymers/carriers, plasticizers, stabilizers and other agents. Nair *et al.* (2020) defined the term solid dispersion as "A dispersion that involves the formation of eutectic mixtures of active drugs with water soluble polymer carriers via melting of their physical mixtures" (Nair *et al.*, 2020). According to Kang *et al.* (2023) the amorphous state which exhibits a disordered structure and possess a higher free energy (thermodynamic driving force) leading to higher aqueous solubility, oral absorption and bioavailability compared to the crystalline state as the crystalline state due to lattice energy drawback is a major constraint in the solubility of crystalline drugs. According to Sathisaran & Dalvi, (2018) the lattice energy is defined " as the measure of the energy released when ions are combined to make a compound. It is a measure of the cohesive forces that bind ions" (Sathisaran & Dalvi, 2018).

In SDs, a fraction of the drug dissolves which saturates the GI fluid, and excess drug precipitates out as fine colloidal particles of submicron size. The advancement of solid dispersions as a practically vital method to enhance bioavailability of BCS class II drugs have overcome the drawbacks of previous methods e.g. salt formation, solubilization, cosolvency, and particle size reduction ((Kaushik, Vikas & Kaushik, 2022).

Many new APIs have appeared on the market (as shown in Figure. 2), these new dosage forms use amorphous polymeric carriers as a carrier (Liu *et al.*, 2013). Therefore, this study will focus on this particular type of SD– amorphous glass solutions which contain hydrophilic polymeric carriers for fast drug release. For this subtype, the molecularly dispersed active drug is released as the hydrophilic polymer carrier dissolves, resulting in a supersaturated solution. Therefore dissolution is adequate for amorphous glass solutions (Luz María *et al.*, 2017).

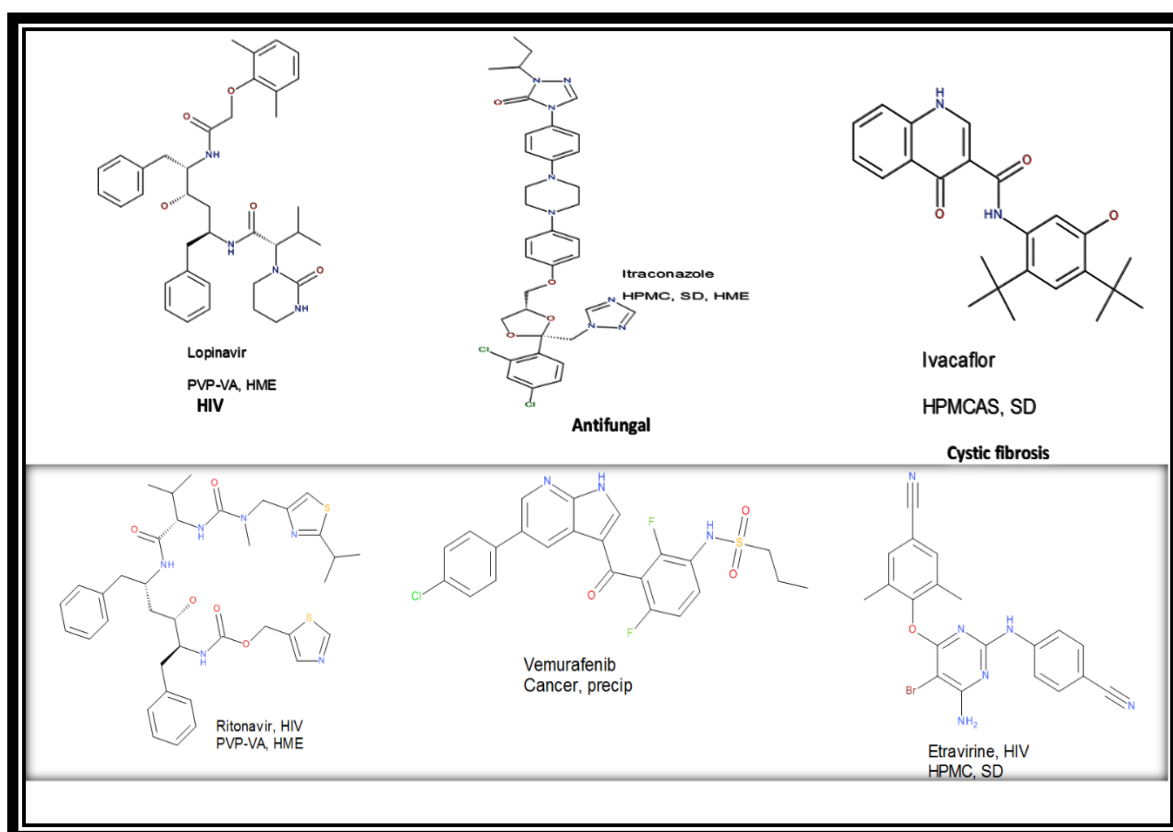


Figure 2. FDA-approved solid dispersion (SD) products (drug, indication, polymer (HPMC is hydroxypropyl methyl cellulose; HPMCAS is hydroxypropyl methyl cellulose acetate succinate; PVP-VA is poly (vinyl pyrrolidinone-co-vinyl acetate)), and processing method (SD is spray-drying; HME is hot-melt extrusion)) (adapted from (Liu *et al.*, 2013)).

The creation of a supersaturated solution on the other hand, requires stabilizing formulation compounds for precipitation. Currently, much research has primarily focused on the physical stability of amorphous solid solutions, which is why only a few amorphous solid solutions are currently on the market (Simões *et al.*, 2020).

This literature review will discuss the various factors that affect the stabilization of SD based solid dosage forms. It will also discuss hot-melt extrusion (HME) as a preparation method used to improve the solubility of BCS class II drugs. Finally, the polymeric materials including the model BCS class II drug that will be used in this study will also be discussed.

2.3 Factors that affect the physical and chemical stability of solid dispersions.

2.3.1 Polymeric carriers used.

In an article by Karsten *et al.* (2021) development of ASD formulations is still very challenging and because it has rapidly evolved it is vital that the correct preparation technique is selected along with the appropriate polymeric matrix and because the main component of an ASD is the polymer this determines the material properties of the system (Karsten *et al.*, 2021).

Polymers that have a high glass transition temperature (T_g) at high concentrations are normally used for amorphous SD systems due to their antiplasticizing effect on the amorphous API. Low polymer weight fractions where there is no difference in T_g ; usually drug-polymer intermolecular interactions will establish their shelf life (Shen *et al.*, 2023). Increasing the molecular weight will increase the T_g of polymeric carriers enhancing antiplasticization of amorphous API's.

However, at a high molecular weight, the increase in T_g is irrelevant because such factors for example viscosity will play a role in the dissolution of the amorphous SDs (Novakovic *et al.*, 2020). Viscosity of polymeric carrier's increases depending on the molecular weight will have an effect on the dissolution properties (Nair *et al.*, 2020). It is essential when formulating amorphous SDs that the polymeric carrier has a low melting point and solubility parameters similar to the model drug that is being used. Also drug-polymer miscibility is vital as highly miscible amorphous systems are resilient to recrystallization (Alzahrani *et al.*, 2022)

The formation of a single stable phase or separate phases depends on the drug-polymer miscibility and on the system thermodynamics at a specific condition (Baghel, Cathcart & O'Reilly, 2016). Table 1 shows the various polymeric carriers used in the formulation of SDs.

Table 1. Examples of various polymers used in the formulation of amorphous solid dispersions (SDs).

Polymer	T_g or T_m (°C)	Drug stabilized	Method of preparation
Poly (vinylpyrrolidone) (PVP) K17	T_g : 126°C	Acetaminophen	Spray Drying
Poly (ethylene glycol) 20,000	T_m : 60-63°C	Carbamazepine	Fusion Method
Soluplus	T_g : 70°C	Carvedilol	Solvent evaporation,/ freeze drying/spray drying
Poly (acrylic acid)	T_g : 110°C	Carbamazepine	Hot melt extrusion
Poloxamer 188	T_m : ~55°C	Nilvadipine	Agitation granulation method
Hydroxypropyl methylcellulose (HPMC)	T_g : 172°C	Indomethacin	Hot melt extrusion
HPMC Acetate succinate	T_g : 113°C	Itraconazole	Film casting method

2.3.2 Amorphous state

A crystalline drug upon heating undergoes melting at a particular temperature i.e. melt temperature (T_m) as shown in Figure. 3. Once cooled it results in the formation of what is called an orderly system. As the molecules have enough time to move from their crystalline state to a thermodynamically point of stability within the crystal lattice (Svärd, Ahuja & Rasmuson, 2020), the molecules arrange in a specific or definite order which results in a crystalline structure once again. If the cooled molten API is cooled straight away it results in a supercooled liquid state which has a temperature below its melting temperature i.e. it is in equilibrium with the molten supercooled drug (Medarević *et al.*, 2019). If the drug is further cooled the thermodynamic stable system is in equilibrium until the T_g is reached, which forms a nonequilibrium state and converts into what is known as a “frozen” glassy state of the API.

A material within this glassy state is a brittle type solid which has no crystalline structure and only small range of order (Luan *et al.*, 2022). This transition from crystalline to amorphous is essential if the supercooled liquid state is to remain below the T_g , the crystals therefore have a higher entropy compared to the supercooled liquid state. This entropy is a negative value before it reaches absolute zero temperature, which disobeys the third law of thermodynamics which states that entropy of a crystal is zero at zero kelvin (Liu, 2020).

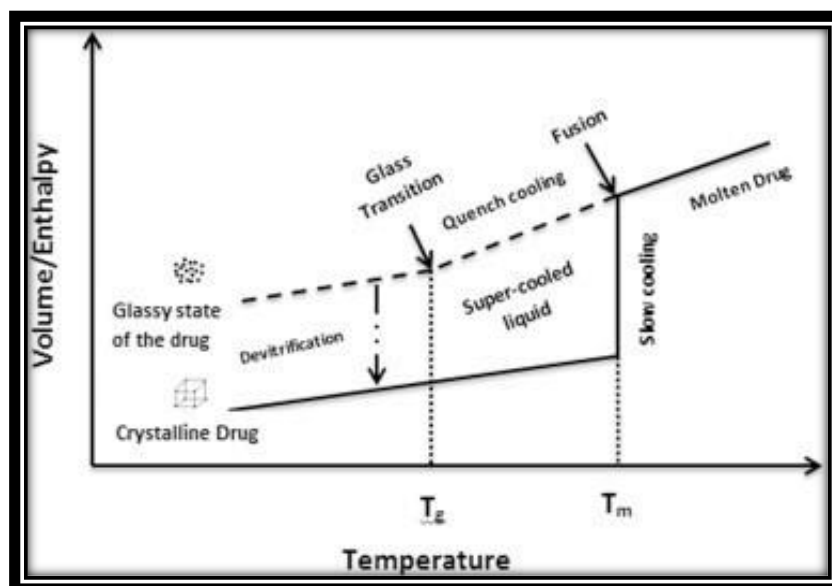


Figure 3. *Enthalpy and volume of various states of crystalline drugs as a function of temperature; glass transition temperature (T_g) and melting temperature (T_m) are glass transition temperature and melting temperature respectively (reproduced from ((Baghel, Cathcart & O'Reilly, 2016)).*

The T_g is a transition characterized by a change in the heat capacity and results in a change of various thermodynamic properties such as volume, enthalpy and entropy. The amorphous state contains a higher enthalpy, entropy and free energy compared to the crystalline form and results in an increase in bioavailability and aqueous solubility of the solid dispersion (Figure. 3).

In relation to dissolution when the amorphous drug is added to the dissolution media, dissolution occurs quickly and appears as a peak on a dissolution graph followed by reduction in aqueous solubility due to the ‘spring and parachute’ effect (Figure. 4) which is a real disadvantage when it comes to dissolution (Handa, Malik & Guarve, 2022).

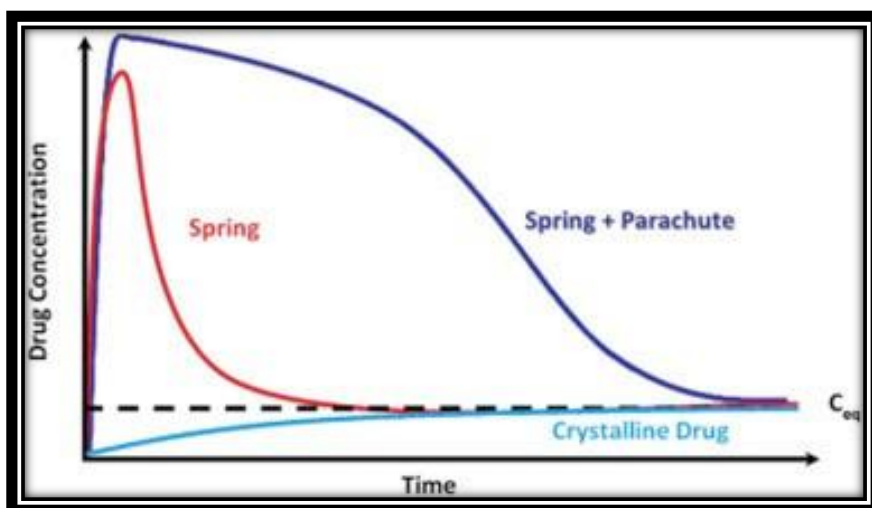


Figure 4. Drug profile based on the aqueous solubility of amorphous and crystalline drug (reproduced from (Handa, Malik & Guarve, 2022))

2.3.3 Intermolecular interactions.

To date predicating inter-molecular interactions is of great interest not just in the pharmaceutical industry but also in SD formulations. The process involves the interaction between a polymeric matrix and a small molecule drug. The thermodynamics of mixing states that for an interaction to exist between a polymer and API, there must be a negative change in the free energy of mixing (Hurley *et al.*, 2019)

This change in the free energy of mixing is related to the entropic and enthalpy contributions according to the following equation (Eq. 1).

$$\Delta G_{\text{mix}} = \Delta H_{\text{mix}} - T \times \Delta S_{\text{mix}}$$

ΔG_{mix} is the Gibbs free energy, ΔH_{mix} is enthalpy of mixing, ΔS_{mix} is the entropy of mixing and T is the absolute temperature. This negative change in free energy is spontaneous due to the increase in the entropy of mixing. However the presence of repulsive and cohesive inter- and intramolecular forces (e.g. dipole-dipole interaction, dispersion force and hydrogen bond interaction) which are present within the solid dispersion system make the interaction between polymer and drug more complicated (Maniruzzaman *et al.*, 2015).

The calculation of the drug-polymer interaction factor and Hansen solubility parameters (HSPs) heavily depends on the various types of intermolecular interactions and the various cohesive and repulsive intra- and intermolecular forces and molecular volumes of each of the components.

The examination of both polymers and drug used in this study in Figure 1, indicate that they are all polar and thus are able to be involved in hydrogen bonding. Maniruzzaman *et al.* (2015) reported that using the lattice-based Flory-Huggins (F-H) theory to describe interactions between drug and polymer is limited as it doesn't take into account the multiple interactions in drug-polymer system. So the HSPs developed by Van Krevelen and Hoftyzer group contribution were used as an alternative in this study to understand the nature of interactions that occur within these systems.

Hydrogen bond formation between the polymeric carrier and the API is thought to play a significant role in preventing recrystallization in amorphous drugs (Hurley *et al.*, 2019). The most common technique used to identify hydrogen bonds between the polymer and API has been Fourier-transform-infrared (FT-IR) spectroscopy. Potter *et al.* (2015) detected the inter-molecular interaction between the carboxylic acid moiety of PVP (Poly (vinylpyrrolidone)) and INM using this conventional technique. Many other researchers also detected the presence of hydrogen bonds between the APIs felodipine and nifedipine using PVP as a polymeric carrier in SDs (Potter *et al.*, 2015).

High resolution ^{13}C solid-state Nuclear magnetic resonance (ssNMR) spectroscopy has often being used to examine hydrogen bonding inter-molecular interactions in SDs (Tran & Tran, 2020). Yuan *et al.* (2015) reported the extent of hydrogen bond formation between PVP and INM increased as the polymeric carrier concentration increased. He also reported that INM hydrogen bonds with PVP VA64 in the same fashion as PVP, however as the vinyl acetate has a weaker hydrogen capability than PVPVA the hydrogen bond formation was less effective. However Yuan *et al.* (2015) could not distinguish between the amide $\text{C}=\text{O}$ carbonyl of INM and PVP VA64/PVP using labelled compounds via solid state NMR spectroscopy (Yuan *et al.*, 2015).

According to Tran & Tran, (2020) Raman spectroscopy is a very effective technique for identifying hydrogen bonding in SDs because APIs such as INM tend to be conjugated aromatic compounds that have strong Raman signals, while excipients tend to have a much weaker Raman spectrum as they are normally aliphatic in nature. Potter *et al.* (2015) prepared binary SDs of INM and PVP via hot-melt extrusion (HME) and reported that the benzoyl $\nu\text{C}=\text{O}$ of INM, which is present at 1698 cm^{-1} in crystalline INM shifted to 1680 cm^{-1} in amorphous INM as a result of hydrogen bonding.

2.3.4 Recrystallization

Recrystallization is a major issue with regard to successful formulation of SDs. Being a thermodynamic high-energy form, the apparent solubility and dissolution rate of amorphous APIs are higher than their crystalline counterparts. However, as mentioned the high free energy of the amorphous form also renders it prone to crystallization and gives rise to physical instability (Baghel *et al.*, 2016). Crystallization of APIs is a two-step process involving nucleation followed by crystal growth. Nucleation is a process in which the drug molecules form small stable clusters or aggregates of a critical size. This is a rate limiting step in the crystallization process and the rate of nucleation depends on the crystallization activation energy (Baghel, Cathcart & O'Reilly, 2018).

The subsequent crystal growth phase is governed by the diffusion of solute molecules to the nuclei interface and addition to the crystal lattice. Thus, one of the main challenges in formulating amorphous SDs is the prevention of nucleation and crystal growth in APIs which results in poor physical stability and compromised oral bioavailability (Baghel, Cathcart & O'Reilly, 2018). In an attempt to delay crystallization and improve physical stability, different polymers (which interfere with either nucleation or crystal growth or both) have been used to prepare binary amorphous SDs (Shi *et al.*, 2020).

Polymers, usually used at high concentrations, reduce the molecular mobility of the amorphous API in a binary dispersion by increasing the T_g of the system. While it is important to improve the physical stability of amorphous SD formulations, generating and maintaining drug supersaturation during dissolution is equally important (Kalepu & Nekkanti, 2015). When the intraluminal concentration of an orally administered drug exceeds its thermodynamic equilibrium solubility, the drug is supersaturated in the gastric media.

Recently, binary SDs (drug-polymer) have gained attention as an effective method of improving the supersaturation concentration of poorly soluble drugs during dissolution (Gan *et al.*, 2023). Different mechanisms have been proposed to explain the improvement in drug dissolution and stability from binary SDs including the formation of fine particles, drug-polymer interaction in solution, formation of a physical barrier to crystallization (adsorption of the polymer molecules onto the crystal surfaces), viscosity enhancement, reduction in Gibb's

free energy and an anti-plasticization effect of polymer on the drug (Baghel, Cathcart & O'Reilly, 2016).

A summary of various factors that can cause recrystallization and/or amorphous instability is summarized in Table 2.

Table 2. *Different factors affecting the stability of amorphous SDs (adapted from (Baghel et al., 2016)).*

Factors	Impact on the stability of amorphous drugs
Glass transition temperature (T_g)	Increasing the T_g increases stability. Polymers therefore can increase the kinetic stability of amorphous API's (Hurley, Potter, Walker, & Higginbotham, 2018).
Preparation method	Various preparation methods result in various different thermal histories and mechanical stress which can alter drug-polymer miscibility and drug mobility (Potter, et al., 2015).
Preparation conditions	Slow cooling of amorphous indomethacin for example can increase its physical stability (Blaabjerg, et al., 2019).
Gibbs free energy	Solid dispersions which have a low Gibbs free energy increase stability of amorphous solid dispersions (Hurley, M.T, Walker, Lyons, & Higginbotham, 2020).
Configurational entropy	Low configurational entropy favours crystallization (Ma & Williams, 2019).
Configurational enthalpy	Increasing the thermodynamic driving force for crystallization increase nucleation rate (Xu, Chen, Gong, & Wang, 2018)
Structural relaxation/molecular mobility	Results in recrystallization. Rate of crystallization is increased at temperatures above T_g . Reducing molecular mobility increases stability (Pandi, Bulusu, Kommineni, Khan, & Singh, 2020).
Humidity, mechanical stress and temperature	Temperature may alter molecular mobility, and humidity can act as a plasticizer by lowering the T_g close to the storage temperature, may also lead to an increase in crystallization and reduces the temperature (Potter, et al., 2015). Mechanical stress may also result in crystallization (Kawakami, 2019).

2.6 A review of the current state of hot melt extrusion used to prepare amorphous SDs.

Methods of manufacturing SDs are well documented in the literature; spray drying (Li *et al.*, 2020) and supercritical fluid impregnation (Han *et al.*, 2019) are just a few relevant examples. HME represents an efficient manufacturing technology capable of dispersing drugs in a melt up to a true molecular solution of the active agent in a matrix. Extrusion is the process of converting a raw material into a product of uniform shape and density by forcing it through a die under controlled conditions (Wang *et al.*, 2022). Extrusion process technology can be divided into two categories; ram extrusion and screw extrusion.

Ram extrusion consists of a positive displacement ram capable of generating high pressures forcing material through a shaping die while screw extrusion consists of a rotating screw or set of screws inside a barrel. Extrusion as a process is a well-established manufacturing method. The first extruder is generally accepted to have been built when Joseph Bramah constructed a hand operated piston press for the manufacture of seamless lead pipes in the United Kingdom in 1797 (Singh, Sharma & Sharma, 2020).

In the following years this technology was adapted to process a range of other materials such as soap, pasta and building materials. Screw extrusion was first developed as a response to the inadequacy of ram extruders in cable covering operations. The first example of a screw extruder can be seen in the 1873 drawing owned by Phoenix Gummiwerke A.G (Xavier, 2022). The first use of a twin-screw extruder was in the manufacture of sausages by Follows and Bates in the United Kingdom in 1869. The first twin screw extruders for polymer processing were developed in Italy in the 1930s by Roberto Colombo and Carlo Pasquetti (Schenkel, 2022) (Lyons, Higginbotham & Blackie, 2007).

In 1939, Troester developed an extruder that incorporated air cooling, automatic temperature control (using a separate control cabinet), nitride-hardened barrel liner, a length/diameter ratio of 10:1, and a variable-speed drive. Figure. 5 illustrates the relevant parts of a modern extruder screw. In recent years twin-screw extrusion has become a reliable process used in a range of applications particularly in polymer processing. Today, twin-screw extruders are used in chemical plants for reactive processing including both polymerisation and grafting reactions.

They are also used in post reactive processing steps such as coagulation and devolatilization. However twin-screw extruders find their main use in bulk processing of polymers. This includes compounding of particulates, blending and reactive processing as well as final shaping operations particularly in profile extrusion.

Twin-screw extruders represent not one technology but several technologies. The screws may be co-rotating or counter-rotating, they may be intermeshing, non-intermeshing or tangential. Intermeshing screws may or may not be self-wiping. In each case a separate historical and technological development may be discerned as well as specific advantages and disadvantages. As described by Martelli, twin-screw extruders were first categorised by Erdmenger who classified them in terms of the flow-path of the material within the screws both along and across the channel (1982). Erdmenger categorised multi-screw extruders as either lengthwise open or crosswise open, the former referring to extruders whose material moves on a path open from the inlet to the outlet and moving from the channels of one of the screws to that of the other screw (Lyons, Higginbotham & Blackie, 2007).

The latter (crosswise open) referring to extruders where there exists a path across the flights common to both the screws such that the material will move along the channel of one of the screws to two channels of the other screw. This may be logical in theory but in practice, it is difficult to categorise screws in such a manner due to the fact that the flow path of the materials does not depend solely on the rotational direction of the screws but also on the geometry of the flights and the channel. Figures. 6 and 7 shows the conventional view to classification of twin-screw extruders.

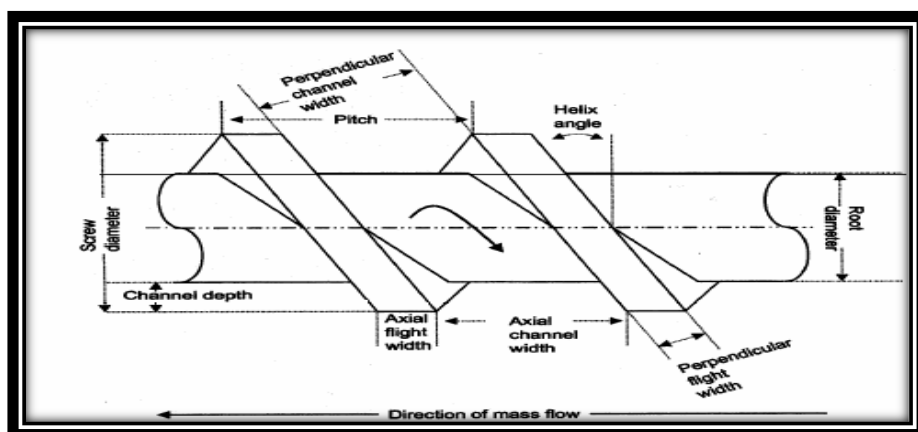


Figure 5. Diagram detailing terms used in relation to screw dimensions (adapted from (Lyons, Higginbotham & Blackie, 2007)).

When the two screws in a twin-screw extruder are intermeshing, the distance from the axis of the screws is less than the outer diameter of the screws and the surfaces of the screws are in ‘near’ contact. Positive conveying of the melt occurs in this configuration. Because of the intermeshing part of one screw not permitting material in the other screw to rotate freely implies that slip at the wall does not occur; this is one of the advantages of such a design. In the non-intermeshing configuration, the distance from the axis of the screws is equal to or greater than the outer diameter of the screws and the surfaces of the screws do not have any contact (Zhuang *et al.*, 2022).

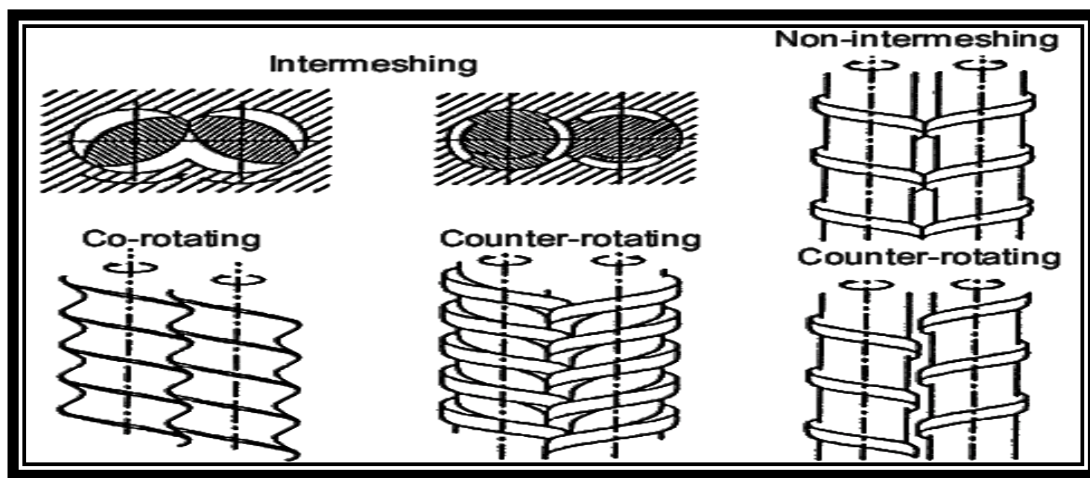


Figure 6. Illustration of various extruder types.

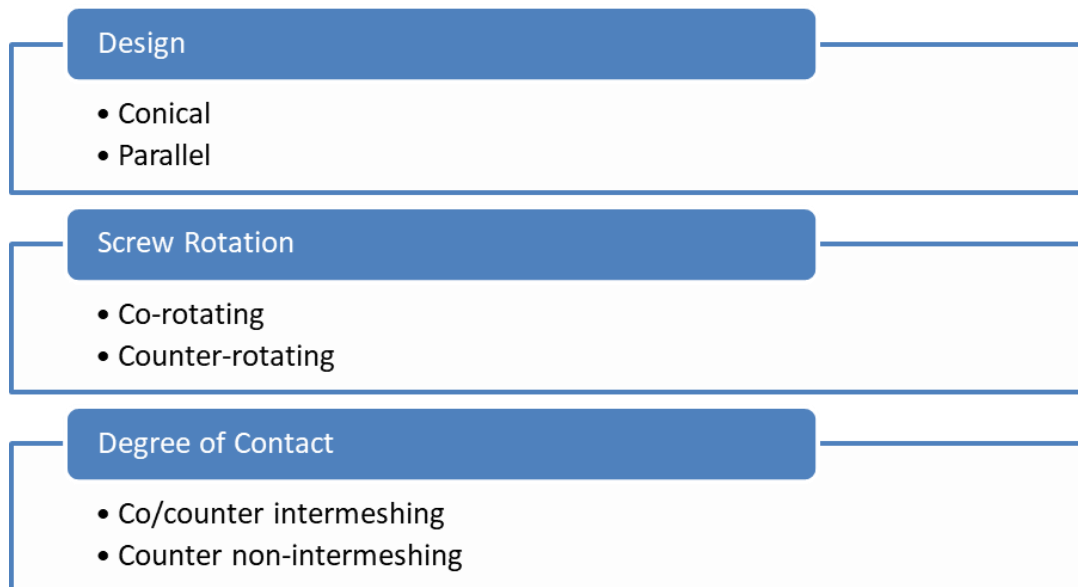


Figure 7. Types of Twin –screw extrusion compounding systems.

From the early 1920s to the 1950s patents were gained by Easton, Pease, Colombo, Meksat and Erdmenger which all expressed the mechanisms of operation of fully intermeshing co-rotating extruders (Lyons, Higginbotham & Blackie, 2007). The surface velocities in the intermesh region for the co-rotating intermeshing twin screw extruder are in opposite directions. With this configuration, materials tend to be wiped from one screw to the other (self-wiping), with a comparatively low percentage entering the intermesh gap. Materials tend to follow a figure-eight pattern in the flighted screw regions, and most of the shear is imparted by shear-inducing kneaders in localised regions (Lyons, Higginbotham & Blackie, 2007).

Forward-flighted screw elements are used to convey materials, reverse-flighted screw elements are used to create pressure fields, while kneaders and shear elements are used to mix and melt. Screws can be made shear intensive or less aggressive based on the number and type of shearing elements integrated into the screw design (figure. 8). As the self-wiping design allows no material to travel through the nib between the two screws, the highest degree of mixing occurs in the transfer area between the screws with little mixing taking place around the outside of the screws. Because the flight from one screw cannot clear the other, co-rotation is limited to bi-lobal mixing elements at standard flight depth (Lyons, Higginbotham & Blackie, 2007).

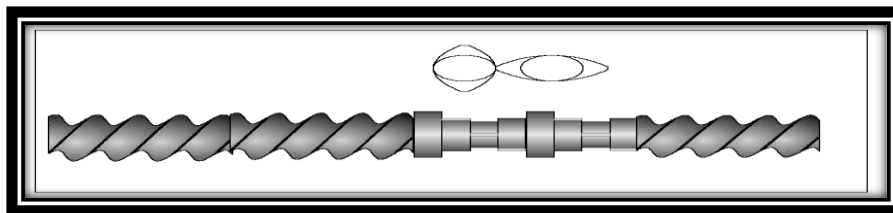


Figure 8. *Transporting and kneading elements in the co-rotating twin screw extruder, number of kneading elements: 8, upper image: front view, lower image: side view.*

Extrusion technology is extensively applied in the plastics and rubber industries, where it is one of the predominant fabrication processes. Examples of products fabricated from extruded polymers include piping, insulated wires, catheter components, and plastic and rubber sheeting. The drawbacks associated with extrusion technology generally relate to the high levels of power input required, mainly resulting from the need to produce elevated temperatures and large shear forces.

Careful control of process parameters can reduce these drawbacks. The largest application of extrusion in the pharmaceutical industry is in the preparation of solid dosage forms and SDs of uniform size, shape and density, containing one or more drug substance.

The reason why HME has gained increased interest in pharmaceutical industry is due to the numerous following benefits offered by this technique (Tambe *et al.*, 2021). HME is an efficient and solvent-free process hence requires less unit steps compared to other techniques. For example, individual excipients can be directly fed into the extruder barrel wherein efficient mixing of the component occurs by the screw elements; hence, pre-blending of the formulation components is not required. Similarly, to manufacture granules wetting and drying of granules is not required as HME is a solvent-free process.

- Formulations with high drug loading can be manufactured by HME with desired release profile.
- Due to intimate mixing of components, good content uniformity can be achieved for very low drug loading.
- HME allows conversion of API to amorphous form or dispersion of API into very small particles, which can result in enhanced bioavailability, less pill burden and *in vivo* plasma concentration variability, reduced side effects, and improved patient compliance.
- HME is a scalable continuous process and product quality can be monitored online.
- Dosage forms of desired shapes can be easily manufactured by HME process (tablets, granules, pellets, films, implants, etc.)

Potter *et al.* (2015) and Hengsawas *et al.* (2017) have reported numerous disadvantages associated with HME because in order for a polymer to be extruded it must exhibit a melt viscosity at acceptable processing temperatures. Therefore, many polymers are not suitable candidates for extrusion as 1) they have too high a glass transition 2) high melt viscosity or 3) narrow processing windows between degradation and glass transition. Thermal stability of the API is also an issue and must be considered, as the high temperatures often required for HME can restrict processing of thermally labile API's. (Potter *et al.*, 2015) & (Tran, Lee & Tran, 2021).

Currently a lot of research has focused on overcoming the various drawbacks associated with HME or using alternative methods such as spray drying and supercritical fluid impregnation to optimize solubility, therefore this study will focus on overcoming the dissolution barrier offered by HME.

Also previous research has focused on spray dried multi-component solid dispersions which, due to the addition of a surfactant, affected the physical stability, amorphous stability and dissolution of selected model drugs (Baghel, Cathcart & O'Reilly, 2018). Therefore, ternary and quaternary hot-melt extruded SDs incorporating a surfactant will be investigated in this study. There are many ways in which limitations associated with HME can be overcome such as

- Lowering processing temperatures to minimize the effect of heat on the HME process and preventing degradation of the drug. This can be done by using hydrophilic polymeric carriers with low thermosensitive properties and melting points such as poloxamers with a low dose drug (Moseson & Taylor, 2018).
- Using supercritical fluids to reduce the processing temperature and torque using carbon dioxide which increases the flexibility and elasticity of the SD formulations. It also decreases operating temperatures by reducing mechanical and shear stresses (Chauvet, Sauceau & Fages, 2017).
- Reducing torque during processing.
- Reducing the residual time at high temperatures (Moseson & Taylor, 2018).
- Improving physical stability during storage.

Other ways of overcoming these limitations which will be explored in this study are as follows;

- Using semi-crystalline polymers to overcome the dissolution barriers offered by HME, it is also important to study how semi-crystalline polymers affect drug-polymer interactions within multicomponent solid dispersions and therefore will be examined also in this study.
- Using various cooling methods to enhance solubility and amorphous stability of SDs. Kawakami, (2019) reported that slow cooling of amorphous INM can increase its physical stability.

- Examining how various cooling rates/methods effect the amorphous nature and stability of APIs can have a significant effect on the solid-state, solubility and crystallization tendency of BCS class II drugs (Kawakami, 2019).

Currently semi-crystalline polymers such as Poloxamer 407 (P407) and its derivatives are being used as aqueous dissolution enhancers or surfactants and have also been used as plasticisers for hot melt extrusion. P188, a block copolymer of poly (propylene oxide) and poly(ethylene oxide) was used as a plasticiser for the poorly soluble API - amorphous polymer system, Aripiprazole – Poly (vinylpyrrolidone) K30 to allow processing by hot melt extrusion despite the relatively high T_g of Poly (vinylpyrrolidone) K30 (Fousteris *et al.*, 2013).

The same study also commented on enhancement of the initial rate of dissolution exhibited by the addition of only 5% w/w of the plasticizer. The addition of a surfactant in the solid dispersion itself could help maintain the degree of supersaturation achieved by the amorphous drug during the dissolution of the solid dispersion (Solanki, Kathawala & Serajuddin, 2019). However, the addition of a low T_g , polymeric excipient such as poloxamers to an amorphous dispersion could contribute to solid state instability of the amorphous drug either by increasing the mobility of the dispersion through lowering the glass transition of the mixture or by acting as a nucleation site.

Gumaste *et al.* (2016) studied Itraconazole-Poloxamer-Soluplus and Itraconazole-Poloxamer-HPMCAS at high drug loadings and the latter was much better at inhibiting crystallisation of both the drug and the poloxamer as shown in figure 9. The interesting thing is that the poloxamer was amorphous. However in this study the SD samples of poloxamer were always present in the semi-crystalline form (Gumaste, Gupta & Serajuddin, 2016).

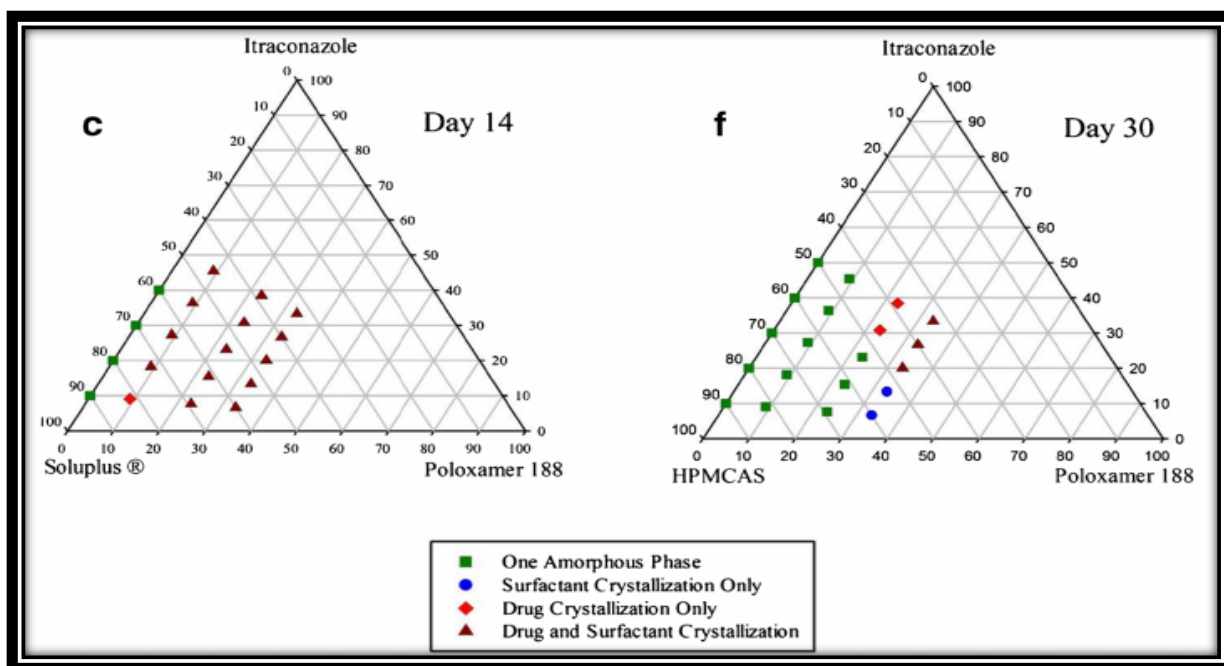


Figure 9. 'Ternary phase diagrams' (experimental not theoretical) of one amorphous polymer, one crystalline excipient and a poorly soluble drug (adopted from (Gumaste, Gupta & Serajuddin, 2016)).

Recently the mechanism of crystallisation of amorphous APIs in a number of semi-crystalline polymer matrices have been investigated and indicates a well-ordered crystallisation in accordance with the 4 lamellar structures of Poly (ethylene glycol) (PEG) (Sangroniz *et al.*, 2021). In an article by Duong *et al.* (2015) it was reported indomethacin when melt quenched with PEG, molecular weight 3350 and transformed into the amorphous form, did not recrystallise immediately and which exhibited a degree of miscibility with the amorphous portion of the semi-crystalline polymer (Duong, Van Humbeeck & Van den Mooter, 2015). Similarly, Gumaste *et al.* (2016) reported miscibility of itraconazole, poloxamer, and hydroxypropylmethylcellulose acetate succinate in the ratio 23:23:54 following exposure to 40°C/75% RH for 1 month after which time the itraconazole remained in the amorphous form (Gumaste, Gupta & Serajuddin, 2016).

Tran *et al.* (2019) reported that air cooling is ideal for the HME process as it does not require high energy removal. It is less expensive with regard to extrusion and it results in slower cooling, it is easy to maintain, has lower operating costs compared to liquid nitrogen and requires less space compared to fluid cooling. It also provides for slower changes in temperature compared to other types of cooling methods. However, it can lead to rapid recrystallization due to the slower change in temperature (Tran *et al.*, 2019).

Liquid nitrogen cools and freezes the formulation rapidly, thereby trapping the drug within its high energy amorphous form preventing nucleation and crystal growth. Very little research has been published with regard to calculating % crystallinity to assess the suitability of a BCS class II drug to form an amorphous phase and how various cooling methods can affect this parameter and aqueous solubility of the API. Therefore, the impact of cooling methods on the amorphous stability of hot-melt extruded multi-component solid dispersions will be investigated.

2.7 Materials used in this study

2.7.1 Indomethacin

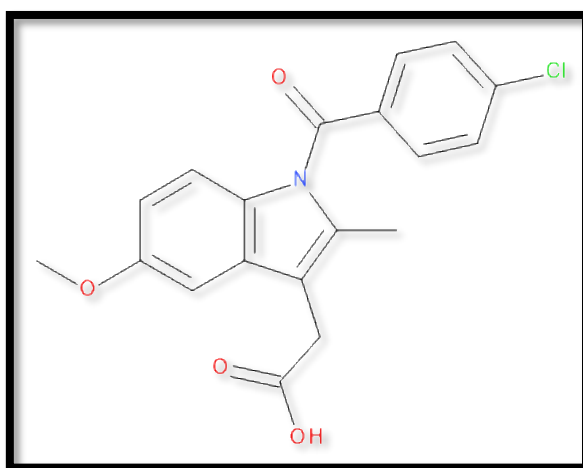


Figure 10. Chemical Structure of the BCS class II drug indomethacin (INM).

1/ Description: According to Merck & Co (2015) INM is supplied in three dosage forms. 1) Capsules for oral administration contain either 25 mg or 50 mg of INM, 2/ Suspension for oral use which contains 25 mg of INM per 5 mL, alcohol 1%, and sorbic acid 0.1% added as a preservative and 3) Suppositories for rectal use which contains 50 mg of INM. INM is a non-steroidal anti-inflammatory indole derivative designated chemically as 1-(4-chlorobenzoyl)-5-methoxy-2-methyl-1H-indole-3-acetic acid (Figure. 10). INM is practically insoluble in water and sparingly soluble in alcohol (Merck, 2005).

2/ Clinical Pharmacology: INM is a non-steroidal anti-inflammatory drug (NSAID) that exhibits antipyretic and analgesic properties. Its mode of action, like that of other anti-inflammatory drugs, is not known (Lucas, 2016). However, its therapeutic action is not due to pituitary-adrenal stimulation. INM is a potent inhibitor of prostaglandin synthesis *in vitro*.

Concentrations are reached during therapy which have been demonstrated to have an effect *in vivo* as well. Prostaglandins sensitize afferent nerves and potentiate the action of bradykinin in inducing pain in animal models. Moreover, prostaglandins are known to be among the mediators of inflammation (Jean-Luc & Marie-Paule, 2023). Since INM is an inhibitor of prostaglandin synthesis, its mode of action may be due to a decrease of prostaglandins in peripheral tissues.

INM has been shown to be an effective anti-inflammatory agent, appropriate for long-term use in rheumatoid arthritis, ankylosing spondylitis, and osteoarthritis (Merck, 2005). It can also suppress inflammation in rheumatoid arthritis as demonstrated by relief of pain, and reduction of fever, swelling and tenderness.

3/ Administration: Immediate-release capsule. INM is usually dosed 2 to 3 times per day and starts at a dose of 25 mg. However, the dose can be increased to 50mg depending on the patient.

4/ Risks/side effects: NSAIDs, including INM, can cause serious gastrointestinal (GI) adverse events including inflammation, bleeding, ulceration, and perforation of the oesophagus, stomach, small intestine, or large intestine, which can be fatal (Jean-Luc & Marie-Paule, 2023). These serious adverse events can occur at any time, with or without warning symptoms, in patients treated with NSAIDs.

INM can cause an increased risk of serious gastrointestinal adverse events including bleeding, ulceration, and perforation of the stomach or intestines, which can be fatal. Therefore, a lot of research has been carried out on the preparation of amorphous INM as a way to overcome these associated risks. The conversion of crystalline INM to its amorphous form has shown to significantly improve its aqueous solubility (Tres *et al.*, 2016). Amorphous INM has shown significantly improved dissolution properties compared to the crystalline form. As mentioned before due to its weakly acidic nature (pKa of 4.5), INM presents a pH-dependent solubility and dissolution rate. The aqueous solubility of indomethacin has been reported to increase from 1.5 µg/mL at pH 1.2 to 105.2 µg/mL at pH 7.4.

In 2022, Jennotte *et al.* (2022) prepared solid dispersions of a poorly water-soluble drug using PVP VA64 and Eudragit EPO as hydrophilic polymeric carriers using HME as a preparation method. The formation of a single-phase amorphous form was confirmed by DSC and XRPD.

The extrudates showed a higher dissolution rate compared to the pure drug. The amorphous drug in solid solutions of PVP VA64, Eudragit EPO and PVPK30 showed tendency to recrystallize, however the rate of recrystallization was dependent on the concentration and nature of the polymer (Jennotte *et al.*, 2022).

It has been shown that INM participates in hydrogen bonding due to its conversion to its amorphous form and as a result increasing aqueous solubility. Yuan *et al.* (2015) studied the type and mechanism of interaction between INM, PVP VA64 and PVP using high resolution ¹³C solid-state NMR spectroscopy and reported that a hydrogen bond was formed between free C=O of carboxylic acid and amide C=O carbonyl of PVP. This was also case for PVP VA64, however its hydrogen bond capability was weaker due to the weaker hydrogen bond potential of the vinyl acetate carbonyl (Yuan *et al.*, 2015).

Furthermore Potter *et al.* (2015) also prepared binary mixtures of INM using PVP and Soluplus as hydrophilic polymeric carriers using supercritical fluid impregnation and HME as preparation methods. The crystalline INM was successfully converted to the amorphous form after careful DSC and XRPD analysis (Potter *et al.*, 2015). Potter and co-workers carried out dissolution studies in pH 1.2 using non-sink conditions, and reported that the maximum aqueous solubility of INM achieved by both preparation methods was 8 µg/ml. pH 1.2 was used as the INM dissociates at a pH greater than 1.2, and since INM displays poor dissolution within the GI tract, a lot of research has focused on optimizing INM solubility within acidic conditions.

In general, sink conditions during the dissolution test are essential for the common dosage forms in order to simulate an *in vivo* situation, where gastrointestinal absorption continuously reduces the concentration of the drug in the fluids. However, the sink condition, obtained by a high concentration of surfactant, may not be an appropriate approach for developing a biorelevant supersaturated dissolution method such as solid dispersion (Zhang *et al.*, 2017). Nucleation and crystallization of drugs in supersaturated conditions are easily observed, and this plays a key role in determining the *in vitro* performance of SDs

In-vitro dissolution studies were performed under non-sink conditions to further increase the understanding of intermolecular interactions between INM and the excipients. Sink conditions are met when the volume of the dissolution medium is at least 3-10 times the volume of saturation (Sun & Lee, 2013).

Any volume less than that will be defined as non-sink conditions, and is normally used when the API is hindered by solubility and to discover the supersaturated drug concentration and the length of time during which it can be maintained (Sun & Lee, 2013).

Non-sink conditions are frequently used when dealing with amorphous solid dispersions using BCS class II drugs as model drugs.

2.7.2 PVP VA64/Plasdone S-630

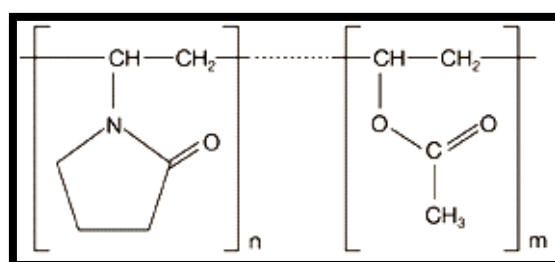


Figure 11. Chemical Structure of Poly (vinylpyrrolidone-vinyl acetate copolymer) (PVP VA64).

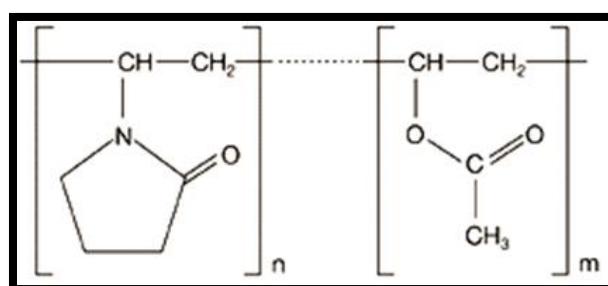


Figure 12. Chemical Structure of Plasdone S-630 (PL-S630) (Poly (vinylpyrrolidone-vinyl acetate copolymer)).

In terms of monographs, Plasdone S-630 (PL-S630) and PVP VA64 are the same product. However, these co-polymers are manufactured from two different manufacture's, and therefore have different solid-state and dissolution properties as a result of their manufacturing process. Differences in the manufacturing process from different suppliers of copovidone can influence the properties of the copovidone produced. Some of these properties may be critical material attributes for the manufacturing process or performance of a drug product.

For example, different supplier's products may have different glass transition temperatures. Therefore, this is why PL-S630 and PVP VA64 was chosen for this study, and very little has been reported in literature on the comparison of PL-S630 and PVP VA64 regarding their solid-state and dissolution properties.

PVP VA64 (molecular weight 45,000, T_g 107 °C, T_m 140 °C) and PL-S630 (molecular weight 12,000, T_g 106 °C, T_m 86.16 °C) (figures. 11 and 12) are a white or slightly yellowish, high molecular weight, amorphous water-soluble polymers that may be used to formulate various solid based dosage forms. Solanki *et al.* (2018) states that PVP VA64 is well suited to thermoplastic processing, with the processing temperature (T_p) ranging from 120 to 160 °C and a glass transition temperature (T_g) of 107°C (Solanki *et al.*, 2018), therefore this carrier is partly crystalline PVP VA64 was used in this study as a result of the above processing temperature range and many researchers have reported an increase in the solubility of INM-PVP VA64 drug-polymer mixtures using HME as a preparation method (Altamimi & Neau, 2015).

Obtained extrudates display modified drug release properties and is primarily based on the actual polymer's molecular weight. PVP VA64 has been used to prepare hot-melt extruded solid dispersion sustained release dosage forms using various BCS class II drugs such as INM (Hurley *et al.*, 2018) (Srinivasan *et al.*, 2023). Hurley *et al.* (2020) investigated the use of PL-S630 as a potential hydrophilic polymeric carrier to improve the aqueous solubility of the BCS class II drug INM using HME as a preparation method. ASD formulations showed an increase in the solubility of both model drugs with INM having an aqueous solubility significantly higher than that reported in literature. XRPD and SEM analysis confirmed INM and FMT exhibited strong plasticization effects with increasing concentrations and were found to be molecularly dispersed within the drug-polymer mixtures.

2.7.3 Poloxamer 407

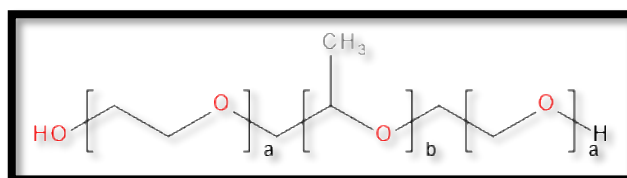


Figure 13. Chemical Structure of Poloxamer 407 (P407) (Ethylene oxide and propylene glycol copolymer) (P407).

Poloxamers are non-ionic poly (ethylene oxide) (PEO)–poly (propylene oxide) (PPO) copolymers (figure. 13). They are used in pharmaceutical formulations as surfactants, emulsifying agents, solubilizing agent, dispersing agents, and in vivo absorbance enhancers. Poloxamers are often considered as “functional excipients” because they are essential components, and play an important role in the formulation (Van der Merwe *et al.*, 2020).

All poloxamers have similar chemical structures but with different molecular weights and composition of the hydrophilic PEO block (a) and hydrophobic PPO block (b). Two of the most commonly used poloxamers are poloxamer 188 (a=80, b=27) with molecular weight ranging from 7680 to 9510 Da, and poloxamer 407 (a=101, b=56) with molecular weight ranging from 9840 to 14600 Da (Almeida *et al.*, 2017). Despite their wide range of applications, limited analytical techniques have been reported in literature for characterizing poloxamers and few are targeted to quantify poloxamer contents in formulations with desired sensitivity and accuracy. For example, the glass transition temperature of P407 has never been reported in literature. Therefore, determining the various solid-state properties especially, the T_g will be explored in this study. Poloxamer is available in different grades based on the physical parameters such as molecular weight, weight % of oxyethylene etc.

P407 was chosen for this study, as surfactants such as P407 when incorporated into amorphous SDs to form ternary and quaternary SDs may further enhance the dissolution rate and BCS class II drugs (Hurle *et al.*, 2020). Surfactants has also been used as plasticizers for polymeric carriers during HME to enhance solubility and drug-polymer miscibility (Correa-Soto *et al.*, 2022). Another reason for choosing P407 was based on the fact that polymeric carriers may dissolve the amorphous drug, leading to a more stable system without phase separation, crystallization and promote wettability increasing aqueous solubility and dissolution rates.

The common available grades are poloxamer (68, 88, 98, 108, 124, 188, 237, 338, and 407). Their surfactant property has been useful in detergency, dispersion, stabilization, foaming, and emulsification. Some of these polymers have been considered for various cardiovascular applications, as well as in sickle cell anaemia. Two polymers from this class, poloxamer 188 and poloxamer 407, show inverse thermosensitivity; therefore, they are soluble in aqueous solutions at low temperature, but will gel at higher temperature which may retard drug released if too high a poloxamer loading is used (Abdeltawab, Svirskis & Sharma, 2020).

Also as P407 is a low T_g polymer, the addition of a P407 to an amorphous dispersion can result in solid-state instability either by increasing molecular mobility or by acting as a nucleation site (Shi *et al.*, 2022). Therefore, choosing the correct loading for poloxamer is essential when formulating amorphous SDs. Currently there is very little literature on how P407 when incorporating within ternary and quaternary hot-melt extruded solid dispersions affects solid-state, intermolecular interactions and dissolution rates of INM and therefore will be investigated in this study.

2.8 Aim and objectives of this study

The aim of this study is:

To determine the effect of P407 and cooling on the solid-state properties, intermolecular interactions, dissolution properties and amorphous stability of various hot-melt extruded multi-component solid dispersions using INM as a model drug.

The objectives of this study are as follows:

- Investigate the effect of P407 on the dissolution properties and amorphous stability of hot-melt extruded multi-component solid dispersions using the BCS class II drug INM, as it was reported in literature that hot melt extrusion resulted in slower dissolution rates compared to alternative methods such as spray drying and supercritical fluid impregnation. Also, previous research has focused on spray dried quaternary mixtures which due to the addition of a surfactant affected the physical stability and amorphous stability of selected model drugs.
- To investigate the role of inter-molecular interactions and the effect of mixed copovidone multi-component hot-melt extruded solid dispersions using PVP VA64 and PL-S630 on the solid-state and dissolution properties of INM, as very little literature has been published in literature on the comparison of PL-S630 and PVP VA64 regarding their solid-state and dissolution properties.
- To examine how cooling methods, affect the crystallization tendency and solubility of the API. As mentioned before very little research has been published with regard to calculating % crystallinity to assess the suitability of a BCS class II drug to form an amorphous phase and how various cooling methods can affect this parameter and crystallization tendency of the API.

- Finally, to significantly improve the aqueous solubility of INM via non-sink conditions, as the maximum kinetic solubility reported in literature is 10 µg/ml after 12 hours. The impact of drug loading will also be investigated.

Chapter Three

Experimental

Details

3.0 Materials & Methods

The aim of chapter 3 of this study is to explain the various methods and materials that were used to prepare and examine how drug-polymer miscibility, system thermodynamics, drug-polymer intermolecular interactions and cooling methods affect kinetic solubility and amorphous stability of SDs overtime using the following methods:

- Twin-screw hot melt extrusion.
- Solubility parameters using the combined group contribution methods of Van Krevelen-Hoftyzer and Fedors (pre-formulation studies).
- Hildebrand and Scott drug-polymer interaction factor (χ) to examine drug-polymer miscibility.
- Attenuated total reflectance-fourier transform infrared (ATR-FTIR) and Raman Spectroscopy to examine drug-polymer intermolecular interactions and molecular mobility.
- Phase solubility studies to determine the apparent 1:1 stability constant K_a of INM within PVP VA64.
- Dissolution USP apparatus type 1 (basket method) (Distek 50947, USA) coupled with UV spectroscopy to examine the nature of drug release and the kinetic solubility of INM within aqueous media.

3.1 Materials

Crystalline γ -INM (1-(4-Chlorobenzoyl)-5-methoxy-2-methyl-3-indoleacetic acid) (INM), purchased from Tokyo Chemical Industry (TCI) (Oxford Science Park, UK), (M_w 357.79 g/mol⁻¹, T_m 160.0 °C T_g 42 °C) was used as a model drug. INM has an aqueous solubility of 1.5 μ g/ml at pH 1.2 (Sun & Lee, 2015).

P407, a hydrophilic non-ionic surfactant, (Ethylene oxide and propylene glycol copolymer), (M_w 12,000, T_m 55 °C, T_g -67 °C) was purchased from BASF Europe GmbH (Burgbernheim, Germany). PVP VA64 (M_w 45,000, T_g 107 °C, T_m 140°C) was received as requested samples from JRS Pharma (Surrey, UK). PL-S630 (T_m 140 °C, T_g 106 °C), was received as a gift from Ashland Specialties Ltd, (UK). See table 3 for more details. All other reagents and chemicals were purchased from Sigma Aldrich (Wicklow, Ireland) and were of analytical reagent grade.

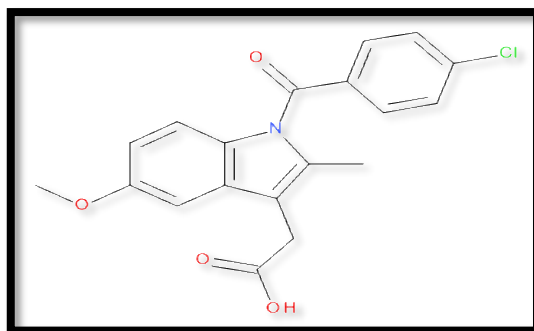


Figure 14. Chemical Structure of the BCS class II drug INM.

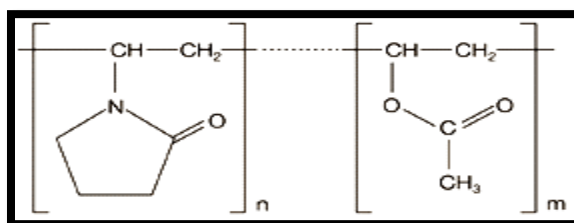


Figure 15. Chemical Structure of PVP VA64/PL-S630.

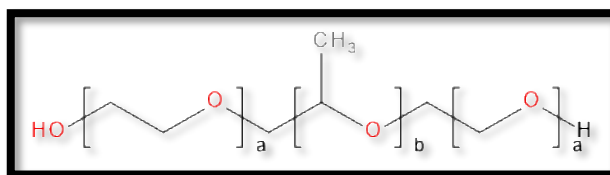


Figure 16. Chemical Structure of P407.

Table 3. Physicochemical properties of model drug and polymers.

	Molecular weight (g/mol)	ΔH_f (KJ/mol)	Tm (°C)	Tg (°C)	pKa	Log p ^b
INM	357.79	37.9	160	42	4.5	3.93
PVP VA64	45,000	-	140.0	107	-	-
PL-S630	47,000	-	86.60	106	-	-
P407	12,000	-	55	-67	-	-

3.2 Preparation of physical mixtures

Prior to HME, physical mixtures of each of the components containing the API INM were weighed and mixed thoroughly in a mortar and pestle for five minutes according to the compositions detailed in tables 4-7. Also, binary drug-polymer mixtures of INM and P407 were also prepared as a control. The % drug-polymer composition used for INM-P407 drug-polymer mixtures were as follows 10/90, 30/70, 50/50 and 70/30%. Amorphous INM (aINM) was prepared by heating to 160 °C in a stainless-steel beaker using a hotplate and quench cooling using liquid nitrogen.

3.3 Hot-melt extrusion conditions

Unless stated otherwise, all the melt compounding detailed in this report was carried out using two bench-top Prism™ twin screw extruder (figures 17 and 19) with 16 mm diameter screws 2 mm diameter die and a length to diameter (L/D) ratio of 25:1 and 15:1 respectively. Prism™ co-rotating screws used for extrusion are manufactured with a certain multi-purpose modular design (Lyons, Higginbotham & Blackie, 2007). The positions of the heating zones and mixing section can be seen on the schematic diagram of the barrel of the Prism™ twin screw extruder with an L/D ratio of 25:1 is shown in figure. 18. The 15:1 L/D ratio twin screw extruder is similar to barrel design to 25:1 L/D ratio extruder except it has 2 heated zones instead of 4. The screws contained various sections that slide into a splined shaft. Therefore, various screw designs that use narrow disk bi-lobal mixing elements can be arranged at a specific location along the shaft to enable mixing effects or shear control (Lyons, Higginbotham & Blackie, 2007).

The screw configuration can have a vital effect on the uniformity and properties of many drugs and excipients as it can degrade APIs and polymeric materials due to its high processing temperatures. In this study the screws are arranged in a co-rotating intermeshing mode (Lyons, Higginbotham & Blackie, 2007).



Figure 17. *The PrismTM twin screw 25:1 length to diameter (L/D) ratio extruder used in this study.*

The screw configurations were assembled via the following sections:

- feed screw sections
- extrusion screw sections
- half feed screw sections
- half reverse feed screw sections
- mixing elements (paddles) 30° offset
- mixing elements (paddles) 60° offset
- mixing elements (paddles) 90° offset

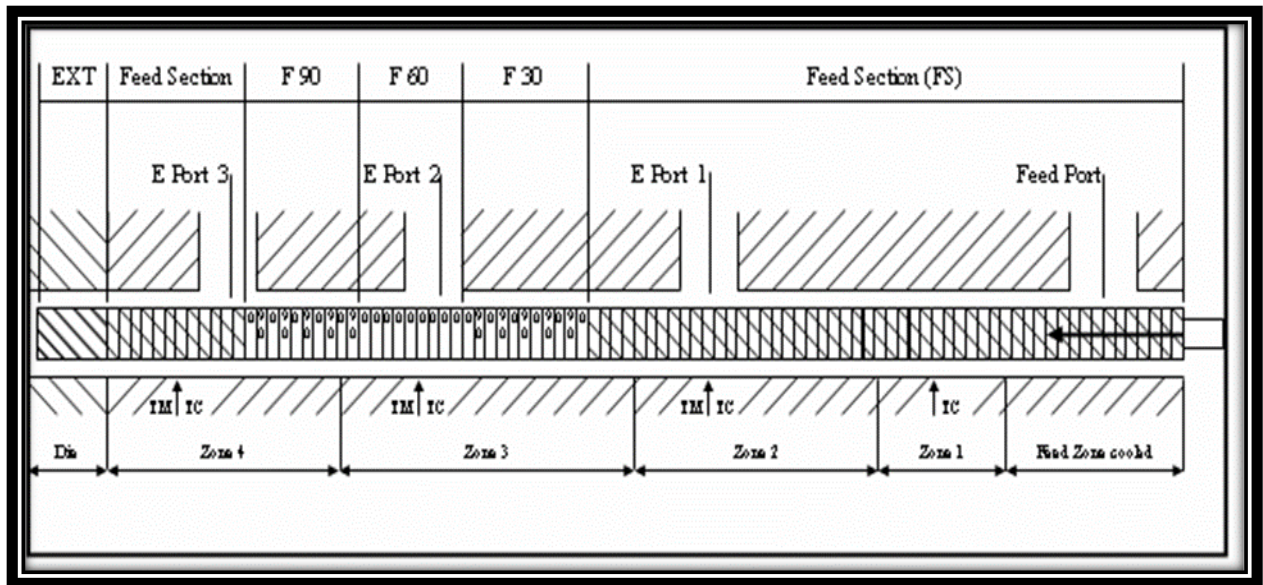


Figure 18. Schematic representation of Prism™ twin screw 25:1 L/D extruder barrel and screw configuration used to compound materials for trials to investigate the drug-polymer miscibility and drug-polymer intermolecular interactions using PVP VA64 as the matrix forming material (adapted from (Lyons, Higginbotham & Blackie, 2007)).



Figure 19. The Prism™ twin screw 15:1 L/D ratio extruder used in this study.

3.3.1 Compounding of materials

The screws assembled contained all-conveying elements that ensured that the transition from conveying to high shear mixing was very gradual to ensure uniformity. The mixing section was positioned towards the die end of the extruder (Lyons, Higginbotham & Blackie, 2007). The batches of drug-polymer matrices described in tables 4-7 were compounded using the extrusion profile outlined in tables 8 and 9 using the Prism twin screw extruders in figure 17 and 18.

To investigate the effect of extrusion parameters and cooling rate on the solid-state and dissolution properties of hot-melt extruded solid dispersions, selected drug-polymer mixtures (table 8) were compounded using the Prism 16mm twin-screw extruders with a 2mm diameter die and L/D ratios of 25:1 (figure 17) and 15:1 (figure 19) 16 mm twin-screw extruders as previously described, using the extrusion profiles outlined in tables 8 and 9, using an automatic feeder at a rate of 13 ± 1 g/min. The diameter of each of the extrudates was 2mm. To investigate the effect of cooling, a selected batch was air cooled, cooled to ambient temperature (25 °C) and quench cooled using liquid nitrogen to investigate the crystallization tendency of the amorphous API.

Table 4. *Batch composition used to investigate the effect of Poloxamer 407 (P407) on the dissolution enhancement of hot-melt extruded SDs compounded using 25:1 L/D ratio extruder (100 grams batch size);*

Identifier	INM [wt%]	P405 [wt%]
SD1	5	0
SD2	5	5
SD3	5	10
SD4	5	15
SD5	5	20
SD6	10	0
SD7	10	5
SD8	10	10
SD9	10	15
SD10	10	20
SD11	15	0
SD12	15	5
SD13	15	10
SD14	15	15
SD15	15	20
SD16	20	0
SD17	20	5
SD18	20	10
SD19	20	15
SD20	20	20
SD21	25	0
SD22	25	5
SD23	25	10
SD24	25	15
SD25	25	20

Table 5. Batch composition used to investigate the role of intermolecular interactions, solid-state and dissolution properties of mixed co-povidone (quaternary) hot-melt extruded SDs compounded using the 15: 1 L/D ratio extruder (50 grams batch size).

Batch No	Composition (% w/w)			
	PL-S630 [wt%]	PVP VA64 [wt%]	P407 [wt%]	INM [wt%]
Quart SD1	42.5	42.5	5	10
Quart SD2	37.5	37.5	15	10
Quart SD3	32.5	32.5	5	30
Quart SD4	27.5	27.5	15	30
Quart SD5	22.5	22.5	5	50
Quart SD6	17.5	17.5	15	50
Quart SD7	12.5	12.5	5	70
Quart SD8	7.5	7.5	15	70

Table 6. Batch composition used to investigate the role of intermolecular interactions, solid-state and dissolution properties of mixed co-povidone (ternary) hot-melt extruded SDs compounded using the 15: 1 L/D ratio extruder (50 grams batch size).

Identifier	Composition (% w/w)		
	PL-S630/PVP VA64 [wt%]	P407 [wt%]	INM [wt%]
PL-S630/PVP VA64 SD1	85	5	10
PL-S630/PVP VA64 SD2	75	15	10
PL-S630/PVP VA64 SD3	65	5	30
PL-S630/PVP VA64 SD4	55	15	30
PL-S630/PVP VA64 SD5	45	5	50
PL-S630/PVP VA64 SD6	35	15	50
PL-S630/PVP VA64 SD7	25	5	70
PL-S630/PVP VA64 SD8	15	15	70

Table 7. Batch composition used to investigate the effect of cooling rate on the solid-state and dissolution properties of hot-melt extruded SDs compounded using the 15: 1 and 25:1 L/D ratio extruders (50 grams batch size).

Identifier	Composition (% w/w)			
	PL-S630 [wt%]	PVP VA64 [wt%]	P407 [wt%]	INM [wt%]
ASD1	32.5	32.5	5	30
ASD2	27.5	27.5	15	30
ASD3	-	65	5	30
ASD4	-	55	15	30
ASD5	65	-	5	30
ASD6	55	-	15	30

Table 8. *Temperature zones of 25:1 L/D ratio extruder used in the hot melt extrusion process.*

Screw speed (RPM)	Temperature (°C)				
	Die	Zone 4	Zone 3	Zone 2	Zone 1
60	160	160	140	120	100

Table 9. *Temperature zones of 15:1 L/D ratio extruder used in the hot melt extrusion process.*

Screw speed (RPM)	Temperature (°C)		
	Die	Zone 2	Zone 1
100	160	160	140

The screw configuration was not varied, however to optimise the processing of the matrix for each individual section the screw speed and temperature profile were varied depending on the processing temperatures of the individual polymeric materials and API (Lyons, Higginbotham & Blackie, 2007). The specific temperature profile required for compounding was determined using the PrismTM extruder via the temperature controllers arranged along the length of the heated barrels. Also to control the temperature of the die another temperature controller was used (Lyons, Higginbotham & Blackie, 2007).

During the hot-melt extrusion process, API's, plasticizers and other excipients are starve fed into a heated barrel, which are then mixed by the rotating screw element and then the homogenous melt is extruded through a cylindrical shaped heated die to form a solid dispersion or strand (Lyons, Higginbotham & Blackie, 2007). The materials inside the barrel are heated via the heat generated by the shearing effect of the rotating screw and the heat conducted from within the heated barrel. The temperatures for processing were chosen based on the glass transition temperature of the polymeric materials and melting point of the drug in this case INM was used (Tian *et al.*, 2020). As a general rule, the extrusion process was conducted at temperatures 20 to 40 °C above the T_g of the polymer and at a temperature close to the melting point of the drug (Hurley *et al.*, 2018). On exiting the die the extrudate was allowed to cool to room temperature, extrudates were next ground under liquid in a mortar and pestle, and passed through a 200 µm sieve to obtain appropriately sized fractions for further studies.

It must be noted that the 15:1 L/D ratio extruder was used to investigate the role of intermolecular interactions and the effect of cooling on the kinetic solubility and amorphous stability of INM due to the reduced batch size.

3.4 Cooling Process

To investigate the crystallization tendency of the API, a selected SD formulation was air cooled (AC) to 25°C by an air pipe connector attached to the 2 mm die of the extruder, cooled to normal room temperature (25°C) (NT), the same as air cooling except with no air pipe connector and quench cooled using liquid nitrogen, (Liq N₂), to examine the effect of slow and rapid cooling processes on the amorphous stability and solubility of INM. For the purpose of this study, only one SD formulation was investigated.

3.5 Pre-Formulation; calculation of solubility parameters (δ), glass transition temperature (T_g) and drug-polymer interaction factor (χ).

Preformation of drug and polymers was conducted using the HSPs which can be calculated using the combined group contribution methods proposed by Van Krevelen-Hoftyzer (Choudhury, Murty & Banerjee, 2023), by considering their chemical structural orientations and the molecular weights of each of the components. These are expressed by the following equations (Eq) 1:

$$\delta^2 = \delta_d^2 + \delta_p^2 + \delta_h^2 \quad \text{Eq. (1).}$$

Where,

$$\delta_d = \frac{\sum F_{di}}{V}, \delta_p = \frac{(\sum F_{pi}^2)^{1/2}}{V}, \delta_h = \left(\frac{\sum F_{hi}}{V}\right)^{1/2}$$

where i is the functional group within the molecule, δ is the total solubility parameter, δ_d is the contribution from dispersion forces, δ_p is the contribution from polar interactions, δ_h is the contribution of hydrogen bonding, F_{di} is the molar attraction constant due to molar dispersion forces, F_{pi} is the molar attraction constant due to molar polarization forces, E_{hi} is the hydrogen bonding energy and V is the molar volume (Hurley *et al.*, 2018).

The drug-polymer interaction parameter, χ , using the solubility parameters difference between the drug and polymer, can be estimated by a method developed by Hildebrand and Scott (Jha, Shah & Amin, 2021).

This is expressed as follows;

$$\chi = \frac{V_0}{RT} (\delta_{\text{drug}} - \delta_{\text{polymer}})^2 \quad \text{Eq. (2).}$$

where V_0 is the volume of the lattice site, R is the gas constant and T is the absolute temperature.

3.6 ATR-FTIR spectroscopy

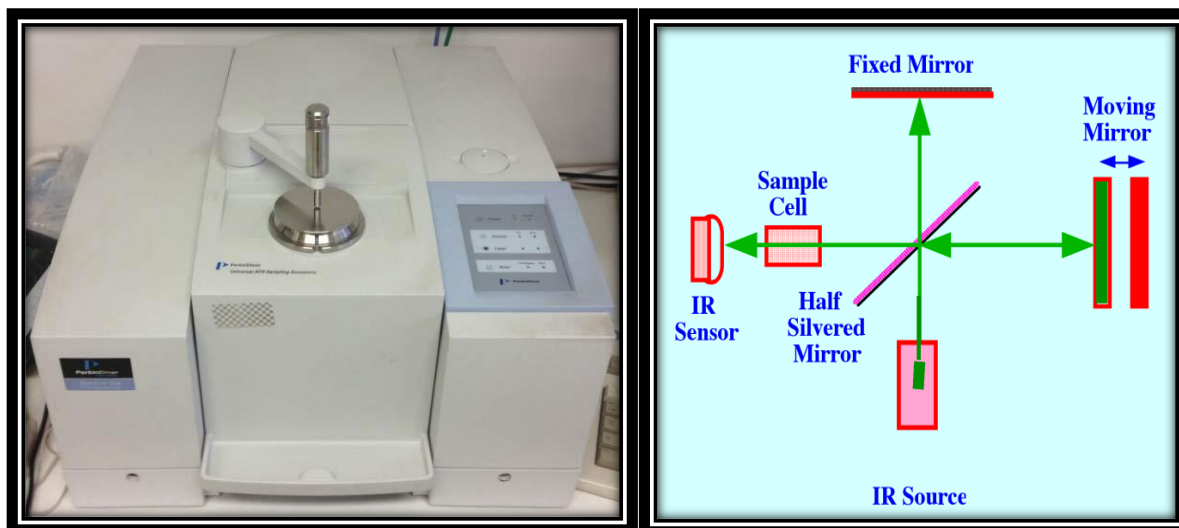


Figure 20. Perkin Elmer Spectrum One attenuated total reflectance-fourier transform infrared spectrometer (ATR-FTIR) (left hand side) and schematic diagram of fourier-transform -infrared spectrometer (FTIR) (right hand side).

ATR-FTIR spectra were collected using a Perkin Elmer spectrum one apparatus fitted with a universal ATR sampling accessory. Data was collected in the spectral range of 4000-420 cm^{-1} , utilising a 16 scan per sample cycle and a fixed universal compression force of 80N. Subsequent analysis was carried out using spectrum software (Hurley *et al.*, 2019).

3.7 Raman Spectroscopy



Figure 21. *Renishaw inVia Raman confocal microscope attached to a motorized stage.*

Raman spectra of selected SD formulations were attained using a Renishaw inVia Raman confocal microscope (Renishaw Instruments, Gloucestershire, UK) which was attached to a motorized stage. A 785 nm laser was used to provide Raman scattered light, the laser operated at 300 mW with a laser power of 100%. The Raman Spectra of each formulation were within the range of 100 and 3200 cm^{-1} , and with an acquisition time of 10s. A $\times 20$ lens was used and had a spot size of 50 μm . A 1200 l/mm (633/780) beam path grating was used.

3.8 X-ray powder diffraction (XRPD)



Figure 22. *Philips PANalytical X'Pert MPD Pro X-ray powder diffractometer (XRPD) with PW3064 sample spinner used in this work.*

XRPD spectra were collected using a Philips PANalytical X'Pert MPD Pro with PW3064 sample spinner. The dried granules of drug-polymer mixtures were gently ground using a pestle and mortar and placed on zero-background silica disks to insure a non-destructive analytical method. The zero background holders are made of 9N semiconductor grade silicon. The XRD pattern obtained, by using the crystals as background plate, was very “clean” (no diffraction on X-rays), so that even at very low-intensity, Bragg reflections of the SD samples were easily detected. The diffraction pattern was collected between 5 and 40° (2θ) with a step size of 0.0167°, a counting time of 29.845s, and a sample rotation of 15 rpm using PANalytical Data Collector, version 2.0. The source was Cu $K\alpha$ ($\lambda = 1.5418 \text{ \AA}$), the accelerating voltage was 40 kV, and the anode current was 35 mA. A fixed divergence slit of 1/4” and a 0.020 mm nickel filter were used (Hurley *et al.*, 2020).

3.9 Scanning electron microscopy (SEM)



Figure 23. *Mira scanning electron microscope (SEM) (left hand side) and Bal-Tec SCD005 sputter coater (right hand side).*

Scanning electron microscopy (SEM) was performed on selected formulations using a Mira SEM (Rescan, Czech Republic) with a magnification of 100kx. Sample preparation involved placing samples on the sticky surface of aluminium stub using double sided sticky tape to increase the electrical conductivity of the sample. After sufficient time (10mins), the samples were coated with a thin layer of gold by placing the samples within a sputter coater (BAL-TEC SCD, sputter, USA) for 110sec at 0.1mBar vacuum. The SEM images were obtained using an acceleration voltage of 15 KV.

3.10 Phase solubility studies

Solubility studies were performed in triplicate using the method reported by Higuchi and Connors (Higuchi *et al.* 1965) in pH buffer 1.2. An excess amount of INM (50-100mg) was added to aqueous solutions of each carrier to increasing concentrations of both polymeric carriers in 10 ml volumetric flasks. The suspensions were maintained at 37 °C for 24 hours. This duration was previously tested to be sufficient to reach equilibrium. 2ml aliquots were withdrawn and were filtered through 25mm Millex - LCR PTFE hydrophilic syringe filters (0.45 µm, Merck Millipore LTD, Ireland). The filtrates were suitably diluted if required and analysed, spectrophotometrically for the dissolved drug at 320 nm.

Shaking was continued until three consecutive readings were performed. The apparent 1:1 stability constant K_a was calculated from the phase solubility graph using the following equation:

$$K_a = \frac{\text{Slope}}{S_0(1-\text{slope})} \quad \text{Eq. (4).}$$

Where S_0 is the intrinsic aqueous solubility of INM.

The Gibbs free energy of transfer (ΔG_{tr}^0) of INM from pure water to the aqueous solution of carrier was calculated by the equation below (Eedara *et al.*, 2021),

$$\Delta G_{tr}^0 = -2.303 RT \log S_0/S_s \quad \text{Eq. (5).}$$

where S_0/S_s is the ratio of molar solubility of INM in aqueous solutions of carrier to that of the same medium without carrier (Hurley *et al.*, 2018).

3.11 *In-Vitro* dissolution studies



Figure 24. *Distek 50947 dissolution apparatus (left hand side) and UV-1280 ultraviolet (UV)-Vis (UV) Spectrophotometer (Right hand side).*

The release rate of INM from SDs and physical mixtures was determined under non-sink conditions using United States Pharmacopeia (USP) dissolution testing apparatus 1 (basket method) (Distek 50947, USA) with a paddle speed of 50 rpm. The dissolution test was performed using 900 ml of pH buffer 1.2 at a temperature of 37 ± 0.5 °C.

A formulation equivalent to 100 mg of INM in SDs and physical mixtures were placed in dissolution medium, with 5 ml aliquots withdrawn at predetermined time intervals (0, 10, 17, 24,45 minutes and 1, 2 and 3 hours), and filtered through a 25mm Millex - LCR PTFE hydrophilic syringe filter (0.45 μ m, Merck Millipore LTD, Ireland).

At each time point, the same volume of fresh medium was replaced as withdrawn. The concentration of INM in each sample was determined using a UV-1280 Ultraviolet (UV)-Vis spectrophotometer (Shimadzu, Japan) and a standard calibration curve. Fresh dissolution medium was used as a blank. Pure INM was used as a control. The concentration of INM dissolved for each formulation (n =3) was plotted as a function of dissolution time with data being expressed as the average \pm standard deviation of replicate absorbance measurements. The ability of the polymeric carriers to prolong and maintain INM supersaturation (SP) in pH buffer 1.2 in selected formulations was qualified by using the SP as reported by Chen *et al.* (2015) (Chan *et al.*, 2015).

3.12 Statistical analysis

The drug dissolution profiles of all SD formulations were compared using an analysis of variance (ANOVA) statistical test. The impact of the amorphous form on the area under the curve (AUC) was statistically examined using (ANOVA) (GraphPad Prism version 5.03 for Windows, GraphPad Software, San Diego, CA). Post-hoc comparisons of the means were performed using Tukey's Multiple Comparison test. A significance level of * $p < 0.05$ was accepted to denote significance in all cases (Hurley *et al.*, 2018) and (Hurley *et al.*, 2020).

3.13 Accelerated amorphous stability studies

Stability studies were conducted under accelerated conditions (40°C, 75% relative humidity) for 5 months by placing SDs in open class vials which were stored in a desiccator which contained a saturated solution of sodium chloride to generate a relative humidity of 75% relative humidity. The relative humidity inside the desiccator was checked regularly using a thermohygrometer. The stored SDs were tested using XRPD (for selected formulations) as previously described (Hurley *et al.*, 2018).

Chapter Four

Results &

Discussion

4.0 Results and Discussion

4.1 Introduction

The optimal design of amorphous SD formulations requires the use of excipients to maintain supersaturation and improve physical stability in order to ensure shelf-life stability and better absorption during intestinal transit, respectively. Previous research has focused on spray dried and supercritical fluid quaternary mixtures which due to the addition of a surfactant affected the physical stability and amorphous stability of selected model drugs.

Very little research has focused on how inter-molecular interactions play a role in the successful formulation of hot-melt extruded quaternary amorphous blends and how they affect physical stability and solubility of amorphous SDs. Also, the effect of cooling on the degree of crystallinity, solid-state and dissolution properties of multi-component hot-melt extruded SDs is of great interest for the successful formulation of amorphous SDs and is an area that is unreported, especially in the context of improving the stability of these specific systems.

Therefore, the main objectives of this study was to prepare SDs via HME using a semi-crystalline polymer to overcome the dissolution and physical stability barriers compared to previous methods and finally investigate the role of inter-molecular interactions and cooling and their effect on the solid-state and dissolution properties of mixed copovidone amorphous solid dispersions. The thermal solid-state properties, degree of crystallinity, drug-polymer interactions, solubility and amorphous stability over time were investigated. X-ray powder diffraction (XRPD) confirmed that INM was converted to the amorphous state, however the addition of P407 had a significant effect on the degree of crystallinity and solubility of the SD formulations.

Spectroscopy studies using infrared and Raman spectroscopy identified the mechanism of interaction and solubility studies showing a higher dissolution rate compared to amorphous and pure INM in pH 1.2 with a kinetic solubility of 20.63 $\mu\text{g/ml}$ and 34.7 $\mu\text{g/ml}$ after 3 and 24 hours. XRPD confirmed that INM remained amorphous after 5 months stability testing in solid solutions with PVP VA64 and PL-S630.

Although cooling had a significant effect on the P407 crystallinity/loading and on solubility of INM, the cooling method used did not have any significant effect on the amorphous stability of INM over time.

4.1.1 Drug-polymer miscibility Studies

Gaikwad *et al.* (2017) reported that within the pharmaceutical industry, HSPs are commonly used to determine the miscibility of an API with pharmaceutical excipients/carriers in SDs. It also has been reported that HSPs have been used within the pharmaceutical industry to determine compatibility of pharmaceutical materials, and are therefore recommended in pre-formulation and in the development of SDs and tablets (Gaikwad *et al.*, 2017).

Maniruzzaman *et al.* (2015) stated that the Flory-Huggins (F-H) lattice-based theory to explain intermolecular interactions between polymer and API is limited as it does not take into consideration the various multiple interactions in drug-polymer systems (Maniruzzaman *et al.*, 2015). Therefore, the HSPs developed by Van Krevelen and Hoftyzer group were used as a substitute for the Flory-Huggins theory to explore the nature of interactions that occur within drug-polymer systems and is mainly based upon the chemical structures of each of the pure components.

For an intermolecular interaction to occur between an API and polymer, the change in the free energy of mixing must be negative according to the laws of thermodynamics of mixing. This specific change in the free energy of mixing is related to enthalpy and entropy contributions according to the following equation (Eq. 4).

$$\Delta G_{\text{mix}} = \Delta H_{\text{mix}} - T \times \Delta S_{\text{mix}} \quad (\text{Eq. 4})$$

Where, ΔG_{mix} , ΔH_{mix} , ΔS_{mix} and T are the Gibbs free energy, enthalpy of mixing, entropy of mixing and absolute temperature respectively. The free energy change is spontaneous as a result of the increase in entropy of mixing and is therefore negative (Maniruzzaman *et al.*, 2015). However, the presence of repulsive and cohesive intermolecular and intramolecular forces (e.g. dispersion force, hydrogen bonding and dipole-dipole interaction) which are present within the amorphous SD making the intermolecular interaction between drug and polymer more complex.

The drug-polymer interaction factor was calculated via the Hildebrand-Scott method which is a hypothetical method used to calculate F-H interaction parameters (Han *et al.*, 2019). It is well reported in literature that unfavourable intermolecular interactions will result in phase separation and recrystallization if $\Delta\delta > 7 \text{ MPa}^{1/2}$, whilst favourable intermolecular interactions and a uniform phase will occur if $\Delta\delta < 7 \text{ MPa}^{1/2}$ (Choudhury *et al.*, 2023).

This is also the case for drug-polymer interactions if the value for χ is close to zero, as shown in table 10. $\Delta\delta$ and χ between INM and the polymers was less than $7 \text{ MPa}^{1/2}$ and close to zero respectively, therefore they are likely to be miscible (Choudhury *et al.*, 2023).

Table 10. Calculated solubility parameters using Hansen solubility parameters (HSPs) (δ) and drug-polymer interaction factor (χ).

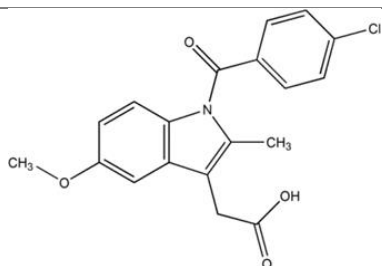
Compound	δ_t (MPa ^{1/2})	$\Delta\delta$ (MPa ^{1/2})	χ
INM	23.00	-	-
PVP VA64	26.40 ^a	3.40 ^a	0.46
PL-S630	26.40	3.40	0.46
P407	25.50 ^b	2.50 ^b	0.36

^a and ^b are values obtained from a previously published report (Hurley *et al.*, 2018).

The molar attraction constant for INM was high (10.37 MPa^{1/2}) and was similar to the values calculated for the polymers (PVP VA64: 11.86 MPa^{1/2} and PL-S630: 11.86 MPa^{1/2}) due to the interaction via hydrogen bonding. The molar attraction constant values are vital for intermolecular interactions between drug and polymer to occur during the transformation to the amorphous state. See tables. 11 to 14 for HSPs calculations used to predict drug-polymer miscibility and drug-polymer interaction factor (χ).

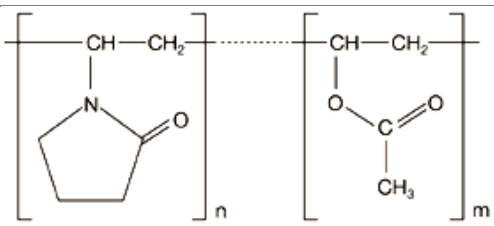
Maniruzzaman *et al.* (2015) prepared amorphous solid dispersions using hot-melt extrusion using the BCS class II drug Verapamil HCL, which had a molar attraction constant of 6.95 MPa^{1/2} and reported that due to the high molar attraction constants of the APIs and polymeric carriers they were able to contribute to hydrogen bonding (Maniruzzaman *et al.*, 2015). As the HSPs are only theoretical, drug-polymer miscibility was further examined using various characterization, thermal analysis and solubility techniques to determine if the drug-polymer mixtures were miscible. In order for a drug and polymer to be miscible it requires the drug to be successfully converted to the amorphous form and to interact with the polymeric carrier. Conversion to the amorphous state will be determined using XRPD to determine if the drug is amorphous. Interaction between drug and polymer will be examined using ATR-FTIR and Raman spectroscopy.

Table 11. Calculation of HSPs and molar volume for INM according to the Hoftyzer-Van Krevelen method.



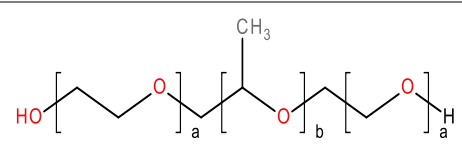
Group	Frequency	$F_{di} (J^{1/2} cm^{3/2} mol^{-1})$	$F_{Pi}^2 (J^{1/2} cm^{3/2} mol^{-1})$	$F_{hi} (J/mol)$	$V_m^a (cm^3/mol)$ (V_o)
-CH ₃	2	840	0	0	67
-CH ₂ -	1	270	0	0	32.2
=CH-	3	600	0	0	40.5
>C=	5	350	0	0	-27.5
Phenylene (o,m,p)	1	1270	12100	0	52.4
-Cl	1	450	302500	400	24
-O-	1	100	160000	3000	3.8
-CO-	1	290	770	2000	10.8
-COOH	1	530	176400	10,000	28.5
-N<	1	20	640000	5000	-9
Ring closure 5 or more atoms	2	380	0	0	32
Conjugation in ring for each double bond	4	0	0	0	-8.8
Σ		5100	1291770	27400	254.7

Table 12. Calculation of HSPs and molar volume for PVP VA64/PL-S630 according to the Hoftyzer-Van Krevelen method.



Group	Frequency	F_{di} ($J^{1/2} \text{ cm}^{3/2} \text{ mol}^{-1}$)	F_{Pi}^2 ($J^{1/2} \text{ cm}^{3/2} \text{ mol}^{-1}$)	F_{hi} (J/mol)	V_m^a (cm^3/mol) (Vo)
-CH ₃	1	420	0	0	33.5
-CH ₂ -	2	540	0	0	32.2
-CH-	2	160	0	0	-2.00
-CO-	1	290	770	2000	10.8
-N<	1	20.0	800	5000	-9.00
-COO-	1	390	490	7000	18.0
Ring 5 or more	1	190	0	0	16.0
Σ		2010.0	1473000	14,000	99.50

Table 13. Calculation of HSPs and molar volume for P407 according to the Hoftyzer-Van Krevelen method.



Group	Frequency	F_{di} ($J^{1/2} \text{ cm}^{3/2} \text{ mol}^{-1}$)	F_{Pi}^2 ($J^{1/2} \text{ cm}^{3/2} \text{ mol}^{-1}$)	F_{hi} (J/mol)	V_m^a (cm^3/mol) (Vo)
-CH ₃	1	420	0	0	33.5
-CH ₂ -	5	2100	0	0	80.5
-OH	2	420	500000	20000	20
-O-	2	200	320000	3000	7.6
Σ		2390	820000	46000	141.6

Table 14. Calculated HSPs of and drug-polymer interaction factor for drug and polymers.

Identifier	Solubility Parameters						χ
	δ_d (MPa ^{1/2})	δ_p (MPa ^{1/2})	δ_h (MPa ^{1/2})	δ_v (MPa ^{1/2})	δ_{total} (MPa ^{1/2})	$\Delta\delta_t$ (MPa ^{1/2})	
INM	20.02	4.46	10.37	20.51	23.00	-	-
PVP VA64	20.20	12.20	11.86	23.59	26.40	3.40	0.46
PL-S630	20.20	12.20	11.86	23.59	26.40	3.40	0.46
P407	16.88	6.40	18.02	18.05	25.50	2.50	0.36

4.1.2 XRPD studies of extruded solid dispersions

The XRPD pattern of PVP VA64 and PL-S630 were amorphous in nature. This can be seen by a slight amorphous halo raised above the baseline. P407 which is semi-crystalline in nature contained two strong principal diffraction peaks at 19.26 and 23.51 respectively due to its semi-crystalline structure. XRPD analysis (Fig. 25) of the SD formulations confirmed the amorphous nature of INM within all SD formulations due to the slight halo raised above the baseline, due to the lack of any sharp, well-defined peaks in the diffractogram. P407 retained its semi-crystalline state in all SD formulations compared to the SD formulations prepared by Gumaste, Gupta and Serajuddin, (2016) who reported that poloxamer was amorphous (Gumaste, Gupta & Serajuddin, 2016).

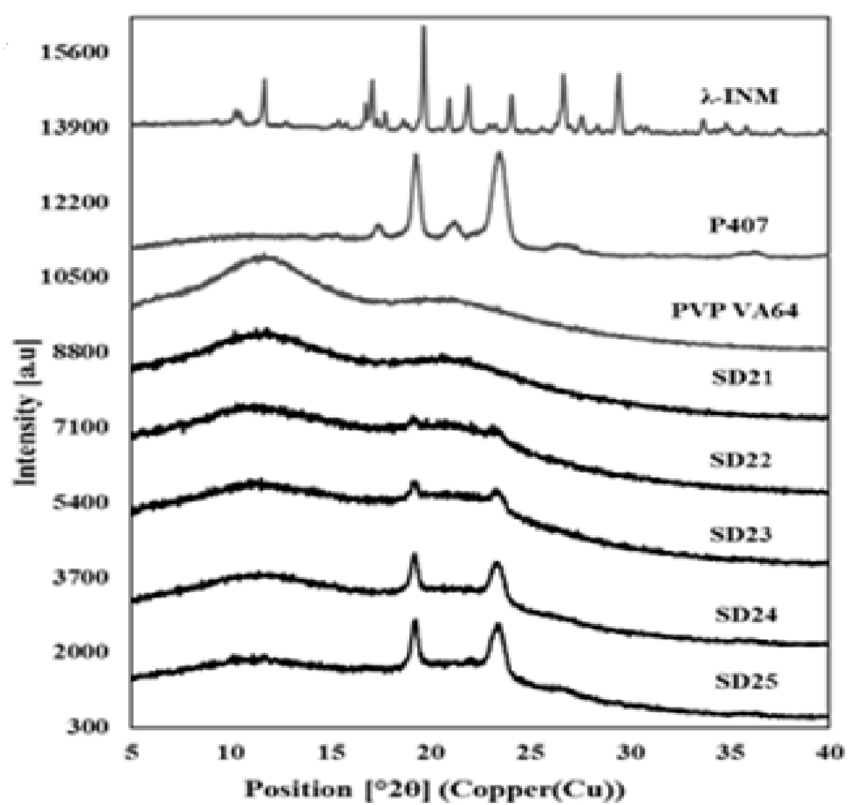


Figure 25: XRPD diffractograms indicating that the INM is present in the amorphous form but the P407 is not solubilised and exists in its crystalline form.

4.1.2.1 An investigation of the inter-molecular interaction, solid-state properties and dissolution properties of mixed copovidone hot-melt Q4 extruded solid dispersions.

The XRPD patterns of the SD formulations are shown in figures. 26 (a) and (b). XRPD pattern for pure INM had several diffraction peaks due to the crystalline nature of the drug. XRPD analysis of the SD formulations confirmed the amorphous nature of INM within all ASD formulations due to the slight halo raised above the baseline, due to the lack of any sharp, well-defined peaks in the diffractograms as shown in figure 26 (a) and (b). However, the 50% and 70% INM SD formulations were not completely amorphous due to the high INM loading as expected. For all other SD formulations both ternary and quaternary SDs, the semi-crystalline peaks associated with P407 was present, compared to the SD formulations reported by Gumaste *et al.* (2016) in which poloxamer was converted to its amorphous form (Gumaste, Gupta & Serajuddin, 2016). However, in the XRPD diffractograms of the 5% P407 loading SD formulations, the semi-crystalline peaks of P407 appear at much weaker intensity compared to the 15% P407 loading samples.

This may be due to the fact that the physical interaction from P407 is much greater at high poloxamer loadings. The conversion from the crystalline to the amorphous form was a result of the possible intermolecular interactions mainly hydrogen bonding and thus formation of molecular solid dispersions. ATR-FTIR and Raman spectroscopy was used to elucidate the type and mechanism of interaction.

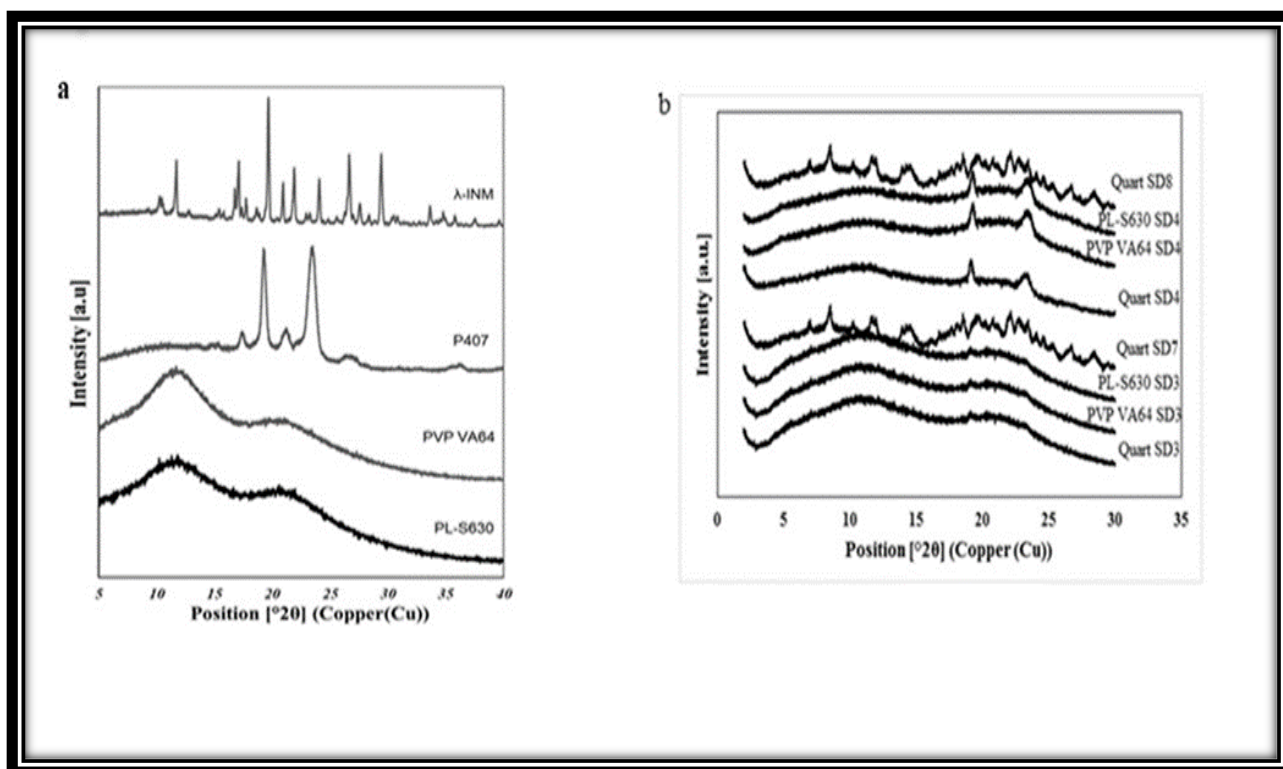


Figure 26. a) XRPD diffractograms of the pure components and (b) XRPD diffractograms of selected ASD formulations indicating that the INM is present in the amorphous form, but the P407 is not solubilized and due to its semi-crystalline nature exists in its semi-crystalline form. The 70% INM ASD formulations remained crystalline.

4.1.2.3 The Effect of Cooling on Hot-Melt Extruded Amorphous Solid Dispersions

XRPD was used to examine the amorphous nature of the drug within the SD formulations. XRPD was performed on a PANalytical Empyrean X-ray diffractometer attached to a computer running High Score Plus to collect and process data. Figure 28 shows the XRPD diffractograms of the SD formulations used to investigate the effect of cooling. The presence of two Bragg peaks of P407 at 19 and 24° respectively indicates that P407 was not converted to the amorphous form as reported by Hurley *et al.* (2018). The drug peaks associated with crystalline INM were completely absent in the melt extrudates with various drug-polymer ratios, indicating that INM was successfully converted to its amorphous form as shown in figure 27. The XRPD diffractograms confirmed that INM was successfully converted to its amorphous form and P407 remained semi-crystalline.

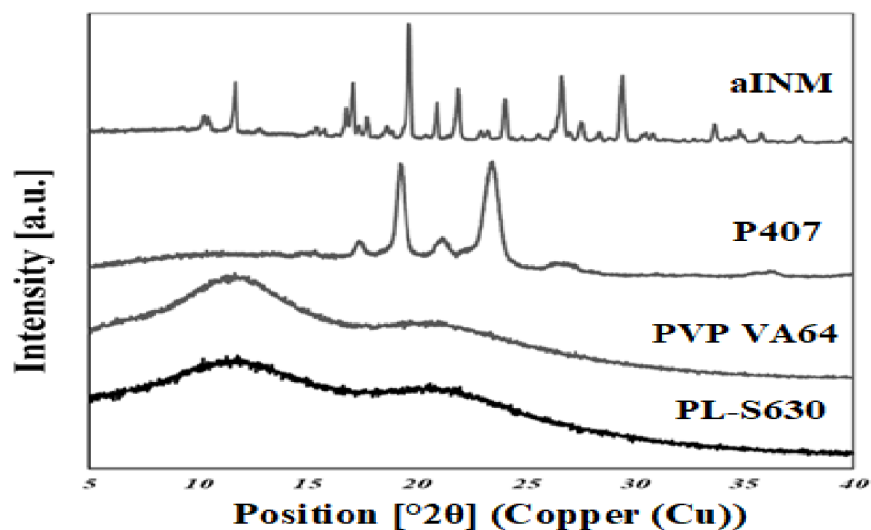


Figure 27. XRPD diffractograms of the pure components. INM is transformed to the amorphous form.

Considering the concentration of plasticizer present in the amorphous SD formulations, it was important to note that the formulations with the higher P407 loadings had significantly higher Bragg peak intensities than formulations with low P407 loading since the APIs can be incorporated into the core of P407 micelle at high loads (Hurley *et al.*, 2020). It is important to note that cooling had a significant effect on the crystallinity (i.e. Bragg peak intensities) of the SD formulations. For example, SD2-NT had the highest Bragg peak intensities indicating that using a high P407 loading with a slow cooling process increases the crystallinity (Hurley *et al.*, 2020).

This analysis confirmed that P407 was not solubilized and is present in its semi-crystalline form with some level of compatibility with PL-S630/PVP VA64-INM system due to the reduction of the enthalpy of fusion and melting temperature in the various SD formulations. This was consistent with higher Bragg peak intensities observed in the XRPD data from the 15% P407 sample with 30% drug loading.

The cooling method used had an effect on the amorphous SDs depending on 1) the cooling method used 2) % P407 loading and 3) the polymeric carrier used. For example in Figure. 28, SD2-Liq N₂ and SD2-NT had much broader and higher Bragg poloxamer peak intensities compared to SD2 and SD2- AC. This is because PL-S630 and PVP VA64 possess different solubility properties with PVP VA64-INM SD formulations having a significantly greater than INM-PL-S630 SDs.

The HSPs alongside XRPD confirmed that the drug and polymer were indeed miscible. XRPD confirmed successful conversion of INM to the amorphous form as mentioned before. As mentioned above ATR-FTIR and Raman spectroscopy was used to confirm hydrogen bonding interaction between PVP VA64/PL-S630 and INM via the interaction between the amide carbonyl C=O of the polymer and the free carboxylic acid C=O of INM. For successful conversion to the amorphous form interaction between drug and polymer is necessary.

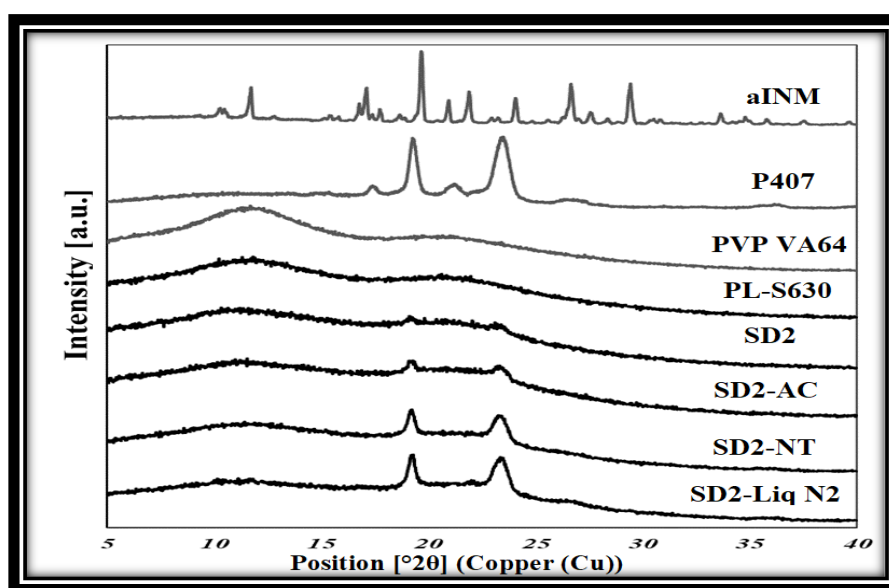


Figure 28. XRPD diffractograms of SD formulations and XRPD diffractograms of the SD formulation used to investigate the effect of cooling. P407 was still present in its crystalline form in all formulations (AC= Air cooled, NT= Normal room temperature and Liq N₂ = Liquid Nitrogen).

4.1.3 ATR-FTIR and Raman Spectroscopic studies

4.1.3.1 Investigation of ethylene oxide-co-propylene oxide for dissolution enhancement of hot-melt extruded solid dispersions

ATR-FTIR spectroscopy is one of the most widely used methods to detect the intermolecular interactions in SDs, such as hydrogen bonds between API's and polymer excipients. PVP VA64 acts a proton acceptor through the carbonyl of the amide group and the vinyl acetate group (Yu *et al.*, 2022), while INM can act as a proton donor through the –OH group of the carboxylic acid (Benmore *et al.*, 2021).

Both γ -INM and α INM exist as dimers with carboxylic acid groups of one molecule directly interacting with another in a cyclic acid-acid dimer (Hurley *et al.*, 2018). Stabilisation of INM in the amorphous phase involves disrupting these intermolecular dimers and involving the carboxylic acid of INM in hydrogen bonding. Figure 29(a) illustrates the ATR-FTIR spectra of γ -INM, α INM, pure polymers, physical mixture and SD formulations (SD21 and SD25).

Pure INM (γ -INM) is characterized by principal absorption peaks and showed two strong non-hydrogen bonding C=O bands at 1714.00 cm^{-1} (free C=O of carboxylic acid) and 1690.00 cm^{-1} (acid-acid dimer C=O Stretch) respectively, the O-H Stretch of the acid is broad however it is superimposed on the sharp C-H stretches, as the free carboxylic acid O-H Stretch may exist as dimers via hydrogen bonding. In α INM this stretching shifts to 1707.00 cm^{-1} and 1679.00 cm^{-1} respectively.

Nyamba *et al.* (2023) reported that PVP VA64 due to its amide structure provide the drug molecule with hydrogen bond acceptors and thus acts as an appropriate polymeric carrier, (Nyamba *et al.*, 2023), for the water-insoluble drug INM which result in thermodynamically stabilized dosage forms since their structure are similar to those of liquid-based solutions. Chan *et al.* (2015) also reported that these carbonyls which can act as proton acceptors appear at 1731 cm^{-1} and 1672 cm^{-1} respectively (Chan *et al.*, 2015). In this study this appeared to be the case as the main principal peaks appeared at 1731.00 cm^{-1} and 1670.00 cm^{-1} due to vinyl acetate and amide carbonyl respectively (figure. 29(a)). However, Hurley *et al.* (2019) also reported that there was no evidence of interaction between PVP VA64 and INM even though a shift was observed. In this study, there was evidence of chemical interaction between INM and PVP VA64.

The ATR-FTIR studies of all SD formulations with PVP VA64 and P407 may indicate that possible potential hydrogen bonding between the INM and PVPVA carbonyl is occurring, due to a broadening of the 1670 cm^{-1} PVP VA64 amide carbonyl peak to 1661 cm^{-1} as well as the appearance of a shoulder around 1650 cm^{-1} . Also, the intensity of the vinyl acetate C=O carbonyl did increase as the drug content increased, however, there was no shift in the vinyl acetate carbonyl peak which possibly is because the amide carbonyl of PVP VA64 is a stronger proton acceptor compared to the vinyl acetate carbonyl of PVP VA64 as reported by Yuan *et al.* (2015).

It must be noted there was a greater broadening and a shift in the amide carbonyl as the % drug loading increased, this was also the case for SD formulations which contained no P407 as shown in figure 29 (b) and (c). This indicates that P407 possibly had no molecular interaction with INM and did not interfere in the interaction between INM and PVP VA64.

In the case of the physical mixture, the amide C=O and vinyl acetate C=O stretch appeared at a much weaker intensity compared to the SD formulations, this may be because INM is still present in its crystalline form, therefore there was no interaction.

The shift and intensity of the carbonyl regions in the SD formulations are not very obvious even in the highest concentration of INM SD formulations. It was also found that this observation is a common phenomenon when FTIR is employed to detect intermolecular interactions in SDs because of the broad peak width and lower drug concentration (Budiman *et al.*, 2023). Thus, it is necessary to have some solid evidence provided from different analytical techniques such as Raman spectroscopy or ssNMR spectroscopy to confirm the formation of hydrogen bonds between INM and PVP VA64.

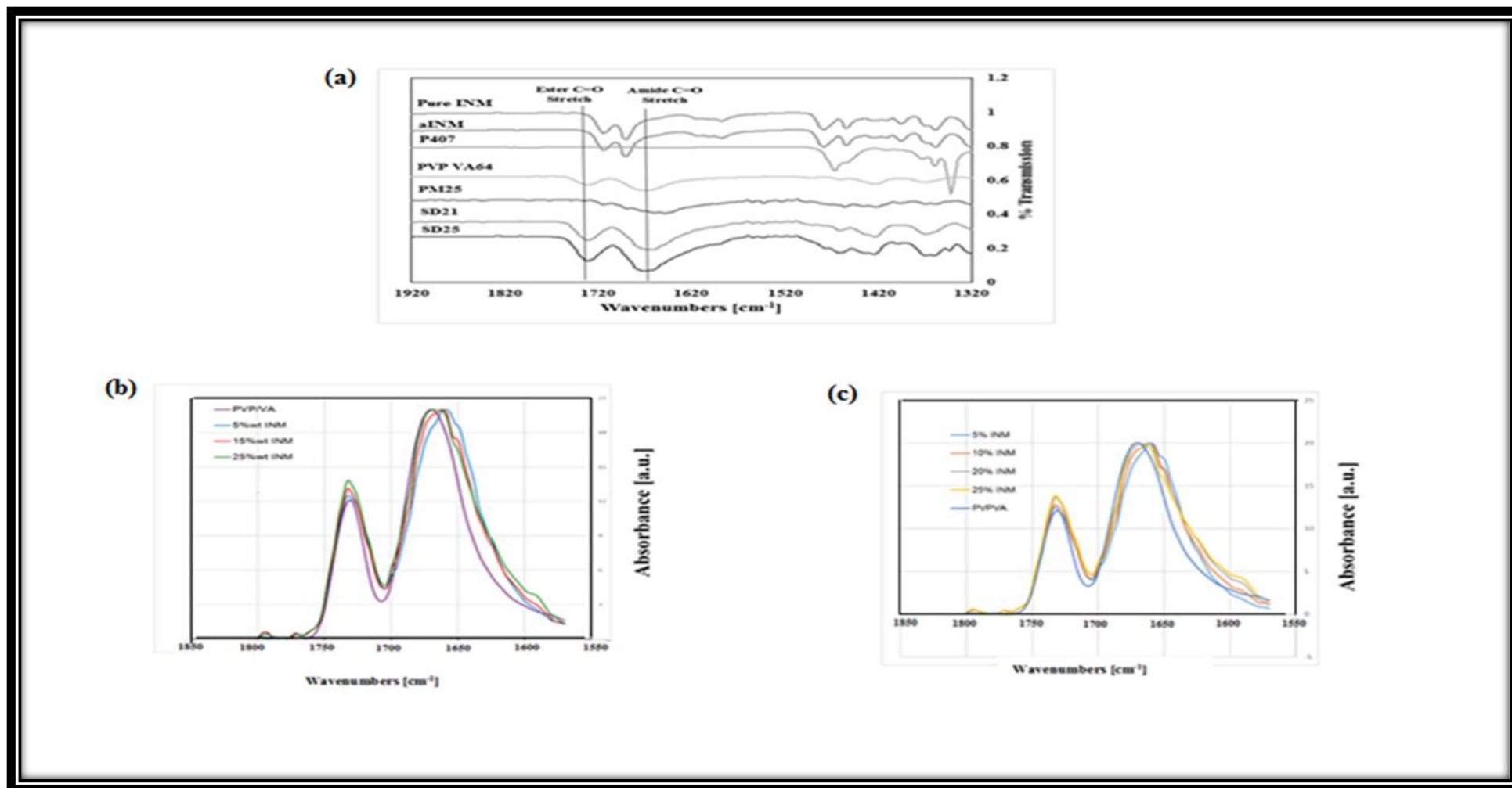


Figure 29: (Top) FTIR spectra of selected 25% SD formulations and pure components indicating a broadening of the amide carbonyl peak of PVP VA64 for both extruded dispersions. Figure 28 (b): (Bottom) SD formulations with 0% P407 loading and Figure 28 (c): (Bottom) SD formulations with 20% P407 loading.

4.1.3.2 An investigation of the inter-molecular interaction, solid-state properties and dissolution properties of mixed copovidone hot-melt extruded solid dispersions

Raman analyses was carried out to further explore the hydrogen bonding interaction between INM, PVP VA64, P407 and PL-S630 in the multi-component solid dispersions prepared by the HME process. Raman spectroscopy is complimentary to ATR-FTIR spectroscopy, and it is quite useful for the analysis of ASDs. Hydrogen bonding was the predicted mechanism of interaction due to high molar attraction constant of INM calculated using the Hansen solubility parameters and polarity of the drug-polymer mixtures. APIs normally tend to be conjugated or aromatic compounds which have strong Raman signals, while excipients have much weaker Raman signals and/or spectra. Similar to the ATR-FTIR studies, Raman spectroscopy showed potential intermolecular interaction between INM and polymeric carriers due to a shift in the amide carbonyl of PVP VA64 and PL-S630. The PVP VA64 amide carbonyl ($\nu\text{C=O}$) peak at 1673.00 cm^{-1} shifted to 1680.00 cm^{-1} in ASD samples due to hydrogen bonding interaction with the $-\text{OH}$ group of INM as a result of hot melt extrusion as shown in Figure 30.

The acid $\nu\text{C=O}$ present at 1702.00 cm^{-1} (free C=O of carboxylic acid) of INM completely disappears in the Raman spectra of the ternary and quaternary ASD formulations as a result of low intensity of INM. Based on the Raman spectra in Figure 30, none of peaks identified in the Raman spectra of amorphous INM were present in the Raman spectra of the ASD formulations. It must be noted even though a hydrogen bond shift was observed in all ASD formulations, the quaternary ASD formulations had a much greater shift as a result of the mixed copovidone present in the quaternary mixtures as shown in Figure 31. However small differences in the intensity and shifts in the peak positions were observed as a result of the HME process in the region of carbonyl group peaks ($1660\text{--}1670\text{ cm}^{-1}$). In summary, the ATR-FTIR and Raman analyses suggest that similar hydrogen bonding interactions were achieved in solid dispersions prepared by the HME process. The Raman analysis confirmed the ATR-FTIR results indicating hydrogen bonding interaction occurred between INM and PVP VA64/Plasdone S-630 as expected and confirmed that the drug and polymer were indeed miscible as predicted by the Hansen solubility parameters.

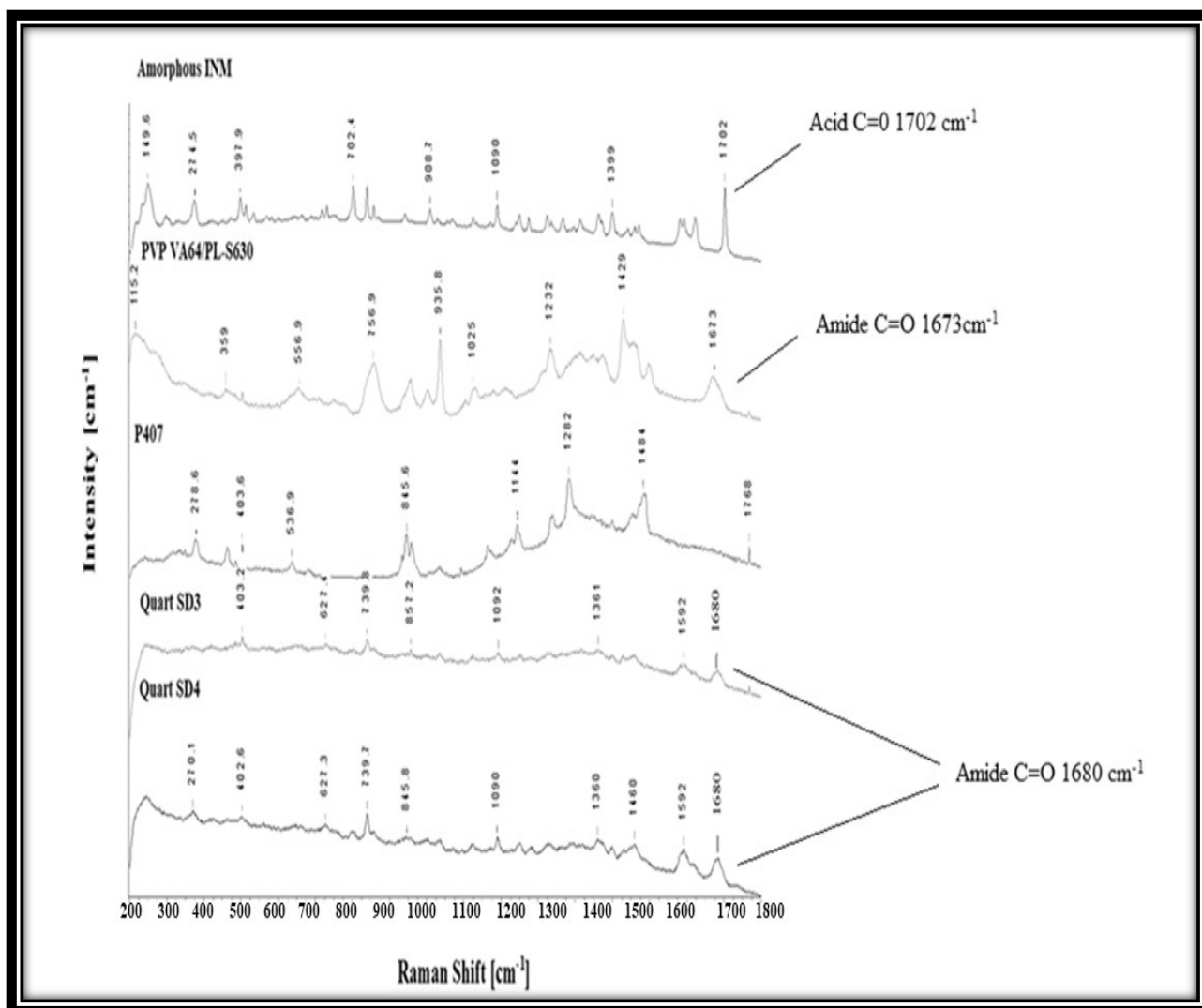


Figure 30. Full Raman spectra of pure components and selected ASD formulations (30% INM), indicating potential hydrogen bonding due to the shift in the amide carbonyl of both PVP VA64 and PL-S630 from 1673 cm^{-1} to 1680 cm^{-1} . The vinyl acetate carbonyl peak appears at a low intensity at 1732.00 cm^{-1} .

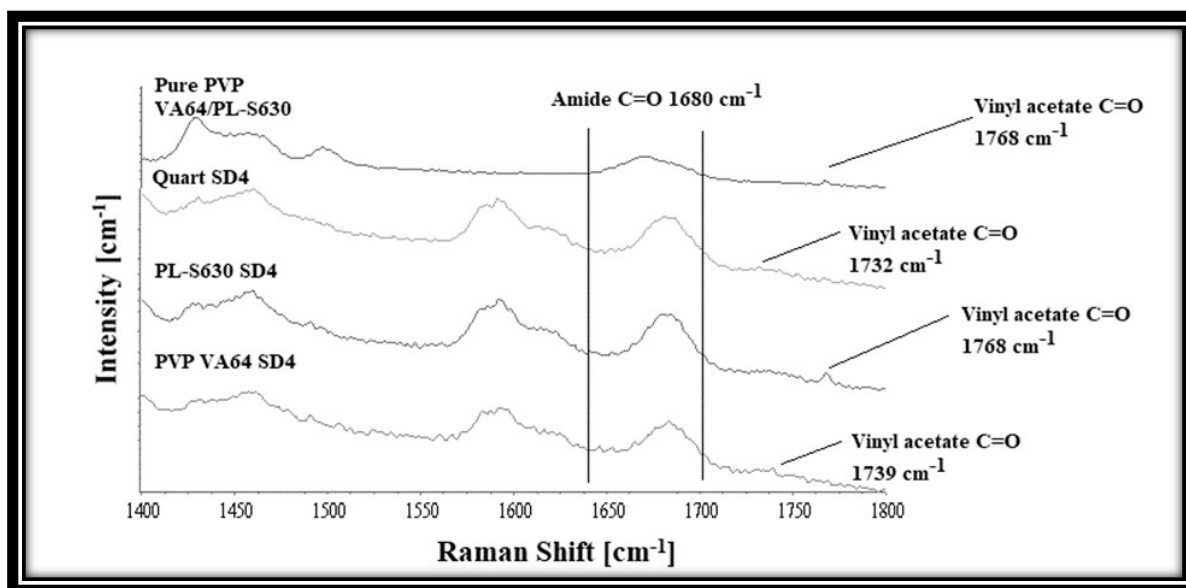


Figure 31. Raman spectra of pure components and selected ASD formulations (30% INM), indicating potential hydrogen bonding. There was a shift in the vinyl acetate C=O carbonyl in the all ASD formulations, however they quaternary ASD formulations had the greatest shift.

In the ATR-FTIR reference spectrum of amorphous INM, the above named peaks shifted to 1707.00 cm^{-1} and 1679.00 cm^{-1} respectively due to conversion to its amorphous form as shown in figure 34, as a result do not align with the polymer peaks (Hurley *et al.*, 2018). See tables 15 to 22 for ATR-FTIR and Raman spectra interpretation.

The ATR-FTIR of all the ASD formulations with PL-S630, PVP VA64 and P407, amorphous INM was present and there was evidence of intermolecular interaction i.e. hydrogen bonding due to the shift of the amide carbonyl of PVP VA64/PL-S630 from 1672.00 cm^{-1} to 1680 cm^{-1} (Figure 32 (a) and figure 32 (b)). There was no shift observed in the C=O of the vinyl acetate carbonyl of PVP VA64/PL-S630 in the ATR-FTIR spectra, however in the Raman spectra it must be noted that there was a shift in the vinyl acetate C=O carbonyl in all ASD formulations, however the quaternary ASD formulations had the greatest shift as shown in Figure 31. This is very significant as most literature states that the vinyl acetate C=O carbonyl is a weak hydrogen bond acceptor which was reported by Yuan *et al.* (2015). Any poloxamer peaks present in the pure P407 sample were not present in the ATR-FTIR spectra of the SD formulations as shown in Figure 32 (c). This may indicate that P407 possibly has no molecular interaction with INM (Méndez *et al.*, 2022).

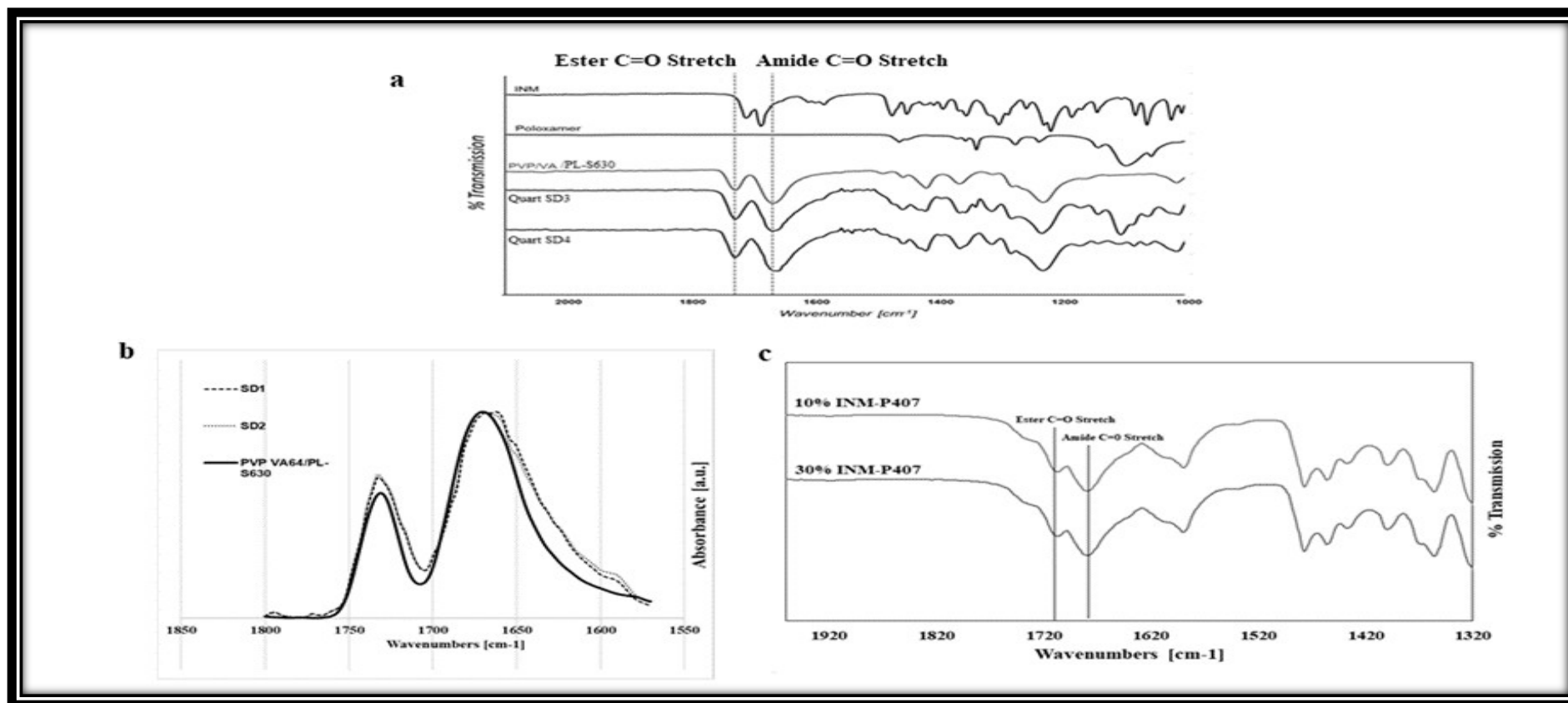


Figure 32. a) ATR-FTIR Spectra of pure components and selected ASD formulations (30% INM). b) ATR-FTIR Spectra of both PVP VA64/PL-S630 and SD1/SD2 indicating potential hydrogen bonding due to the shift in the amide carbonyl of both PVP VA64 and PL-S630 from 1672 cm^{-1} to 1685 cm^{-1} . There is no shift in the vinyl acetate carbonyl peak as a result of its weaker hydrogen bond potential. (c) ATR-FTIR spectra of binary ASDs of 10 and 30% INM-P407 drug-polymer mixtures

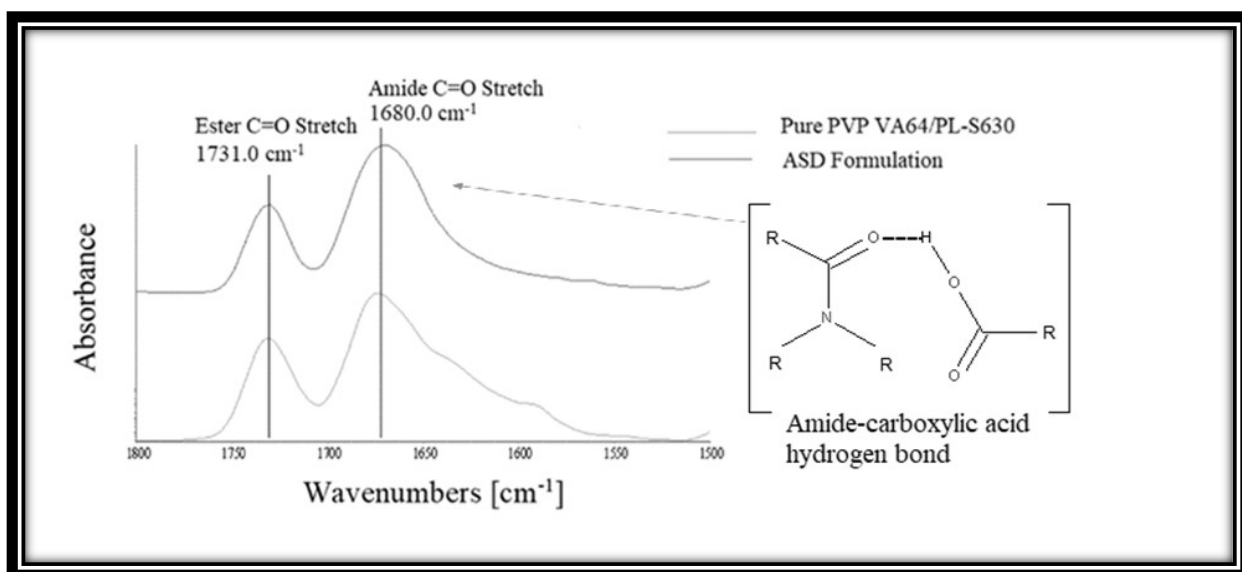


Figure 33. a) ATR-FTIR Spectra of a selected ASD formulation (*Quart SD2*) illustrating the hydrogen bond between PVP VA64/PL-S630 and INM due to the shift in the amide carbonyl of both PVP VA64 and PL-S630 from 1672 cm⁻¹ to 1685 cm⁻¹

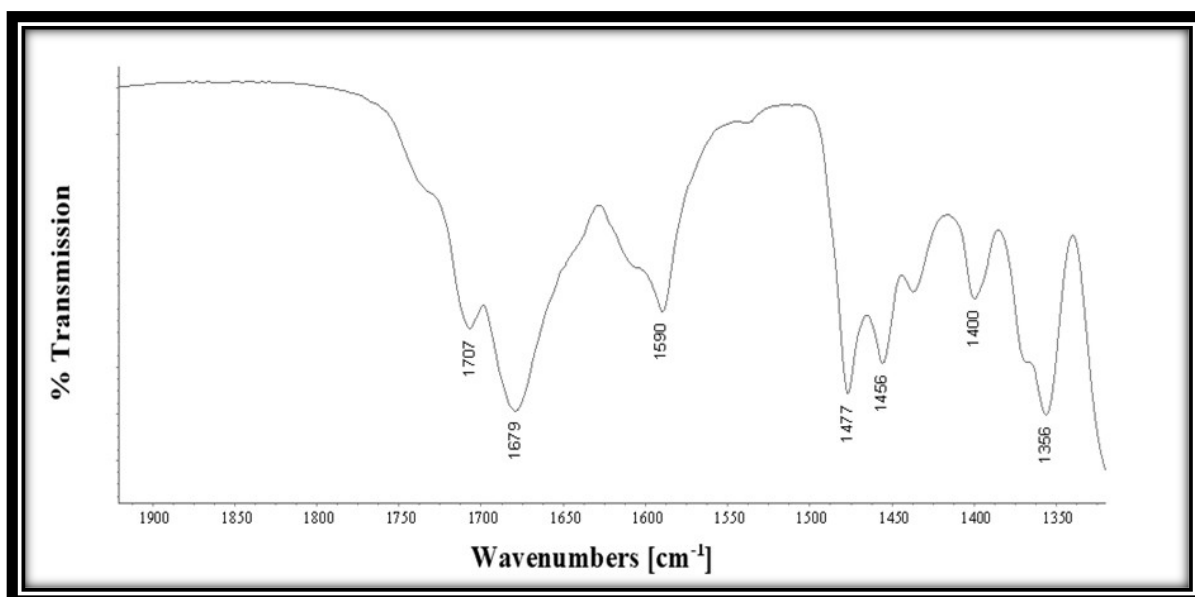


Figure 34. ATR-FTIR reference spectrum of amorphous INM, indicating a shift in the acid-acid dimer C=O stretch (1690 cm⁻¹ to 1679 cm⁻¹) and the free carboxylic acid C=O (1714 cm⁻¹ to 1707 cm⁻¹).

Table 15. *Interpretation of ATR-FTIR Spectrum of INM.*

Bond Vibration	Frequency (cm⁻¹)
C-Cl Stretch	751.01
-COOH out of plane Stretch	924.22
C-O Stretch	1222.22
O-CH ₃ Stretch	1453.61
Aromatic C=C Stretch	1588.10
C=O Stretch (Two bands)	1689.62, 1712.67
Aromatic C-H Stretch, -COOH (superimposed)	2927.60

Table 16. *Interpretation of ATR-FTIR Spectrum of PVP VA64/PL-S630.*

Bond Vibration	Frequency (cm⁻¹)
C-O Stretch (Two bands)	1019.22, 1234.09
Ester C=O Stretch	1730.88
Amide C=O Stretch	1672.00
C-N Stretch of amine	1369.30
Alkyl C-H Stretch	3100.00
C-H bending	1422.92

Table 17. *Interpretation of ATR-FTIR Spectrum of P407.*

Bond Vibration	Frequency (cm⁻¹)
Aliphatic C-H Stretch (Two bands)	2978.76, 2883.93
In plane O-H bend	1342.20
C-O Stretch	1099.59

Table 18. *Interpretation of ATR-FTIR Spectrum of SD formulations.*

Bond Vibration	Frequency (cm⁻¹)
C-O Stretch (Two bands)	1019.22, 1234.09
Ester C=O Stretch	1730.88
Amide C=O Stretch	1680.00
C-N Stretch of amine	1369.30
Alkyl C-H Stretch	3100.00
C-H bending	1422.92

Table 19. *Interpretation of Raman Spectrum of INM*

Bond Vibration	Frequency (cm⁻¹)
ν C-Cl Stretch	702.40
δ CH ₃	1399.00
ν (C-O-C) asym	1090.00
ν (C-O-C)	906.30
Amide ν C=O Stretch	1680.00
Acid ν C=O	1702.00

Table 20. *Interpretation of Raman Spectrum of PVP VA64/PL-S630*

Bond Vibration	Frequency (cm⁻¹)
ν (C-O-C)	935.6
ν (C-O-C) asym	1026.00
ν (CC), aliphatic chain vibrations	1232.00
δ CH ₃ asym	1420.00
δ CH ₂	1423.00
Amide ν C=O Stretch	1673.00
Vinyl acetate ν C=O	1768.00

Table 21. *Interpretation of Raman Spectrum of P407.*

Bond Vibration	Frequency (cm⁻¹)
ν (C-O-C)	845.6
ν (C-O-C) asym	1145.00
ν (CC), aliphatic chain vibrations	1202.00
δ CH ₃ asym	1484.00
δ CH ₂	1482.00

Table 22. Interpretation of Raman Spectrum of a selected SD formulation (Quart SD4).

Bond Vibration	Frequency (cm ⁻¹)
$\nu(\text{C-O-C})$	845.80
$\nu(\text{C-O-C})$ asym	1092.00
δCH_3 asym	1460.00
δCH_2	1458.00
$\nu\text{C-N}$ Stretch	1592.00
Amide $\nu\text{C=O}$ Stretch	1680.00
Vinyl acetate $\nu\text{C=O}$	1732.00

4.1.3.3 The Effect of Cooling on Hot-Melt Extruded Amorphous Solid Dispersions

ATR-FTIR was used in conjunction with Raman studies to elucidate the mechanism of interaction between INM and each of the polymers which is necessary for drug-polymer miscibility. When INM was converted to the amorphous form via hot melt extrusion, the amide carbonyl C=O of PVP VA64 and PL-S630 shifted to 1680 cm⁻¹. This indicates that hydrogen bonding had taken place between the amide carbonyl of the polymer and the free C=O bond of the carboxylic acid of INM (Hurley *et al.*, 2018). This was the case for all SD formulations as shown in figure 35 (a).

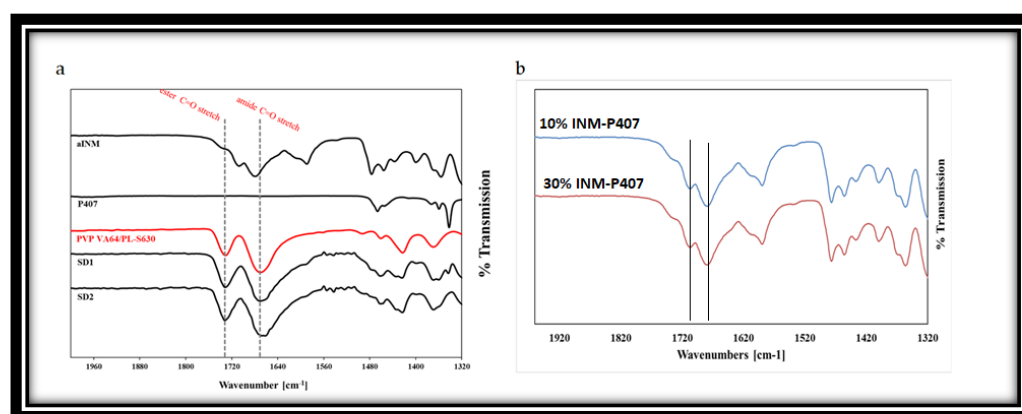


Figure 35. a) ATR-FTIR Spectra of pure components and selected SD formulations (30% INM) showing a shift in the amide carbonyl C=O from 1672 cm⁻¹ to 1680 cm⁻¹. There is no shift in the vinyl acetate carbonyl peak as a result of its weaker hydrogen bond potential. (b) ATR-FTIR spectra of binary SDs (controls) of 10 and 30% INM-P407 drug-polymer mixtures.

There was no change in the vinyl acetate C=O carbonyl due to weaker hydrogen bonding potential of the vinyl acetate carbonyl as reported by Yuan *et al.*, (2015) as shown in figure 35 (b) (Yuan *et al.*, 2015). Any P407 peaks within the pure P407 sample were completely absent in the ATR-FTIR spectra of the SD formulations as shown in figure 35 (a) and figure 36. This indicates that P407 possibly has no intermolecular interaction with INM at a molecular level (Hurley *et al.*, 2018).

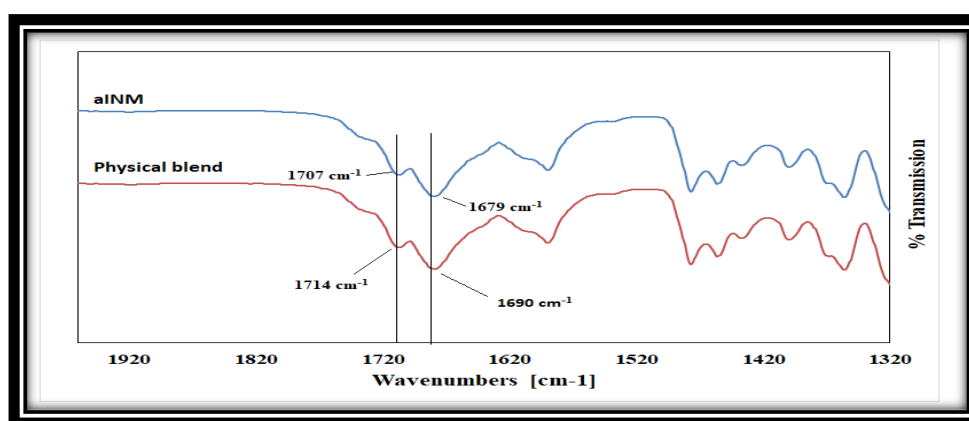


Figure 36. ATR-FTIR Spectra of aINM and Physical blend. Crystalline INM is still present in physical blend as expected.

It is also important to note that in the ATR-FTIR reference spectrum of aINM, the two C=O bands at 1714 cm⁻¹ (free C=O of carboxylic acid) and 1690 cm⁻¹ (acid-acid dimer C=O stretch) shifted to 1707 cm⁻¹ and 1679 cm⁻¹ respectively due to transformation to its amorphous form as shown in figure 37, and therefore do not align with the polymer peaks. The physical blends contained crystalline INM as expected as shown in figure 36 (Hurley *et al.*, 2018).

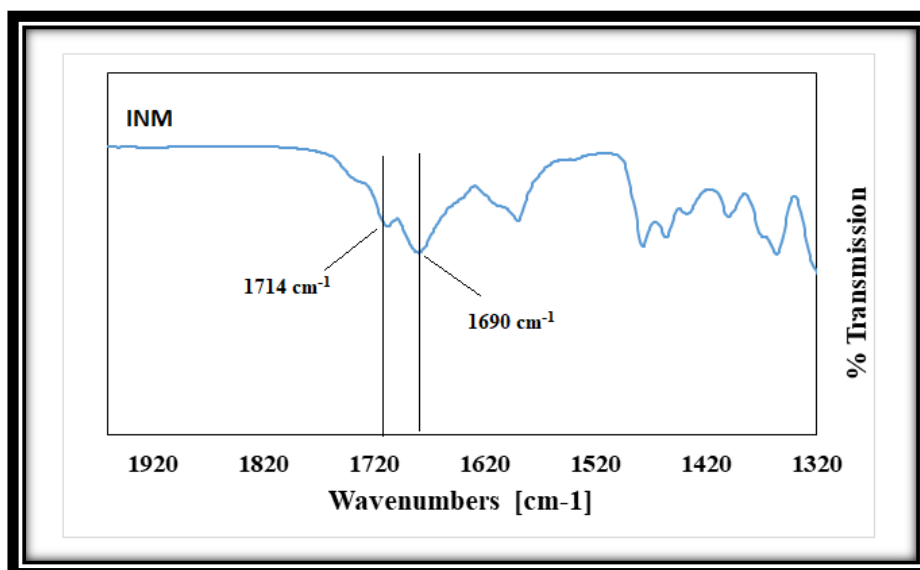


Figure 37. ATR-FTIR Spectrum of crystalline INM.

Hydrogen bonding was the predicted mechanism of interaction due to polarity of INM and polymeric carriers as a result of the relatively high INM molar attraction constant calculated using the HSPs. The amide carbonyl ($\nu\text{C}=\text{O}$) peak at 1673 cm^{-1} shifted to 1680 cm^{-1} in all SD formulations due to hydrogen bond interaction with the $-\text{OH}$ carboxylic acid of INM as shown in figure 38. The intensity of the vinyl acetate carbonyl group is weak and appears at 1745 cm^{-1} due to the weaker hydrogen bonding potential as reported by Yuan *et al.* (2015).

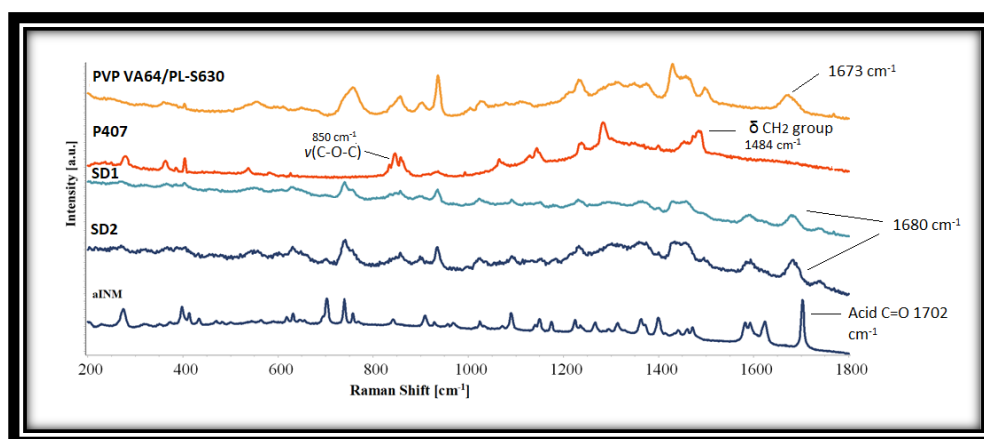


Figure 38. Raman spectra of crystalline INM, polymeric carriers and chosen SD formulations (30% INM), which shows interaction via hydrogen bonding as a result of the shift in the amide $\text{C}=\text{O}$ carbonyl stretch of PL-S630 and PVP VA64. The low intense peak at 1732.00 cm^{-1} corresponds to the vinyl acetate $\text{C}=\text{O}$ carbonyl.

The acid $\nu\text{C}=\text{O}$ present at 1702 cm^{-1} (free $\text{C}=\text{O}$ of carboxylic acid) of INM disappears in the Raman spectra of the quaternary and ternary SD formulations due to the low intensity of INM. Based on the Raman spectra in figure 38, the peaks identified in the Raman spectra of aINM were not present in the Raman spectra of the amorphous SD formulations. The broad peak at 1482 cm^{-1} in the Raman spectrum of solid-state P407 reflected the deformation vibration of the δCH_2 group.

The $\nu(\text{O-H})$ of P407 was present at 3200 cm^{-1} and $\nu(\text{C-O-C})$ was present at 850 cm^{-1} . Careful analysis of the SD formulations indicates that the bands associated with P407 were not present in the SD formulations due to the lack of intermolecular interaction. Raman spectroscopy similar to ATR-FTIR spectroscopy identified that hydrogen bonding occurred between PVP VA64/PL-S630 regardless of the cooling method used.

4.1.4 SEM studies

4.1.4.1 Investigation of ethylene oxide-co-propylene oxide for dissolution enhancement of hot-melt extruded solid dispersions

SEM was used to examine the surface morphology of selected SD formulations and pure INM. The particle morphology of pure INM, Pure polymers and SDs are illustrated in Figures 39-43. Pure P407 (figure 41) appeared as smooth-surfaced spherical particles. Pure INM (figure 40) appear irregular in size and shape and were much smaller than the P407 and SD particles. PVP VA64 appeared as spheres that are hollow in nature (figure 39). While examining the physical mixture (Figure 42) no specific interaction was observed between drug and matrix material. From the SEM image of the SD (Figure 43) the INM crystals seem to be incorporated into the polymer matrix. From the SEM images it can be deduced that the drug was successfully dispersed in the carrier material. No agglomeration was present resulting in a smooth surface and showed that the individual surface properties of PVP VA64, P407 and INM were lost during the extrusion process indicating INM possibly may be present in its amorphous form.

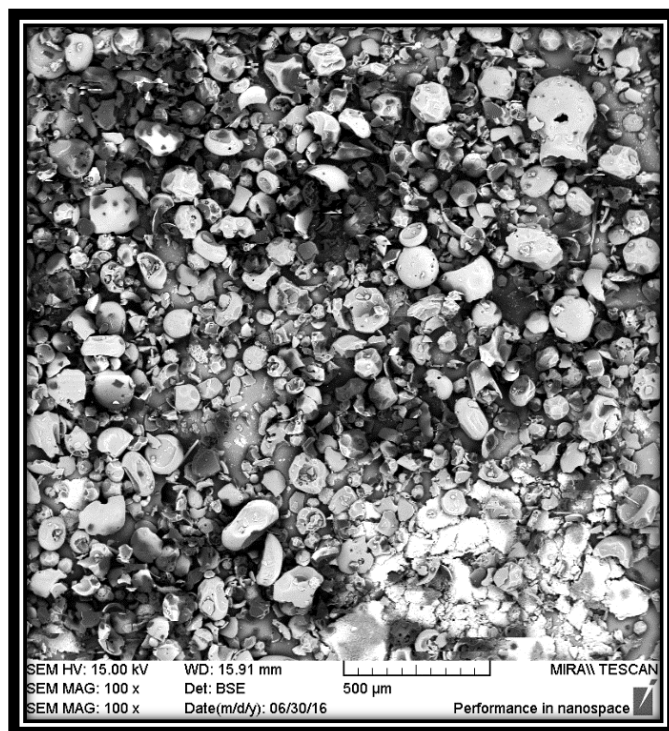


Figure 39. SEM image of Pure PVP VA64 at 100kx magnification.

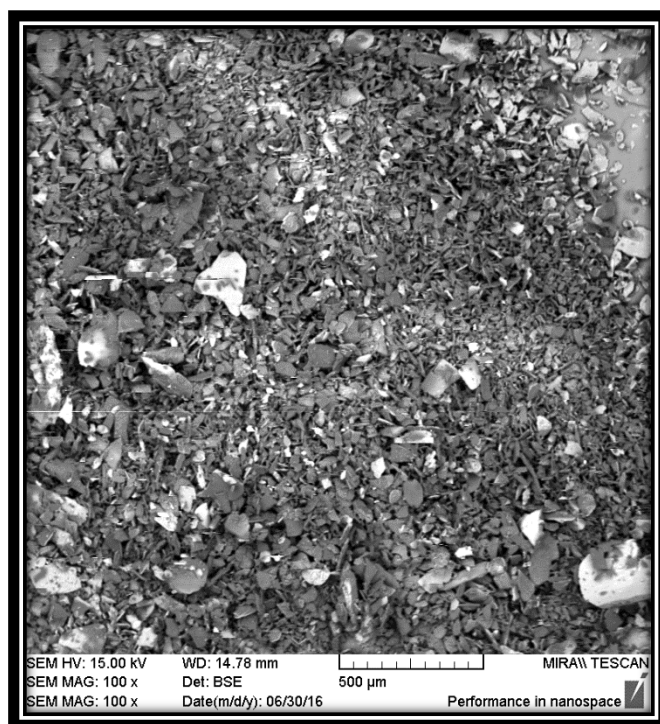


Figure 40. SEM image of Pure INM at 100kx magnification.

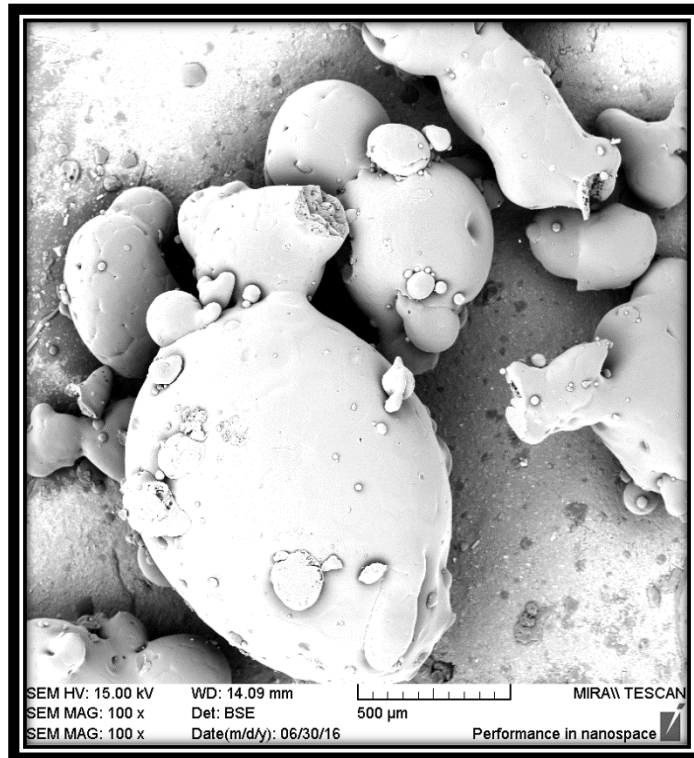


Figure 41. SEM image of Pure P407 at 100kx magnification.

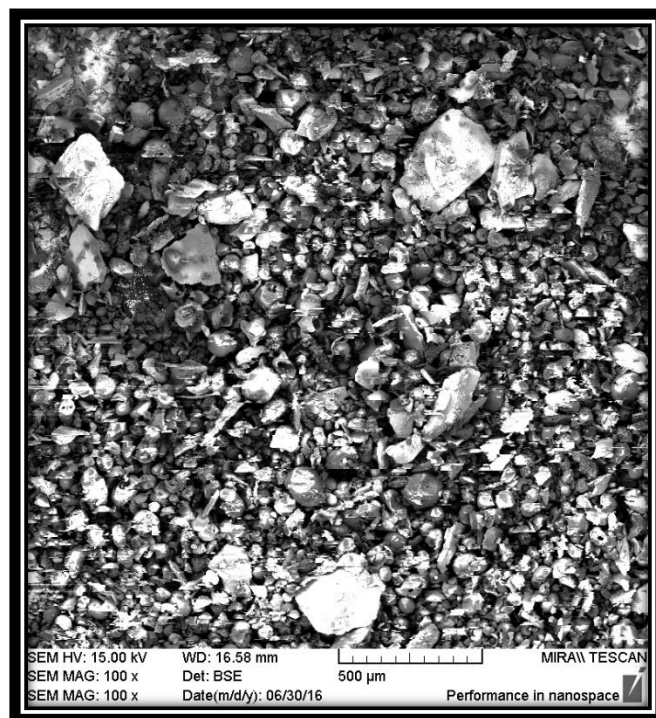


Figure 42. SEM image of physical mixture at 100kx magnification.

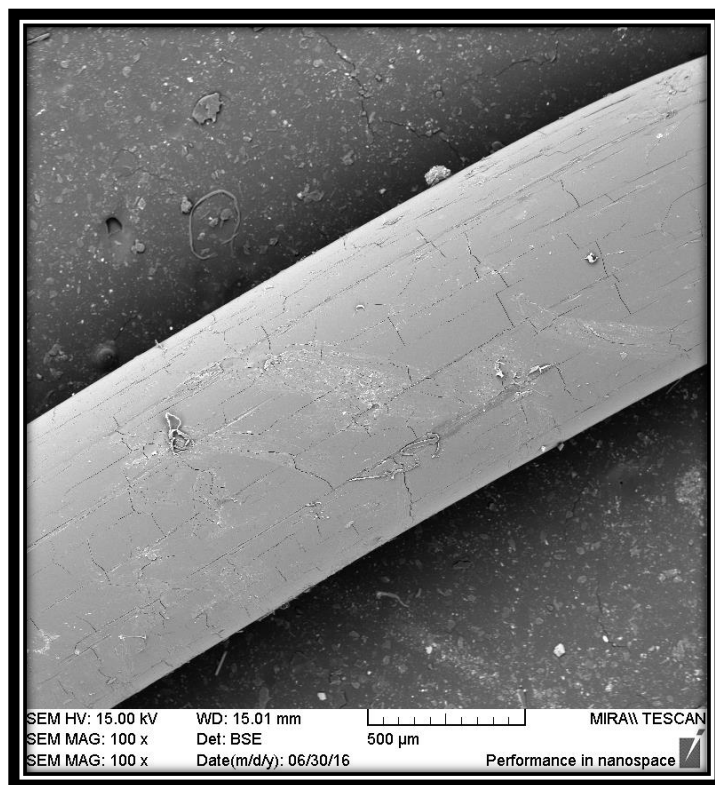


Figure 43. SEM image of SD1 (0% P407-10% INM loading) at 100kx magnification.

4.1.5 Phase solubility studies

4.1.5.1 Investigation of ethylene oxide-co-propylene oxide for dissolution enhancement of hot-melt extruded solid dispersions

Figure 44 represents the kinetic solubility of INM in aqueous solutions of PVP VA64 and P407. The Gibbs free energy of transfer (ΔG_{tr}^0) and apparent solubility constants derived from Figure 44 are shown in Table 23.

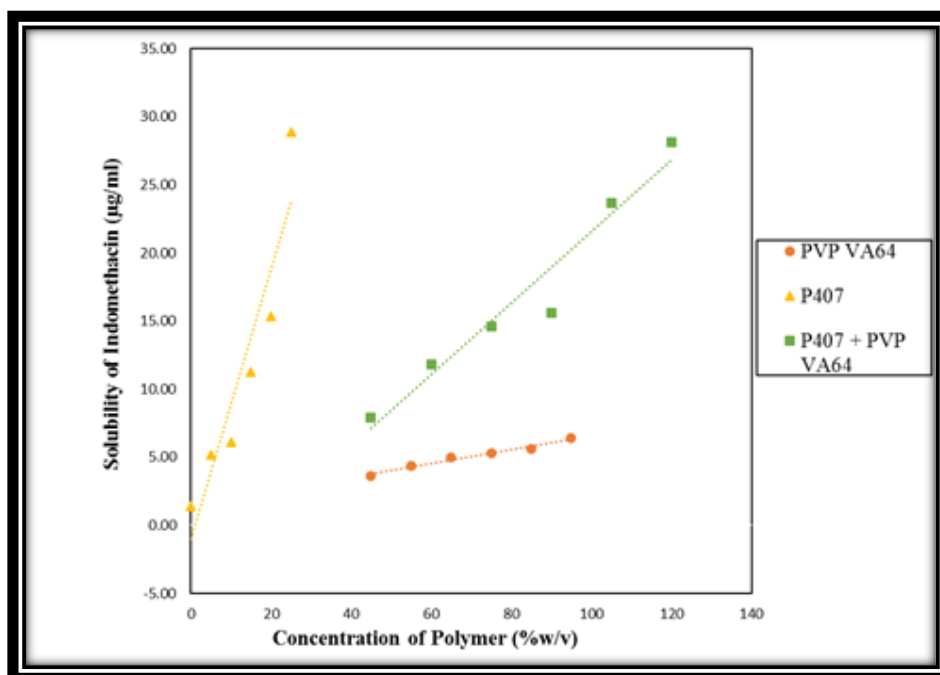


Figure 44. Solubility of INM ($\mu\text{g/ml}$) in aqueous solutions of PVP VA64 and P407 at 37 °C (Each point represents the average \pm SD of three independently prepared samples).

The phase solubility plot of solubility of INM ($\mu\text{g/ml}$) against combined polymer concentration (% w/v) exhibits a linear relationship (which is AL type of plot) in the polymer concentration range that was investigated (Figure 44). Table 23 shows that all Gibbs free energy of transfer values are negative at all carrier levels. This demonstrates that the drug solubilization process is spontaneous (Bertoni *et al.*, 2023). In drug-polymer SD mixtures the entropy of mixing is always favoured and thus negative.

A-type phase solubility profiles are obtained when the solubility of the drug INM increases with increasing polymer concentration. When the complex is first order in nature with respect to ligand (polymeric matrix) and linear with respect to the substrate (drug), then the AL-type phase solubility profile is obtained (Srinivasan *et al.*, 2023).

The AL-type phase-solubility curve is obtained when the solubility curve is first order with respect to polymer concentration (Bertoni *et al.*, 2023). Under AL-type phase-solubility diagram, the kinetic solubility of the API dispersed within a water-soluble polymer can be described with the slope (S) of the solubility curve and the intrinsic solubility (S_0) of the drug. As the concentration of carrier increased the ΔG_{tr}^0 values decreased as the process at higher carrier levels is more favourable.

Table 23 also shows that INM-P407–PVP VA64 mixture has more favorable interactions in pH buffer 1.2 due to its higher K_a value compared to INM-P407 and INM-PVP VA64 mixtures respectively. In both cases, the solubility of INM increased as the polymeric carrier concentration increased. A negative value of K_a signifies an increase in solubility. In this study, all K_a values were positive indicating an increase in the kinetic solubility of INM at pH 1.2 (Hurley *et al.*, 2018) and (Hurley *et al.*, 2020).

The K_a value represents the higher solubility gained from a metastable state of the compound. For example, amorphous drugs have a higher solubility than their crystalline counterparts but this solubility is unstable as the amorphous form has a tendency to revert to crystalline form. Thus, it is referred to as the apparent stability constant, negative values signify a decrease in the solubility (Hurley *et al.*, 2018).

Table 23. Gibbs free energy values and apparent stability constants (K_a) of INM-P407, INM-PVP VA64 and INM-P407-PVP VA64 interactions.

Concentration of P407 (%w/v)	Concentration of PVP VA64 (%w/v)	Quantity of INM added (mg)	Combined Concentration of Polymer (% w/v)	ΔG_{tr}^0 (kJ/mol)		
				P407	PVP VA64	P407 + PVP VA64
0	45	50	45	0.00	-2.44	-4.46
5	55	50	60	-3.38	-2.93	-5.50
10	65	50	75	-3.80	-3.27	-6.05
15	75	50	90	-5.37	-3.43	-6.22
20	85	50	105	-6.17	-3.58	-7.29
25	95	50	120	-7.81	-3.92	-7.74
	Intercept		0.99	1.43		4.68
	Slope		0.98	0.05		0.26
	K_a ($\mu\text{g/ml}$)		0.001	0.034		0.041

4.1.5.2 An investigation of the inter-molecular interaction, solid-state properties and dissolution properties of mixed copovidone hot-melt extruded solid dispersions

The kinetic solubility of INM from the various quaternary ASD formulations are shown in Table 25. Also, a phase solubility plot of solubility of INM ($\mu\text{g/ml}$) against polymer concentration (% w/v) was drawn and exhibited a linear relationship in the chosen polymer

concentration range that was examined. With regards to Figure 45, the Gibbs free energy values decreased as the % polymeric carrier loading decreased as shown in Table 24, which indicates that the drug solubilization process was indeed spontaneous (Singla *et al.*, 2019) and (Hurley *et al.*, 2018). The process is spontaneous due to the increase of ΔS_{mix} in mixing (due to increase in randomness) (Maniruzzaman *et al.*, 2015). According to the first condition of the thermodynamics of mixing, for a drug and polymer to interact there must a negative change in the free energy of mixing.

The entropy of mixing is always favoured for drug-polymer ASD mixtures. For the ASD formulations, after 24 hours the quaternary SD formulations had the highest kinetic solubility with a value of 76.30 $\mu\text{g/ml}$ (Quart SD1) with 10% INM loading as shown in Table 24. The physical mixtures with the exception of PVP VA64 SD1, PL-S630 SD1 and Quart SD1 had a greater solubility for INM compared to the SD formulations. This may have been due to recrystallization of INM due to high loading of P407 in the SD formulations.

This is a significant improvement in the solubility of INM compared to the solubility reported by Chokshi *et al.* (2008) who reported that the maximum solubility of INM achieved after 24 and 72 hours was 10 $\mu\text{g/ml}$ and 30 $\mu\text{g/ml}$ respectively, using 30, 50 and 70% INM loading. It also has been reported in literature that high poloxamer loading at high drug loads can retard drug release as a result of the gelling properties of poloxamer at high drug concentrations.

Physical mixtures tend to have a higher solubility because when the drug-polymer mixtures in the dry state are dispersed in aqueous solutions of polymer, polymeric particles hydrate rapidly due hydrophilic nature of P407 within polymer solutions resulting in the increased wettability of the drug particles (Hurley *et al.*, 2020). This is related to surface activity and wetting effect which results in reduced agglomeration and solubilizing effect of P407.

The kinetic solubility of the mixed PVP VA64 and PL-S630 systems was significantly higher than the ternary systems (Table 24). This may be due to greater vinyl acetate hydrogen bonding interaction as shown in Figure 45 in quaternary SD formulations.

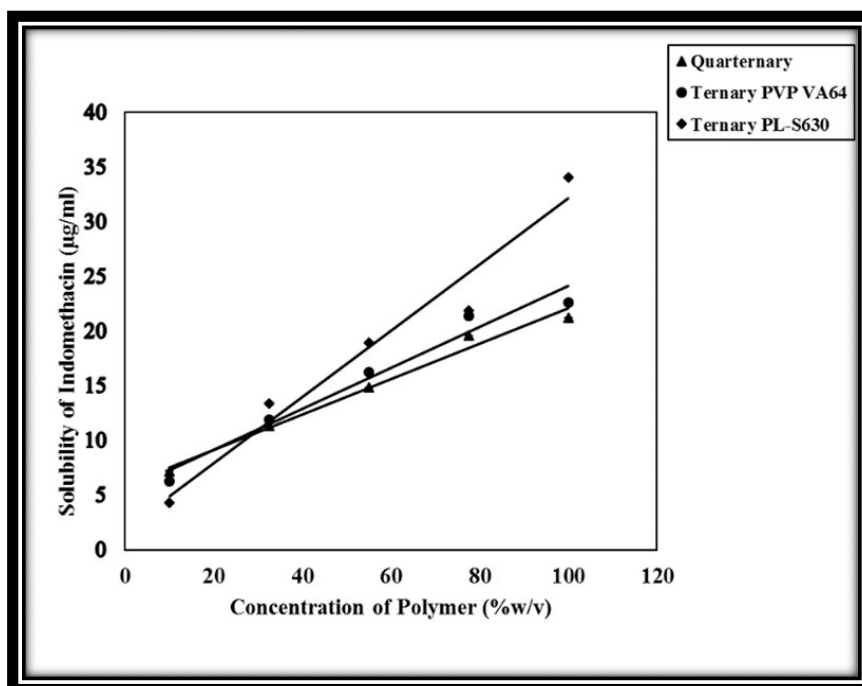


Figure 45. Solubility of INM ($\mu\text{g/ml}$) in aqueous solutions of PL-S630, PVP VA64 and P407 at 37°C (each point represents the average \pm SD of 3 independently prepared ASD samples) with a maximum kinetic solubility of $34 \mu\text{g/ml}$.

Table 24. Gibbs free energy Values and Apparent stability constants (K_a) of ternary and quaternary drug-polymer-surfactant interactions.

Concentration of P407 (%wt/vol)	Concentration of PL-S630 (%wt/vol)	Concentration of PVP VA64 (%wt/vol)	Quantity of INM added (mg)	Combined Concentration of Polymer (% wt/vol)	ΔG_{tr}^0 (kJ/mol)		
					PL-S630+P407	PVP VA64+P407	Quaternary
5	5	5	50	5	1.56	0.58	0.23
7.5	25	25	50	25	-1.37	-1.07	-0.94
10	45	45	50	45	-2.27	-1.87	-1.63
12.5	65	65	50	65	-2.64	-2.57	-2.35
15	85	85	50	85	-3.78	-2.72	-2.56
Intercept					1.90×10^0	5.42×10^0	5.96×10^0
Slope					0.30×10^0	0.19×10^0	0.16×10^0
K_a ($\mu\text{g/ml}$)					0.12	0.04	0.03

Table 25. Comparison of the solubility of INM from various quaternary and ternary SD formulations and corresponding physical mixtures in pH buffer 1.2 after 3 and 24 hours respectively.

4.1.5.6 The Effect of Cooling on Hot-Melt Extruded Amorphous Solid Dispersions

Formulation	Solubility of INM ($\mu\text{g/ml}$) after 3 hrs.		Solubility of INM ($\mu\text{g/ml}$) after 24 hrs.	
	ASD	Physical Mixture	ASD	Physical Mixture
PVP VA64 SD1	4.43	4.57	11.20	5.67
PVP VA64 SD2	7.90	21.23	5.67	4.00
PVP VA64 SD3	7.80	21.93	4.00	2.13
PVP VA64 SD4	20.73	26.50	2.13	1.50
PVP VA64 SD5	6.86	29.17	1.50	4.17
PVP VA64 SD6	9.20	19.77	4.17	0.93
PVP VA64 SD7	1.33	18.83	0.93	6.73
PVP VA64 SD8	6.47	16.23	6.73	14.00
PL-S630 SD1	13.83	4.40	14.00	14.00
PL-S630 SD2	14.03	14.80	14.00	6.43
PL-S630 SD3	8.40	7.77	6.43	10.60
PL-S630 SD4	10.60	11.57	10.60	4.37
PL-S630 SD5	0.50	7.63	4.37	8.07
PL-S630 SD6	3.37	6.70	8.07	6.90
PL-S630 SD7	2.03	7.27	6.90	4.50
PL-S630 SD8	2.83	7.13	4.50	73.60
Quart SD1	6.40	53.87	73.60	31.23
Quart SD2	12.67	45.63	31.23	23.47
Quart SD3	5.50	26.13	23.47	34.17
Quart SD4	8.03	24.30	34.17	16.77
Quart SD5	4.30	29.00	16.77	14.13
Quart SD6	4.87	22.57	14.13	16.53
Quart SD7	9.43	20.23	16.53	21.17
Quart SD8	9.53	18.50	21.17	

The INM aqueous solubility from the several ternary and quaternary SD formulations are shown in table 26. For the SD formulations, after 24 hours the quaternary SD formulations had the highest aqueous solubility with a value of 34.17 $\mu\text{g/ml}$ (Quart SD1) with 30% INM loading as shown in table 26. The SD formulations after 3 hours had a higher solubility for INM compared to the physical mixtures.

This may have been due to the conversion to the amorphous form, drug-polymer interaction and drug-polymer miscibility. Crystalline INM is present in the physical mixtures resulting in recrystallization. After 24 hours the physical mixtures had a significantly higher solubility as polymeric particles hydrated rapidly resulting in the increased wettability of the

drug particles (Hurley *et al.*, 2019). However, this depends on the % composition of drug and polymer used as shown in table 26. The kinetic solubility of the mixed copovidone systems was considerably higher than the ternary systems (Table 26) possibly because of the greater shift in the vinyl acetate carbonyl of PVP VA64/PL-S630 due to hydrogen bonding as shown in the ATR-FTIR spectra. However higher shifts do not guarantee higher kinetic solubility.

This is true when the SD comes into contact with water causing a change in the kinetics and thermodynamics of the system. The decrease in INM solubility was due to recrystallization of the API. The cooling method used also had a significant effect on the solubility of INM. For example, SD2-NT had a significantly higher solubility than SD2-AC and SD2-Liq N₂.

Table 26. Comparison of the aqueous solubility of INM and standard deviation (STD) from various quaternary and ternary SD formulations and physical blends in pH buffer 1.2 after 3 and 24 hours respectively. Physical blends contain crystalline INM.

Identifier No	Solubility of INM (µg/ml) after 3 hrs.				Solubility of INM (µg/ml) after 24 hrs.			
	SD	STD	Physical blend	STD	Physical blend	STD	SD	STD
SD1	5.50	0.40	3.27	0.03	26.13	0.01	23.47	0.03
SD2	13.00	0.15	3.30	0.00	27.30	0.02	34.17	0.00
SD3	7.80	0.69	2.74	0.00	21.93	0.00	4.00	0.00
SD4	20.73	0.65	2.59	0.01	26.50	0.01	6.13	0.01
SD5	8.40	1.20	0.97	0.01	7.77	0.01	6.43	0.01
SD6	10.60	1.20	1.47	0.01	11.57	0.015	10.60	0.01
SD2-AC	13.00	0.15	3.03	0.00	24.30	0.03	32.17	0.00
SD2-NT	14.03	0.26	4.03	0.01	27.30	0.02	34.00	0.01
SD2-Liq N ₂	12.00	1.35	2.03	0.00	15.12	0.04	20.00	0.00

The effect of cooling on the SD formulations with PVP VA64 and PL-S630 had a significant effect on the dissolution properties. After 24 hours, the SD formulation cooled to normal room temperature (NT) and air-cooled formulations had the highest aqueous solubility of INM as slow cooling of aINM increases physical stability as reported by Baghel *et al.* (2016). As SD2-NT had the highest degree of crystallinity due to the slow cooling process, it increased the solubility of INM significantly.

There was also a significant improvement in the kinetic solubility of INM after 24 hours with a maximum kinetic solubility of 34.17 $\mu\text{g/ml}$, compared to 30 $\mu\text{g/ml}$ after 72 hours reported by Chokshi *et al.* (2008) (Chokshi *et al.*, 2008). SD2-NT had the highest solubility with a value of 34.17 $\mu\text{g/ml}$ after 24 hours, which again shows that slow cooling increases solubility. Like the degree of crystallinity, there was a significant difference between SD4 and SD6 due to different solubility properties of PVP VA64 and PL-S630 as mentioned before.

4.1.7 *In-vitro* dissolution studies

4.1.7.1 Investigation of ethylene oxide-co-propylene oxide for dissolution enhancement of hot-melt extruded solid dispersions

The dissolution was performed under non-sink conditions in pH buffer 1.2 for 3 hours and pure INM was used as a control. Non-sink conditions were used to determine the supersaturated drug concentration, which could be achieved by each SD formulation. Pure crystalline INM is a weak acid with a pKa of 4.5 and displays pH-dependent solubility and dissolution rates; hence pH buffer 1.2 was used. The AUC was calculated to examine any statistical difference (* $p < 0.05$) between the SD formulations, pure INM and amorphous INM.

The mechanism of dissolution of amorphous solid dispersions, including the role of the polymer, has been discussed in literature and was clearly shown in this study. During dissolution the solubility advantage offered by the amorphous form is realised as an initial high rate of dissolution as shown in Figures 46 and 47. In the case of dissolution of the pure amorphous drug the supersaturated concentration will quickly decrease due to a high recrystallization tendency which is dependent on the extent of supersaturation.

However it has been observed that in the presence of polymer the supersaturated concentration is maintained at a higher level for a longer period of time, thus increasing the area under the dissolution curve (Huang, Staufenbiel & Bodmeier, 2022).

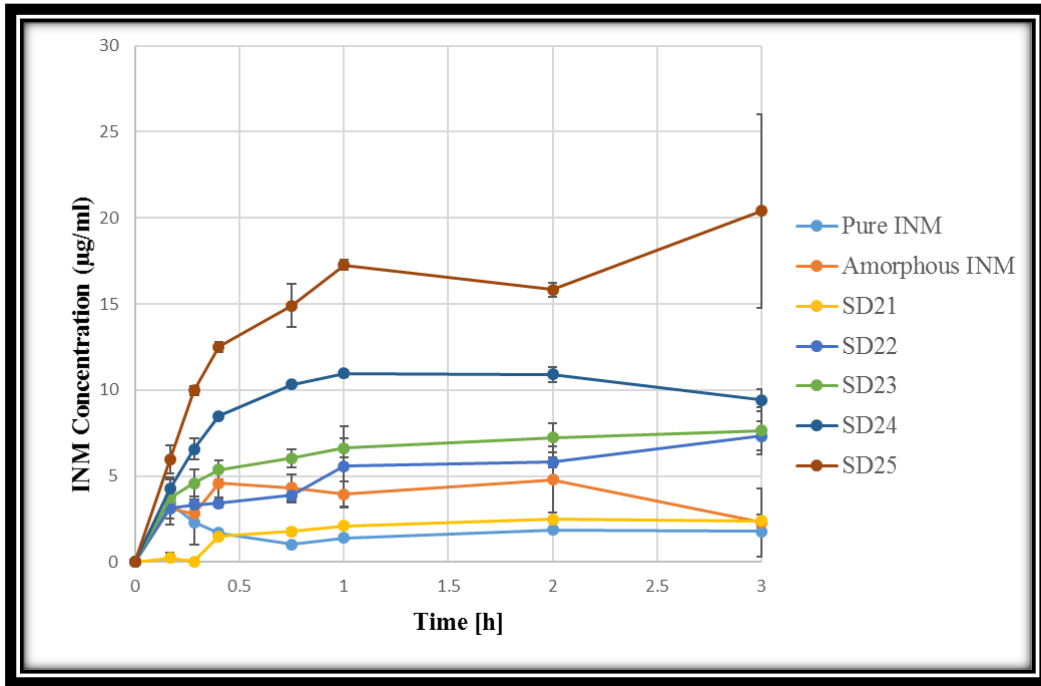


Figure 46. *Dissolution profile of 25% INM SD formulations in pH buffer 1.2.*

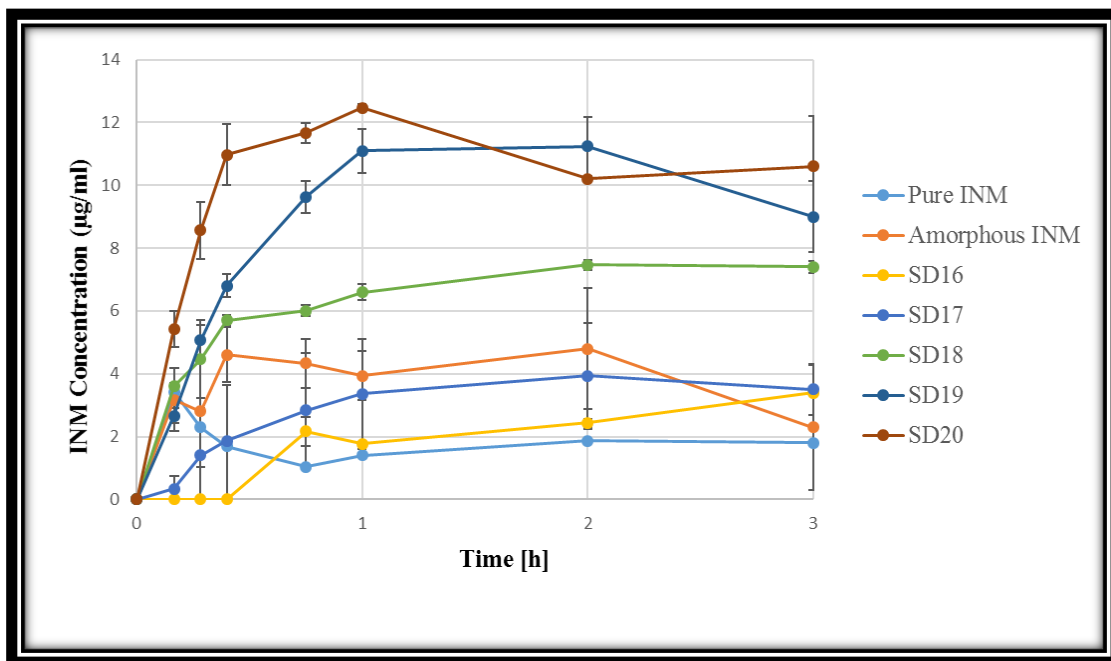


Figure 47. *Dissolution profile of 20% INM SD formulations in pH buffer 1.2.*

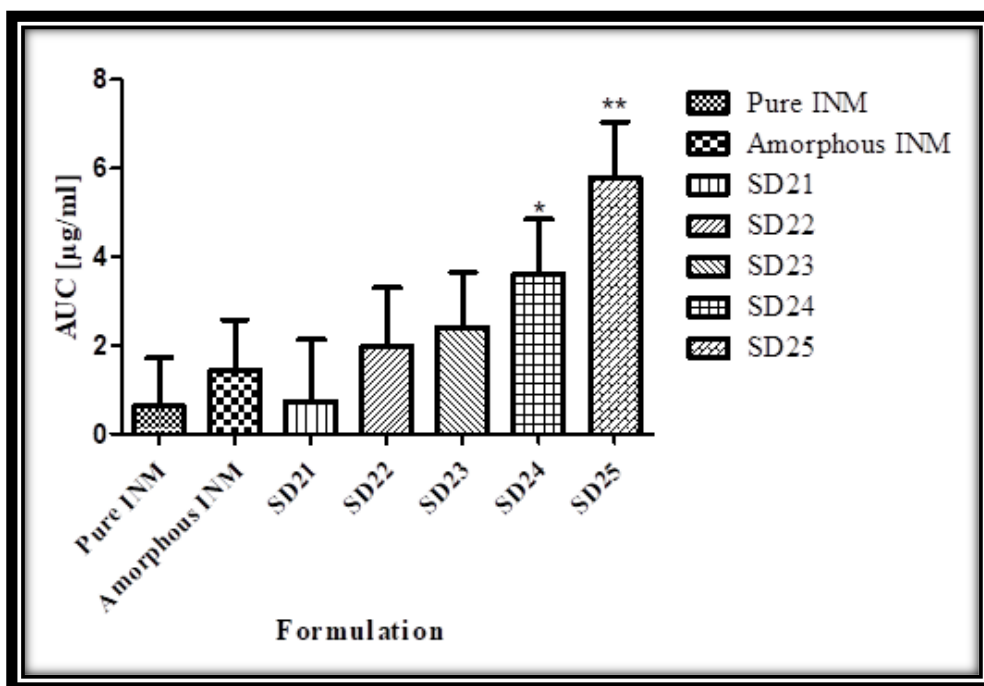


Figure 47. Graphical representations of the area under the curve (AUC) for 25% SD formulations in pH 1.2, ** and * represents statistical difference ($p < 0.05$) between SD and pure INM and aINM respectively, for a one way ANOVA and Tukey Kramer post-hoc test.

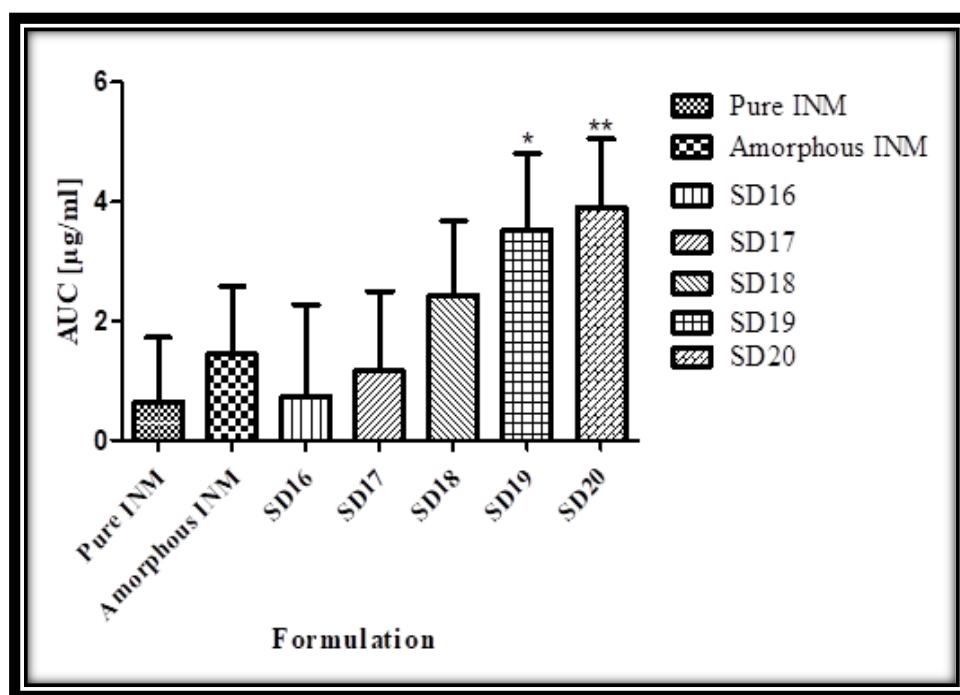


Figure 48. Graphical representations of AUC for 25% SD formulations in pH 1.2, ** and * represents statistical difference ($p < 0.05$) between SD and pure INM and aINM respectively, for a one way ANOVA and Tukey Kramer post-hoc test.

The initial high dissolution rate, attributed to the morphological form of the drug and the subsequent stabilisation effect of the polymer is known as a ‘spring and parachute’ mechanism (Li *et al.*, 2021). It has been suggested that the polymer acts to reduce the rate of recrystallization of drug, through the mechanism of stabilising the supersaturated concentration through the production of polymeric nanoparticles (Huang, Staufenbiel & Bodmeier, 2022).

The initial rate of drug release has been attributed to the rate at which the polymer dissolves, the spring parachute mechanism occurring when there is an initial fast drug release, brought about by an initial fast dissolution of polymer, producing a supersaturated drug concentration. In this way it has been observed at low drug loadings, where the drug is molecularly dispersed in the polymer, that dissolution is carrier controlled (Pina *et al.*, 2014).

Pina *et al.* (2014) proposed carrier-controlled dissolution through their work with both partially and completely amorphous dispersions (Pina *et al.*, 2014). It was observed that polymer type had more of an influence on dissolution than the morphology of the drug, partially crystalline formulations in some cases showing a higher rate of drug release than completely amorphous, suggesting a carrier-controlled mechanism.

Drug release was investigated under non-sink conditions to discover the supersaturated drug concentration which could be achieved by each formulation (figures 48 and 49). The AUC was used to calculate the dissolution efficiency for dissolution testing under sink conditions (Aldeeb *et al.*, 2022), but in the case of non-sink conditions is calculated as a measure of the supersaturated concentration and the length of time during which it can be achieved or maintained (Sun & Lee, 2013).

It is vital to take into account that the free concentration of drug within the aqueous media depends upon the aqueous solubility of the amorphous or crystalline API which depends upon the following; crystallization kinetics of the drug, interactions between drug and polymer and drug-polymer miscibility ratio. Successful formulation of amorphous solid dispersions depends on the capability of the polymeric carrier to sustain supersaturation without precipitation long enough to allow for drug absorption.

The ‘‘spring and parachute’’ effect i.e. dissolution is bought about as a rapid burst release of API due to fast dissolution of polymeric carrier produced a supersaturated drug concentration. This mechanism has been observed at all drug loadings as the drug is molecularly dispersed in the polymeric carriers, therefore dissolution is carrier controlled. P407 played a significant role in these experiments, dissolution profile of pure and amorphous INM was not significantly improved, however the SDs showed a fast release of INM as expected due to reduction of particle size, transformation of crystalline INM into its amorphous form, reduction of aggregation and agglomeration and finally improvement of drug wettability.

The phase solubility studies showed that the kinetic solubility of INM in aqueous solutions of P407 and PVP VA64 was 28 µg/ml (Figure 44). However, the kinetic solubility achieved during real - time dissolution was 21 µg/ml. This is because when the polymer and drug mixtures in the dry state were dispersed in aqueous polymer solutions, the polymer particles hydrated rapidly (because of the high hydrophilic potency of P407 into polymer solution contributing to the increased wettability of the drug particles (Hurley *et al.*, 2019).

Enhanced solubility and dissolution of INM from physical mixtures could thus be related to the surface activity, wetting effect which may lead to reduced agglomeration and hence increased surface area, and solubilizing effect of P407. The kinetic solubility of INM in the SDs increased in comparison to crystalline INM and amorphous INM. Pure INM had a kinetic solubility of 1.2 µg/ml as expected, which is in good agreement with the value reported in the literature (Tres *et al.*, 2016).

Pure amorphous INM has a kinetic solubility of 2.4 µg/ml as expected due to the conversion to the amorphous form. The increase in kinetic solubility was dependent on polymer concentration. There is a trend that as the P407 is increased so too does the concentration of drug in solution (Figures 46 and 47). The kinetic solubility of INM was increased by at least 10 times over 3 hours compared to the kinetic solubility of INM reported by Chokshi *et al.* (2008). Chokshi *et al.* (2008) prepared binary mixtures of INM-PVP VA64 and reported a kinetic solubility of 10 µg/ml for all SD formulations using 30%, 50% and 70% INM drug loading in pH buffer 1.2.

There was also an improvement in solubility achieved from the 25% drug load formulations in comparison to the 20% drug load formulations. This is shown in Figures 46 and 47 where the maximum kinetic solubility achieved from the 20% INM SD formulations was 12 µg/ml. It can be concluded from the obtained results that 0.55:0.2:0.25 ratio (SD25) was found to be superior to other ratios of the polymer.

The AUC values of each of the SD formulations was compared to the crystalline INM and aINM using a one-way ANOVA and Tukey Kramer post-hoc test (figures 48 and 49). For the 20% SDs and 25% SDs. There was no statistical difference between crystalline INM and amorphous INM for all SD formulations except for SD19, SD20, SD24 and SD25. SD20 and SD25 which were statistically different to pure and amorphous INM and SD19 and SD24 were only statistically different to pure INM. The overall effect of drug loading and wt % of polymer did have an effect on AUC and solubility of INM in solution.

The increase in the kinetic solubility of INM solid dispersions may be due to the reduction in the drug crystallinity and its colloidal and molecular dispersion within the polymeric carriers. As the polymeric carrier dissolved, the drug was exposed to dissolution medium in the form of very fine particles resulting in rapid dissolution. P407 existed in solution as a unimer but self-assembled into micelles. At concentrations that are above the critical micelle concentration, unimer molecules aggregate to form micelles (Hurley *et al.*, 2018). The hydrophobic P407 propylene oxide core of the micelle incorporated into the water-insoluble molecules of INM, which may have resulted in increased solubility of the drug molecule (Morita *et al.*, 2021).

It must be noted that apart from the higher hydrophilicity and surface properties of P407, increased wettability and dispersibility and particle size reduction of the drug, (Morita *et al.*, 2021), also may have contributed to the improved kinetic solubility of INM.

Higher hydrophilicity and surfactant properties of P407 result in greater wetting and increase in the surface available by reducing interfacial tension between the water-insoluble drug and dissolution medium.

Hurley *et al.* (2019) reported that in high P407 loading can retard drug release. This may be due to the gelling property of poloxamer at higher concentrations. In this study this may also have been the case as recrystallization of the INM was shown at higher drug ratios of P407 and may have resulted in retarded drug release after 3 hours. As P407 was present in its semi-crystalline form, this may also have contributed to the recrystallization of the INM during *in-vitro* dissolution studies.

4.1.7.2 An investigation of the inter-molecular interaction, solid-state properties and dissolution properties of mixed copovidone hot-melt extruded solid dispersions

To further understand how the intermolecular interactions within multi-component i.e. quaternary and ternary SDs affect the INM dissolution profile in pH buffer 1.2, *in-vitro* dissolution experiments were performed under non-sink conditions. The aim of this study was to examine the synergistic effect of the various polymer combinations within SDs and how it affected the maintenance of INM supersaturation. Pure INM and amorphous INM were also used as a control similar to the previous study. The AUC was calculated as a measure of the length of time that the supersaturated concentration could be maintained or achieved i.e., a measure of the supersaturated concentration (Potter *et al.*, 2015). The AUC was used to compare the solubility of INM between selected SD formulations and pure/amorphous INM. Particle size was controlled in this study, the initial drug dosage within the dissolution vessels was 100mg as the particle size of each formulation was 200 microns as they were sieved prior to analysis.

Pina *et al.* (2014) proposed dissolution that is carrier controlled through their work with both completely and partially controlled amorphous dispersions (Pina *et al.*, 2014). It was observed that the type of polymer used had a significant effect on the dissolution compared to the morphology of the drug, partially crystalline formulations showed a higher rate of drug release in some cases compared to completely amorphous, therefore they proposed a controlled carrier mechanism.

The drug release curves however in this study did not exhibit the spring and parachute effect; however, they showed an increase in the drug concentration over 3 hours of dissolution.

However, it must be noted that a spring and parachute effect can still be seen as SDs readily show a ‘spring’ and the parachute effect, may however be a slow parachute with supersaturation sustaining for many hours before precipitation starts to occur to define the parachute phase. It must be noted that all SD formulations did not completely dissolve over the entire duration of the dissolution study. Therefore, it is assumed that neither the polymer nor the drug completely dissolves over the 3 hours in pH buffer 1.2. Potter *et al.* (2015) prepared ASDs containing 10, 30 and 50% INM via supercritical fluid impregnation and hot melt extrusion and reported that polymer and INM did not completely dissolve even after 8 hours of dissolution (Potter *et al.*, 2015).

The kinetic solubility of all SD formulations increased compared to pure and amorphous INM (Figure 50). Amorphous and crystalline INM had a kinetic solubility of 2.4 µg/ml and 1.2 µg/ml as expected due to its conversion to the amorphous form. The increase in the kinetic solubility of INM was dependent upon both surfactant and polymeric carrier loading. The kinetic solubility of INM in this study increased by at least 10 times over 3 hours. Chokshi *et al.* (2008) prepared binary drug-polymer mixtures of PVP-VA64-INM using HME and achieved a maximum kinetic solubility of 10 µg/ml after 12 hours for all solid dispersions prepared using 70, 50 and 30% INM in pH buffer 1.2 (Chokshi *et al.*, 2008). It was also a significant improvement compared to the kinetic solubility of INM reported by Potter *et al.* (2015) who prepared binary mixtures of INM and PVP via hot melt extrusion and supercritical fluid impregnation and achieved a maximum kinetic solubility of 8 µg/ml after 8 hours.

There was very little difference in terms of solubility between both the ternary SD formulations and quaternary SD formulations after 3 hours as shown in Figure 50. In this study PVP VA64 had the highest kinetic solubility with a value of 20.73 µg/ml (PVP VA64-SD4 (30% INM)) after 3 hours of dissolution. This was a similar result to the solubility from the previous study where the maximum solubility reported was 20 µg/ml with a 25% drug loading (Hurley *et al.*, 2018). The SDs with highest poloxamer loading had the highest solubility after 3 hours. This increase in solubility was related to the intermolecular interaction between drug and polymer and drug-polymer miscibility.

The hydrophobic P407 propylene oxide core of the micelle which incorporated into the INM water-insoluble molecules also played a significant role in the increase in solubility of INM. P407 exists as a unimer self-assembled into micelles in solution. This may have resulted in the increased kinetic solubility of INM molecules. P407 results in greater wetting and increases the surface that is available by reducing the interfacial tension between the dissolution medium and the poorly water-soluble drug. Reduced interfacial tension reduces the nucleation activation energy (Thakur, Sheokand & Bansal, 2019), therefore reducing recrystallization.

The AUC values of all SD formulations were compared with pure and amorphous INM using a 1-way ANOVA and Tukey Kramer post hoc test (figure 50). For both the quaternary, PL-S630 and PVP VA64 ternary ASD formulations with the exception of Quart SD2, Quart SD4, Quart SD7, Quart SD8, PVP VA64 SD2, PVP VA64 SD4, PL-S630 SD1, PL-S630 SD2 and PL-S630 SD4 there was no statistical difference between crystalline and amorphous INM. The overall effect of drug and % wt of poloxamer did have a significant effect on the solubility of INM and AUC in solution.

After 3 hours, the SD formulations did have a higher kinetic solubility compared to the pure and amorphous drug due to the conversion to the amorphous form (figure 50). The samples that contained the highest drug loading recrystallized because of 1) the presence of crystalline INM, as it is higher to achieve the amorphous state using a high drug loading, 2) no inter-molecular interaction between drug and polymer and 3) drug-polymer immiscibility. For the quaternary mixtures only all ASDs with the highest % of poloxamer loading recrystallized with the exception of Quart SD4 and Quart SD8 as previously reported by Hurley *et al.* (2018) due to its gelling properties and its semi-crystalline nature of P407.

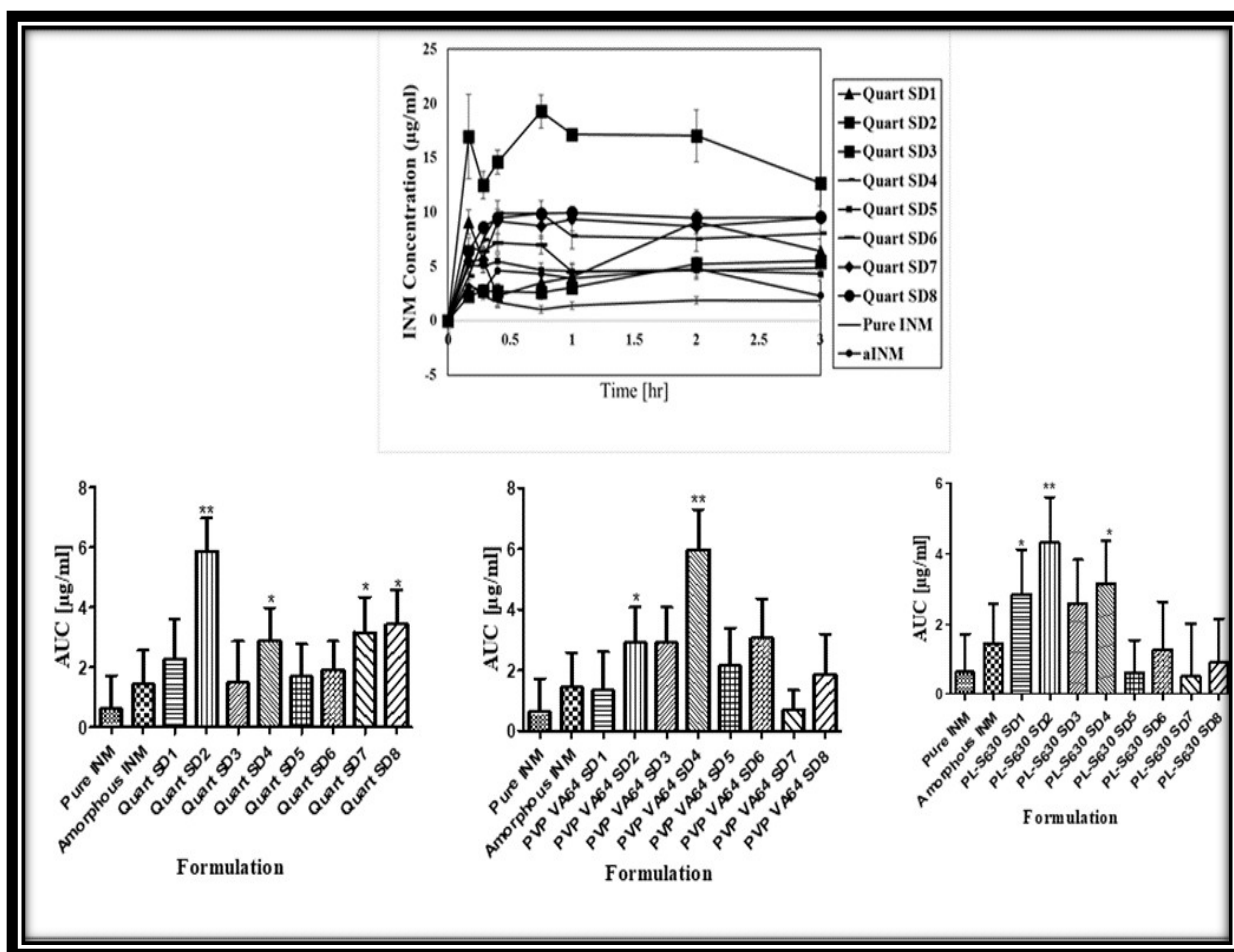


Figure 50. *In-vitro* dissolution profiles of quaternary SDs and graphical representations of AUC of quaternary and ternary SD formulations in pH 1.2. ** and * represents the statistical difference ($p < 0.05$) between SD, aINM and pure INM respectively, for 1-way ANOVA and Tukey Kramer post hoc test.

4.1.7.3 The Effect of Cooling on Hot-Melt Extruded Amorphous Solid Dispersions

The *in-vitro* dissolution rates of INM and selected SD formulations, shown in Table 9 and 10, were performed using non-sink conditions in pH buffer 1.2. Table 27 shows the concentration of INM ($\mu\text{g/ml}$) at various time intervals over 3 hours. Control of the particle size of each formulation was vital in this study, as it can affect dynamic solubility of each formulation. The particle size of each formulation was 200 microns to ensure uniformity. The formulation equal to 100 mg of INM was placed within the dissolution vessels.

It is important to note that there was no interference from the polymers and therefore did not affect the value of UV absorption. The λ max for both PL-S630 and PVP VA64 is 440 nm for vinyl-pyrrolidone and 258 nm for vinyl acetate as stated in literature (Hurley *et al.*, 2020). INM has a λ max of 320 nm.

The aqueous solubility of crystalline and amorphous INM was 1.2 and 2.4 $\mu\text{g/ml}$ respectively (Hurley *et al.*, 2018). Non-sink conditions were used for this study as crystallization of APIs and nucleation within supersaturated dissolution conditions can be observed (Zhang *et al.*, 2017). An illustration of non-sink conditions is shown in figure 51. In figure 50, the SD has no initial crystallinity due to the conversion to the amorphous state, but several crystals grow during the dissolution test as the supersaturation generated results in phase separation and nucleation (Liu *et al.*, 2013). The dissolution of dissolved INM depended upon the dissolution rate comparative to the rate of crystallization. If the dissolution rate is too rapid relative to crystallization, then 100% release may be achieved, with a subsequent decrease in the solution concentration as crystallization occurs (shown in figure 51). If the rate of crystallization is rapid compared to the dissolution rate, then 100% drug release will not be achieved and will display a “spring” and “parachute” effect which is the case in this study.

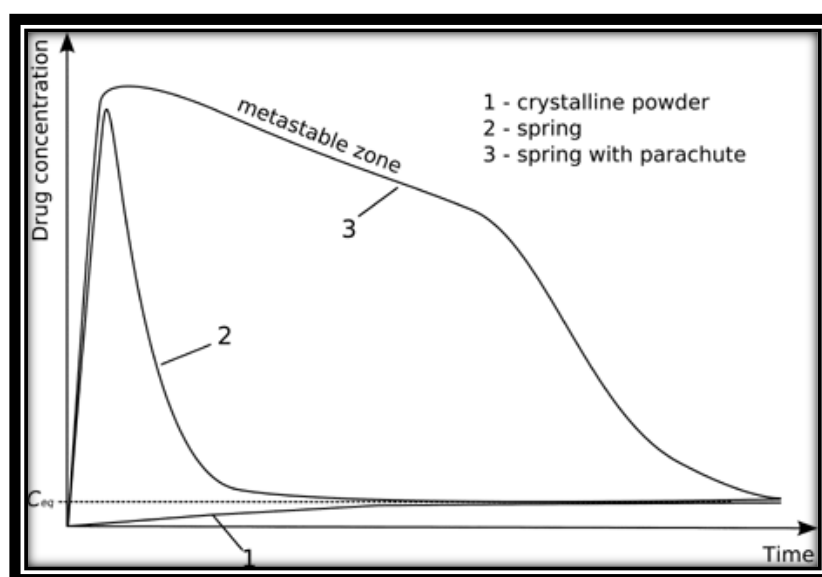


Figure 51. Illustration of non-sink conditions used in the dissolution test. Dissolution profile 1: dissolution of the crystalline API; profile 2: dissolution of a “spring” effect of the API without the presence of dissolution enhancers profile 3: dissolution of a ‘spring’ and ‘parachute’ form of the API in the presence of dissolution enhancers act as a “parachute.” C_{eq} represents equilibrium solubility.

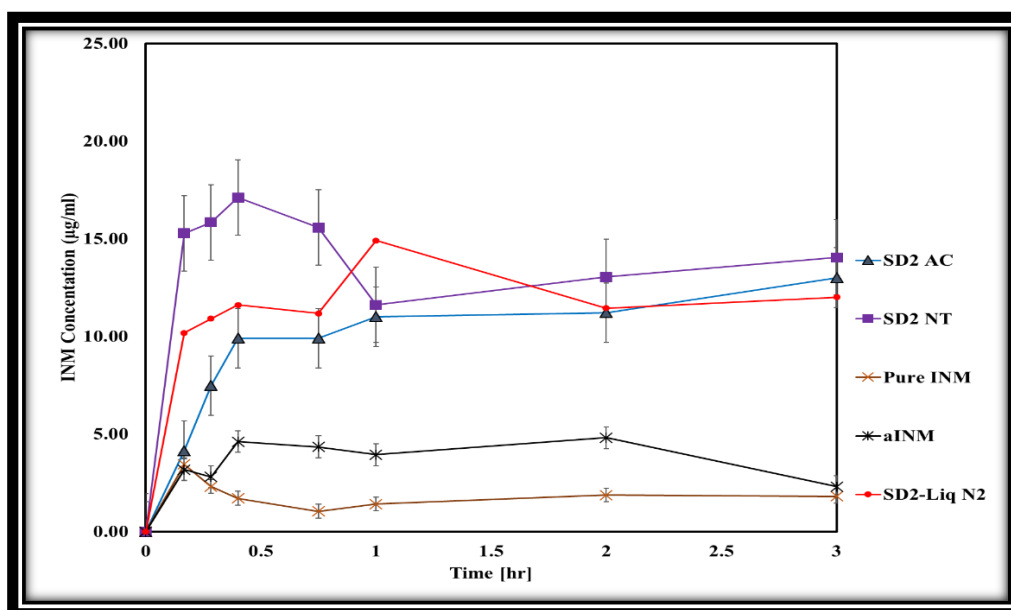


Figure 52. *In-vitro* dissolution profiles of air-cooled SD formulations performed in buffer of pH 1.2.

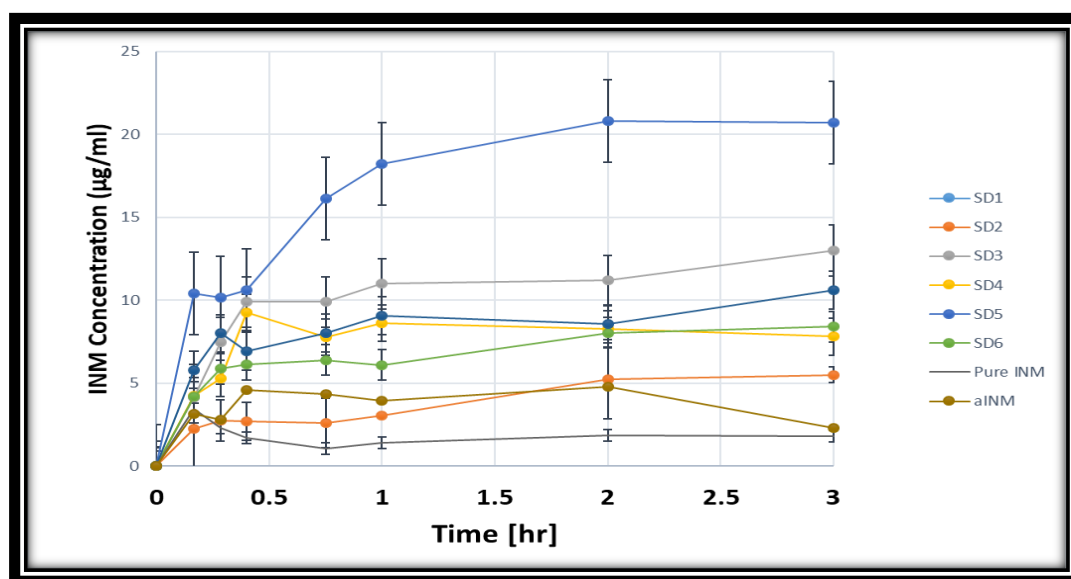


Figure 53. *In-vitro* dissolution profiles of quaternary SD formulations performed in buffer of pH 1.2. The maximum aqueous solubility is 20.73 µg/ml after 3 hours. (AC= Air cooled, NT= Normal room temperature and Liq N₂ = Liquid Nitrogen).

Table 27. Comparison of the aqueous solubility of INM from various quaternary and ternary SD formulations in pH buffer 1.2 taken at various time intervals over 24 hours.

Identifier	Conc. of INM (µg/ml) at 0 hours.	Conc. of INM (µg/ml) at 0.2 hours.	Conc. of INM (µg/ml) at 0.3 hours.	Conc. of INM (µg/ml) at 0.4 hours.	Conc. Of INM (µg/ml) at 0.75 hours.	Conc. of INM (µg/ml) at 1 hours.	Conc. of INM (µg/ml) at 2 hours.	Conc. of INM (µg/ml) at 3 hours.
SD1	0.00	2.27	2.73	2.70	2.60	3.07	5.23	5.50
SD2	0.00	4.13	7.46	9.90	9.90	11.00	11.20	13.00
SD3	0.00	4.23	5.30	9.27	7.77	8.63	8.27	7.80
SD4	0.00	10.40	10.17	10.63	16.13	10.80	20.83	20.73
SD5	0.00	4.17	5.87	6.13	6.40	6.10	8.03	8.40
SD6	0.00	5.80	8.00	6.93	8.03	9.07	8.57	10.60
SD2-AC	0.00	4.13	7.46	9.90	9.90	11.00	11.20	13.00
SD2-NT	0.00	15.27	15.83	17.10	15.57	11.60	13.03	14.03
SD2-Liq N ₂	0.00	10.17	10.90	11.60	11.17	14.90	11.43	12.00

Table 28. Comparison of the aqueous solubility of INM from various quaternary and ternary SD formulations in pH buffer 1.2 after 3 and 24 hours. Supersaturation parameter (SP) was calculated for SD formulations after 3 hours.

Identifier No	No. of Phases	Conc. of INM, 3 hours. (µg/ml)	STD	Conc. of INM, 24 hours. (µg/ml)	STD	SP of INM after 3 hours.
SD1	2	5.50	0.40	23.47	0.01	0.97
SD2	2	13.00	0.15	34.17	0.02	0.98
SD3	2	7.80	0.69	4.00	0.00	0.49
SD4	2	20.73	0.65	6.13	0.01	0.24
SD5	2	8.40	1.20	6.43	0.01	0.56
SD6	2	10.60	1.20	10.60	0.015	0.45
SD2-AC	2	13.00	0.15	32.17	0.03	0.49
SD2-NT	2	14.03	0.26	34.00	0.02	0.70
SD2-Liq N ₂	2	12.00	1.35	20.00	0.04	0.30

In this study there was a tendency that as the concentration of P407 increased, the drug concentration also increased (figures 52 and 53). The aqueous solubility of dissolved INM significantly increased compared to the values reported in literature. Chokshi *et al.* (2008) prepared INM-PVP VA64 binary mixtures and recorded a kinetic solubility of 10 µg/mL and 30 µg/ml in pH buffer 1.2 after 24 and 72 hours using 30% INM.

Table 28 shows the SP of INM after 3 hours in pH buffer 1.2 under non-sink conditions. For the purposes of this work, only the supersaturation parameter (SP) of SD formulations after 3 hours was selected and calculated. According to Chen *et al.* (2015), SP apparently is a dimensionless parameter with a range between zero and one. Zero means no supersaturation power, while one indicates the tendency of drug precipitation to occur is reduced (Chen *et al.*, 2015). SP is a function of the chemical structure of the drug, initial drug concentration, type of polymer and concentration of polymer (Hurley *et al.*, 2020).

Table 28 shows that all formulations had a SP value of 0.24 or above indicating that the INM was resilient against drug precipitation, however the quaternary formulation SD1 contained the highest SP value indicating that polymer type and concentration of polymer had a significant effect on the ability of the SD to inhibit drug precipitation and recrystallization.

During the extrusion process, INM was transformed to the amorphous state in all SD formulations. Therefore, as a result the aqueous solubility of INM was significantly greater compared to both amorphous and crystalline INM with a maximum aqueous solubility of 20.73 µg/ml. This study also showed that the cooling method used for extrusion had a significant impact on the kinetic solubility of INM. The highest aqueous solubility observed was 34.00 µg/ml for SD2 NT containing 30% INM after 24 hours. The dissolution concentration increased by 10 times as compared to pure and amorphous drug.

All SD formulations with highest P407 loading (15%) had a significantly higher solubility compared to the 5% P407 formulations after 3 hours. The significant increase in aqueous solubility was related to the degree of crystallinity, cooling process used and interaction between polymeric carrier and API including polymer-drug miscibility. The P407 micelle core contains propylene oxide which is hydrophobic which when incorporated into INM resulted in increased solubility of INM. P407 in nature is a unimer which when placed into solution can form micelles via self-assembly (Hurley *et al.*, 2020).

According to Suksiriworapong *et al.* (2013) the critical micelle concentration of P407 is 2.8×10^{-8} M (0.03 $\mu\text{g/ml}$), as the concentration of drug and SD formulations in this study was greater than 0.03 $\mu\text{g/ml}$ it resulted in micelle formation as shown in table 28 (Suksiriworapong *et al.*, 2014). Also, the degree of crystallinity was significantly lower in the higher P407 loadings, increasing solubility. P407 can result in many benefits such as greater wetting, increasing surface area and decreasing interfacial tension between API and the dissolution medium. It is stated in literature that reducing the interfacial tension decreases nucleation (Zhao *et al.*, 2020).

The recrystallization of amorphous INM in solid solutions was dependent upon three factors; % P407 loading, degree of P407 crystallinity and cooling method used. It is well reported in literature that high P407 loading can lead to recrystallization due to the hydrophobic P407 propylene oxide core (Hurley *et al.*, 2018). Slow cooling is ideal for a process that does not require high energy removal. It is less expensive regarding extrusion, it is easier to maintain, has lower operating costs compared to liquid nitrogen and requires less space compared to fluid cooling.

The AUC of pure and aINM was compared to the AUC of each SD formulation using statistical analysis. The statistical tests used were Tukey Kramer post hoc test and 1-way ANOVA (figure 53). For both the quaternary and ternary SD formulations with the exception of SD2, SD4, and SD6 there was no statistical difference between amorphous and crystalline INM. The overall effect of drug, polymer concentration and % wt. of P407 did have a significant effect on the solubility of INM and AUC in solution.

Figure 54 shows that the formulations containing the highest P407 loading were statistically different to crystalline INM which shows that the increase in P407 increased the solubility of INM as reported by Hurley *et al.* (2018). Figure 54 also shows that cooling had a significant effect on solubility. SD2-NT had the highest solubility after 3 and 24 hours with values of 14.03 $\mu\text{g/ml}$ and 34.00 $\mu\text{g/ml}$. Whereas the rapid cooling method SD2- Liq N₂ had a solubility of 12.00 $\mu\text{g/ml}$ and 20.00 $\mu\text{g/ml}$ respectively. This corresponds to the XRPD results for the degree of crystallinity, with SD2-NT having the highest XRPD Bragg peak intensities compared to SD2- AC for example. The greater the solubility, the greater the crystallinity present. SD2-NT had the highest aqueous solubility due to the slow cooling process. Therefore, cooling influenced the solubility of INM and AUC in solution (Hurley *et al.*, 2018).

The solubility also depended upon the polymeric carrier used as mentioned already. There was a significant difference in solubility between SD4 and SD6 which contain PVP VA64 and PL-S630 respectively. SD4 had a kinetic solubility of 20.73 $\mu\text{g/ml}$ compared to 10.60 $\mu\text{g/ml}$ for SD6. It is important to note that the different solid-state and dissolution properties of PVP VA64 and PL-S630 significantly affect the solubility of INM achieved.

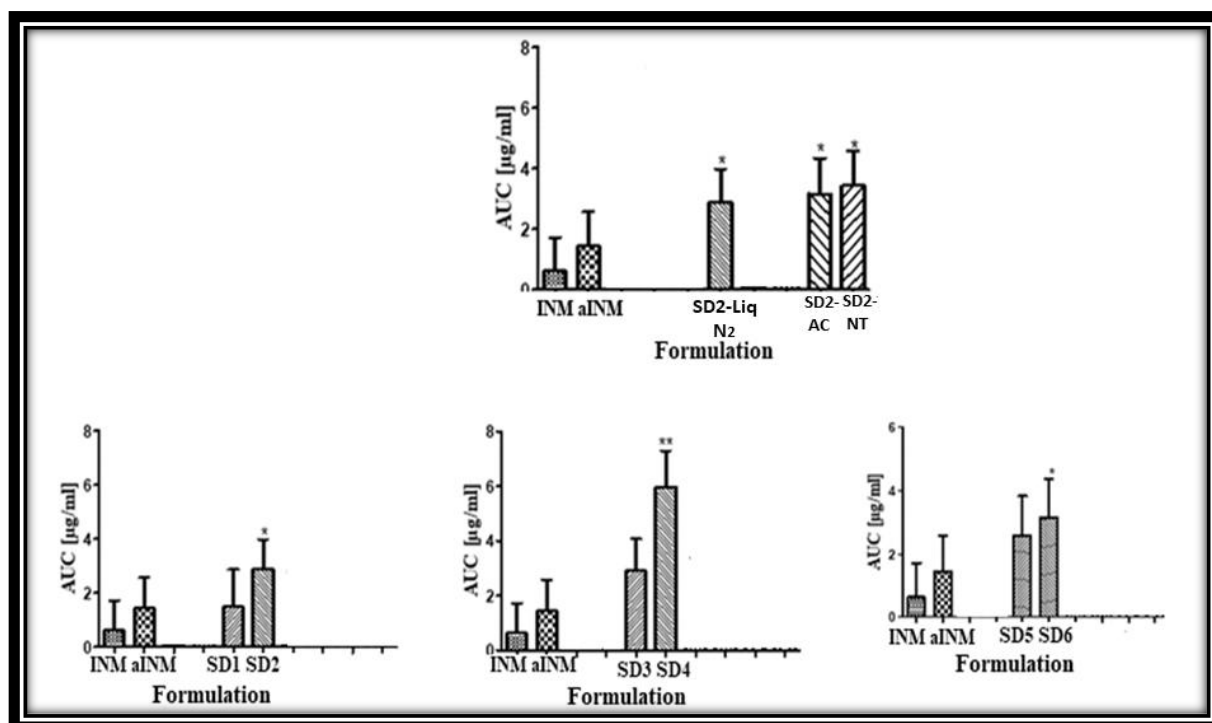


Figure 54. Graphical representations of AUC of quaternary and ternary SD formulations in pH 1.2. ** and * represents the statistical difference ($p < 0.05$) between SD, aINM and pure INM respectively, for 1-way ANOVA and Tukey Kramer post hoc test. (AC= Air cooled, NT= Normal room temperature and Liq N₂ = Liquid Nitrogen).

4.1.8 Accelerated stability studies

The 25 completely amorphous hot-melt extruded formulations were subjected to conditions of 40°C and 75% relative humidity for 5 months, after which XRPD was used to examine the crystalline nature of the samples. XRPD was only for the SD formulations used to examine the effect of cooling on SD formulations in relation to amorphous stability. Potter *et al.* (2015) and Sinclair *et al.* (2011) reported the relatively instability of SD formulations as a result of moisture uptake due to the hygroscopic nature of PVP.

As water can act as a plasticizer, it has been reported in literature that water can lower the glass transition temperatures of SD Formulations and enhances the mobility of polymer and drug (Sinclair *et al.*, 2011).

Monzural *et al.* (2010) also reported that the addition of semi-crystalline polymers can result in recrystallization of the API over long periods of time. P407 which is semi-crystalline in nature did not seem to have any effect on the amorphous stability of INM after 5 months and no recrystallization was observed, the SD formulations which contained 0% P407 were also amorphous. Therefore, the addition of P407 did not contribute to the amorphous stability of the SD formulations as shown in Figure 55.

XRPD confirmed that after 5 months INM remained amorphous for all SD formulations (figure 55). The Bragg peaks associated with crystalline INM were completely absent in all XRPD diffractograms of SDs after 5 months. In the XRPD diffractograms shown in figure 55 after 5 months' stability, the Bragg peaks associated with crystalline INM were completely absent. XRPD confirmed that INM was stable after 5 months' stability studies. This was also shown by Hurley *et al.* (2018) where SDs were prepared using INM as a model drug. All SDs remained amorphous as a result of conversion from the crystalline to amorphous state and as a result of the high molar attraction constant of INM, hydrogen bonding and drug-polymer miscibility. This shows that all ASD formulations are miscible as predicted by the HSPs in Table 1. The results also confirm that the cooling method used did not have significant impact on the amorphous stability of INM, (Hurley *et al.*, 2020), as the higher Bragg peak intensities in SD2 AC, SD2 Liq N₂ and SD2 NT were the same before and after 5 months stability.

This was also shown by Hurley *et al.* (2018) where SDs were prepared using INM as a model drug. All SDs remained amorphous as a result of conversion from the crystalline to amorphous state and as a result of the high molar attraction constant of INM, hydrogen bonding and drug-polymer miscibility (Hurley *et al.*, 2020). This shows that all ASD formulations are miscible as predicted by the HSPs in Table 1.

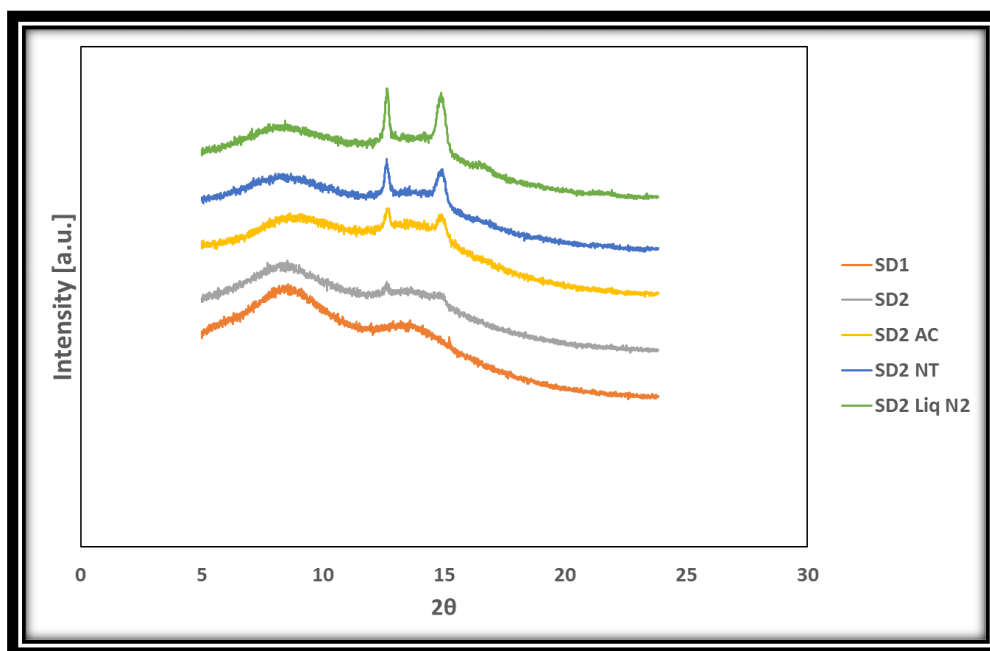


Figure 54. XRPD diffractograms of SD formulations and XRPD diffractograms of the SD formulation used to investigate the effect of cooling after 5 months of a stability study under accelerated conditions of 40 °C and 75% RH. P407 was still present in its crystalline form in all formulations (AC= Air cooled, NT= Normal room temperature and Liq N₂ = Liquid Nitrogen).

Chapter five

Conclusion

and future

work

5.0 Conclusion & future work

5.1 Conclusion

XRPD confirmed that INM was successfully converted into the amorphous form via the hot melt extrusion process. The cooling method used did have any effect on the amorphous stability when air cooled, cooled to normal room temperature and cooled via liquid nitrogen. However, cooling and the type of polymeric carrier used had a significant effect on the nature of crystallinity and solubility of INM. It is also important to note that in the formulations with the higher P407 loadings had a much higher Bragg peak intensity.

Both ATR-FTIR and Raman spectroscopy confirmed the presence of hydrogen bonding between the amide carbonyl of PVP VA64/PL-S630 and the –OH group of the carboxylic acid of INM as expected. Raman spectroscopy confirmed that there was a shift in the vinyl acetate carbonyl meaning that the vinyl acetate carbonyl is involved in hydrogen bonding. ATR-FTIR spectroscopy also confirmed that P407 does not interact with INM at a molecular level. Solubility studies of INM showed a significant increase in the kinetic solubility of INM compared to crystalline INM at 37 °C in pH 1.2. The SD formulations showed a significantly higher dissolution rate of 20.63 µg/ml. The XRPD stability data showed that the cooling method used did have a significant effect on the amorphous stability of INM as all SD formulations remained amorphous after 5 months' stability testing.

The results of the solubility studies show that the greater the P407 loading used and/or crystallinity, the greater the solubility. However, the cooling process used, significantly affected the crystallinity and solubility also as SD2-NT had the highest aqueous solubility for dissolved INM and the highest crystallinity due to the slow cooling process. Slow cooling therefore enhances physical stability and solubility as reported by Baghel *et al.* (2015). This work illustrates the significance of examining the cooling method used in order to improve the aqueous solubility, amorphous stability and solid-state properties of BCS class II drugs.

5.2 Future work

A comparative study of the effect of different processing techniques (spray drying, HME and supercritical fluid) on SDs using semi-crystalline polymers (ternary and binary) would be of great interest in establishing the ideal method for a drug-polymer formulation. The resulting SDs could be analysed via hyper DSC, XRPD, FTIR, SEM and ssNMR to examine drug loading within a polymeric material, % yield efficiency, drug-polymer miscibility, phase separation, molecular mobility and amorphous stability of the dispersion. In-vitro dissolution studies should also be performed in simulated gastric and intestinal fluids and drug release kinetics could be examined. Furthermore, the SDs should also be assessed to see if additional polymers or surfactants are required to stabilise the supersaturated state.

The recrystallization kinetics of amorphous APIs in SDs (ternary and binary) and the role of polymers in decreasing the rate of crystallization could be studied. The amorphous SDs should be subjected to accelerated stability studies at different temperatures and relative humidity. Humidity-adjusted Arrhenius kinetics could be employed to model the recrystallization kinetics. Although this has been used in the study of drug degradation, it is novel to apply this technique for same. The stability study could show the effect of humidity and temperature on the SD and may help in predicting and determining the storage conditions and shelf life of the product. The different mechanism in which polymers stabilize the amorphous API such as hydrogen bonding, anti-plasticization or reduction in molecular mobility could be assessed via hyper DSC, FTIR, XRPD and NMR.

Formulating SDs into dosage forms and examining their characteristics is a logical and common-sense approach and/or progression of this work. Various multi-component SDs and excipients should be studied. The final dosage form should be characterized for micromeritics properties, uniformity of weight and content, friability test and hardness test as per United State Pharmacopoeia (USP) guidelines. Further in-vitro dissolution studies should be performed using gastric and intestinal fluid to determine the drug-release profile. A long term stability study could be carried out in order to study the stability of the preliminary dosage formulation as per ICH guidelines.

References

References

1. Abdeltawab, H., Svirskis, D & Sharma, M. (2020). Formulation strategies to modulate drug release from poloxamer based in situ gelling systems. *Expert Opinion on Drug Delivery*, 17(4), pp. 495–509.
2. Aldeeb, R., El-Miligi, M., El-Nabarawi, M., Tag, R., Amin, H & Taha, A. (2022). Enhancement of the Solubility and Dissolution Rate of Telmisartan by Surface Solid Dispersions Employing Superdisintegrants, Hydrophilic Polymers and Combined Carriers. *Scientia Pharmaceutica*, 90(4), pp. 71.
3. Almeida, M., Magalhães, M., Veiga, F & Figueiras, A. (2017). Poloxamers, poloxamines and polymeric micelles: Definition, structure and therapeutic applications in cancer. *Journal of Polymer Research*, 25(1), pp. 31.
4. Altamimi, M & Neau, S. (2015). Use of the Flory–Huggins theory to predict the solubility of nifedipine and sulfamethoxazole in the triblock, graft copolymer Soluplus. *Drug Development and Industrial Pharmacy*, 42(3), pp. 446-455.
5. Alzahrani, A; Nyavanandi, D; Mandati, P; Adel Ali Youssef, A; Narala, S; Bandari, S & Repka, M. (2022). A systematic and robust assessment of hot-melt extrusion-based amorphous solid dispersions: Theoretical prediction to practical implementation. *International Journal of Pharmaceutics*, 624, pp. 121951.
6. Baghel, S., Cathcart, H & O'Reilly, N. (2016). Polymeric Amorphous Solid Dispersions: A Review of Amorphization, Crystallization, Stabilization, Solid-State Characterization, and Aqueous Solubilization of Biopharmaceutical Classification System Class II Drugs. *Journal of Pharmaceutical Sciences*, 105(9), pp. 2527-2544.
7. Baghel, S., Cathcart, H & O'Reilly, N. (2018). Investigation into the Solid-State Properties and Dissolution Profile of Spray-Dried Ternary Amorphous Solid Dispersions: A Rational Step toward the Design and Development of a Multicomponent Amorphous System. *Molecular Pharmaceutics*, 15(9), pp. 3796–3812.
8. Baghel, S., Cathcart, H., Redington, W & O'Reilly, N. (2016). An investigation into the crystallization tendency/kinetics of amorphous active pharmaceutical ingredients: A case study with dipyridamole and cinnarizine. *European Journal of Biopharmaceutics*, 104, pp. 59–71.
9. Benmore, C., Benmore, S., Edwards, A., Shrader, C., Bhat, M., Cherry, B & Weber, J. (2021). A High Energy X-ray Diffraction Study of Amorphous Indomethacin. *Journal of Pharmaceutical Sciences*, 111(3), pp. 818-824.

10. Bertoni, S., Albertini, B & Passerini, N. (2023). Investigating the physicochemical properties of solid dispersions based on semicrystalline carriers: A case study with ketoprofen. *International Journal of Pharmaceutics*, 632, 122576.
11. Blaabjerg, L., Bulduk, B., Lindenberg, E., Löbmann, K., Rades, T & Grohganz, H. (2019). Influence of Glass Forming Ability on the Physical Stability of Supersaturated Amorphous Solid Dispersions. *Journal of Pharmaceutical Sciences*, 108(8), pp. 2561–2569.
12. Budiman, A., Lailasari, E., Nurani, N., Yunita, E., Anastasya, G., Aulia, R & Aulifa, D. (2023). Ternary Solid Dispersions: A Review of the Preparation, Characterization, Mechanism of Drug Release, and Physical Stability. *Pharmaceutics*, 15(8), pp. 2116.
13. Chan, S., Chung, Y., Cheah, X., Tan, E & Quah, J. (2015). The characterization and dissolution performances of spray dried solid dispersion of ketoprofen in hydrophilic carriers. *Asian Journal of Pharmaceutical Sciences*, 10(5), pp. 372-385.
14. Chauvet, M., Sauceau, M & Fages, J. (2017). Extrusion assisted by supercritical CO₂: A review on its application to biopolymers. *The Journal of Supercritical Fluids*, 120, pp. 408-420.
15. Chen, Y., Liu, C., Chen, Z., Su, C., Hageman, M., Hussain, M & Qian, F. (2015). Drug–Polymer–Water Interaction and Its Implication for the Dissolution Performance of Amorphous Solid Dispersions. *Molecular Pharmaceutics*, 12(2), pp. 576-589.
16. Chokshi, R., Shah, N., Sandhu, H., Malick, A & Zia, H. (2008). Stabilization of Low Glass Transition Temperature Indomethacin Formulations: Impact of Polymer-Type and Its Concentration. *Journal of Pharmaceutical Sciences*, 97(6), pp. 2286–2298.
17. Choudhury, D., Murty, U & Banerjee, S. (2023). Selection of appropriate dapsone and poly(1-vinylpyrrolidone-co-vinyl acetate) ratios for the preparation of amorphous solid dispersions. *Heliyon*, 9(3), pp. 14167.
18. Correa-Soto, C., Gao, Y., Indulkar, A., Zhang, Z & Taylor, L. (2022). Role of surfactants in improving release from higher drug loading amorphous solid dispersions. *International Journal of Pharmaceutics*, 625, pp. 122120.
19. Csicsák, D., Szolláth, R., Kádár, S., Ambrus, R., Bartos, C., Balogh, E & Völgyi, G. (2023). The Effect of the Particle Size Reduction on the Biorelevant Solubility and Dissolution of Poorly Soluble Drugs with Different Acid-Base Character. *Pharmaceutics*, 15(1), pp. 278.
20. Davis, D. M., Supawan Santitewagun, J., Axel Zeitler, S & Williams, R. (2021). Formulating a heat- and shear-labile drug in an amorphous solid dispersion: Balancing drug degradation and crystallinity. *International Journal Of Pharmaceutics: X*, 3, pp. 100092.

21. De Mohac, L., Raimi-Abraham, B., Caruana, R., Gaetano, G & Licciardi, M. (2020). Multicomponent solid dispersion a new generation of solid dispersion produced by spray-drying. *Journal of Drug Delivery Science and Technology*, 57, pp. 101750.
22. Duong, T., Van Humbeeck, J & Van den Mooter, G. (2015). Crystallization Kinetics of Indomethacin/Polyethylene Glycol Dispersions Containing High Drug Loadings. *Molecular Pharmaceutics*, 12(7), pp. 2493-2504.
23. Eedara, B., Nyavanandi, D., Narala, S., Veerareddy, P., & Bandari, S. (2021). Improved Dissolution Rate and Intestinal Absorption of Fexofenadine Hydrochloride by the Preparation of Solid Dispersions: In Vitro and In Situ Evaluation. *Pharmaceutics*, 13(3), pp. 310.
24. Fael, H & Demirel, A. (2021). Indomethacin co-amorphous drug-drug systems with improved solubility, supersaturation, dissolution rate and physical stability. *International Journal of Pharmaceutics*, 600, pp. 120448.
25. Fousteris, E., Tarantili, P., Karavas, E & Bikiaris, D. (2013). Poly(vinyl pyrrolidone)–poloxamer-188 solid dispersions prepared by hot melt extrusion. *Journal of Thermal Analysis and Calorimetry*, 113(3), pp. 1037-1047.
26. Francisco Javier, A., Domínguez-Martín, A., Alarcón-Payer, C., Sevillano-Páez, A., Cristóbal Verdugo, E., Josefa María González, P & Choquesillo-Lazarte, D. (2023). Enhanced NSAIDs Solubility in Drug–Drug Formulations with Ciprofloxacin. *International Journal of Molecular Sciences*, 24(4), pp. 3305.
27. Gaikwad, E., Khabade, S., Sutar, T., Bhat, M & Payghan, S. (2017). Three-dimensional hansen solubility parameters as predictors of miscibility in cocrystal formation. *Asian Journal of Pharmaceutics*, 11(4), pp. 302-318.
28. Gan, Y., Baak, J., Chen, T., Ye, H., Liao, W., Lv, H & Zheng, S. (2023). Supersaturation and Precipitation Applied in Drug Delivery Systems: Development Strategies and Evaluation Approaches. *Molecules*, 28(5), pp. 2212.
29. Gumaste, S., Gupta, S & Serajuddin, A. (2016). Investigation of Polymer-Surfactant and Polymer-Drug-Surfactant Miscibility for Solid Dispersion. *The AAPS Journal*, 18(5), pp. 1131-1143.
30. Han, F., Zhang, W., Wang, Y., Xi, Z., Chen, L., Li, S & Xu, L. (2019). Applying Supercritical Fluid Technology to Prepare Ibuprofen Solid Dispersions with Improved Oral Bioavailability. *Pharmaceutics*, 11(2), pp. 67.
31. Han, R., Xiong, H., Ye, Z., Yang, Y., Huang, T., Jing, Q & Ouyang, D. (2019). Predicting physical stability of solid dispersions by machine learning techniques. *Journal of Controlled Release*, 311-312, pp. 16-25.

32. Handa, U., Malik, A & Guarve, K. (2022). A Review on the Concept of Superfluity Mechanism in Solubility Enhancement. *Research Journal of Pharmacy and Technology*, 15(8), pp. 3769-3775.
33. Huang, Z., Staufenbiel, S & Bodmeier, R. (2022). Kinetic solubility improvement and influence of polymers on controlled supersaturation of itraconazole-succinic acid nano-co-crystals. *International Journal of Pharmaceutics*, 616, pp. 121536.
34. Hurley, D. D., M.T, Walker, G., Lyons, J.G., & Higginbotham, C.L. (2020). The Effect of Cooling on the Degree of Crystallinity, Solid-State Properties, and Dissolution Rate of Multi-Component Hot-Melt Extruded Solid Dispersions. *Pharmaceutics*, 12(3), pp. 212.
35. Hurley, D., Carter, D., Yee, L., Davis, M., Walker, G., Lyons, J.G & Higginbotham, C.L. (2019). An investigation of the inter-molecular interaction, solid-state properties and dissolution properties of mixed copovidone hot-melt extruded solid dispersions. *Journal of Drug Delivery Science and Technology*, 53, pp. 101132.
36. Hurley, D., Potter, C., Walker, G & Higginbotham, C.L. (2018). Investigation of Ethylene Oxide-co-propylene Oxide for Dissolution Enhancement of Hot-Melt Extruded Solid Dispersions. *Journal of Pharmaceutical Sciences*, 107(5), pp. 1372-1382.
37. Jean-Luc, W & Marie-Paule, W. (2023). Pro- and Anti-Inflammatory Prostaglandins and Cytokines in Humans: A Mini Review. *International Journal of Molecular Sciences*, 24(11), pp. 9647.
38. Jelić, D. (2021). Thermal Stability of Amorphous Solid Dispersions. *Molecules*, 26(1), pp. 238.
39. Jennotte, O., Koch, N., Lechanteur, A & Evrard, B. (2022). Development of amorphous solid dispersions of cannabidiol: Influence of the carrier, the hot-melt extrusion parameters and the use of a crystallization inhibitor. *Journal of Drug Delivery Science & Technology*, 71, pp. 103372.
40. Jha, D., Shah, D & Amin, P. (2021). Effect of Hypromellose Acetate Succinate Substituents on Miscibility Behavior of Spray-dried Amorphous Solid Dispersions: Flory–Huggins Parameter Prediction and Validation. *Carbohydrate Polymer Technologies and Applications*, 2, pp. 100137.
41. Józó, M., Simon, N., Yi, L., Móczó, J & Pukánszky, B. (2021). Improved Release of a Drug with Poor Water Solubility by Using Electrospun Water-Soluble Polymers as Carriers. *Pharmaceutics*, 14(1), pp. 34.
42. Kalepu, S & Nekkanti, V. (2015). Insoluble drug delivery strategies: review of recent advances and business prospects. *Acta Pharmaceutica Sinica. B*, 5(5), pp. 442-453.

43. Karsten, F., Schmidt, K., Mareczek, L., Gäbe, M., Hennig, R & Thommes, M. (2021). Impact of incorporated drugs on material properties of amorphous solid dispersions. *European Journal of Pharmaceutics and Biopharmaceutics*, 159, pp. 88-98.
44. Kaushik, R., Vikas, B., & Kaushik, D. (2022). Recent Patents on Drug Delivery & Formulation. *An Overview on Recent Patents and Technologies on Solid Dispersion*, 14(1), pp. 63-74.
45. Kawakami, K. (2019). Crystallization Tendency of Pharmaceutical Glasses: Relevance to Compound Properties, Impact of Formulation Process, and Implications for Design of Amorphous Solid Dispersions. *Pharmaceutics*, 11(5), pp. 202.
46. Kumar, R., Thakur, A., Chaudhari, P & Banerjee, N. (2021). Particle Size Reduction Techniques of Pharmaceutical Compounds for the Enhancement of Their Dissolution Rate and Bioavailability. *Journal of Pharmaceutical Innovation*, 17, pp. 333-352.
47. Li, N., Cape, J., Mankani, B., Zemlyanov, D., Shepard, K., Morgen, M & Taylor, L. (2020). Water-Induced Phase Separation of Spray-Dried Amorphous Solid Dispersions. *Molecular Pharmaceutics*, 17(10), pp. 4004–4017.
48. Li, Y., Zhang, H., Cui, B., Hao, C., Zhu, H., Guan, J & Shi, N. (2021). Felodipine-indomethacin” co-amorphous supersaturating drug delivery systems: “Spring-parachute” process, stability, in vivo bioavailability, and underlying molecular mechanisms. *European journal of pharmaceutics and biopharmaceutics*, 166, pp. 111-125.
49. Liu, P., De Wulf, O., Laru, J., Heikkilä, T., van Veen, B., Kiesvaara, J & Laaksonen, T. (2013). Dissolution Studies of Poorly Soluble Drug Nanosuspensions in Non-sink Conditions. *AAPS PharmSciTech*, 14(2), pp. 748-756.
50. Liu, Z. (2020). Computational thermodynamics and its applications. *Acta Materialia*, 200, pp. 745-792.
51. Lu, J. X., Tupper, C & Murray, J. (2022). *Biochemistry, Dissolution and Solubility*. Florida, United States of America: StatPearls Publishing.
52. Luan, H., Zhang, X., Dai, H., Zhang, F., Luan, J., Jiao, Z & Yao, K. (2022). High-entropy induced a glass-to-glass transition in a metallic glass. *Nature Communications*, 13(1). pp. 2183.
53. Lucas, S. (2016). The Pharmacology of Indomethacin. *Headache*, 56(2), pp. 436-446.
54. Luz María, M., Videa, M., Tania López, S., Castro, S., Caballero, A., Díaz, V & Castorena-Torres, F. (2017). Two-phase amorphous-amorphous solid drug dispersion with enhanced stability, solubility and bioavailability resulting from ultrasonic dispersion of an immiscible system. *European Journal of Pharmaceutics and Biopharmaceutics*, 119, 2 pp. 43-252.

55. Lyons, J., Higginbotham, C & Blackie, P. (2007). *Development of novel monolithic matrices for drug delivery*. PHD Thesis, Technological University of Shannon.
56. Ma, X., & Williams, R. (2019). Characterization of amorphous solid dispersions: An update. *Journal of Drug Delivery Science and Technology*, 50, pp. 113-124.
57. Malkawi, R., Malkawi, W., Al-Mahmoud, Y & Tawalbeh, J. (2022). Current Trends on Solid Dispersions: Past, Present, and Future. *Advances in Pharmacological and Pharmaceutical Sciences*, pp. 1-17.
58. Maniruzzaman, M., Snowden, M., Bradely, M & Douroumis, D. (2015). Studies of intermolecular interactions in solid dispersions using advanced surface chemical analysis. *RSC Advances*, 5(91), pp. 74212–74219.
59. Medarević, D., Djuriš, J., Barmpalexis, P., Kachrimanis, K & Ibrić, S. (2019). Analytical and Computational Methods for the Estimation of Drug-Polymer Solubility and Miscibility in Solid Dispersions Development. *Pharmaceutics*, 11(8), pp. 372.
60. Méndez, F., Verma, V., Kujawski, J., Geertman, R., Tajber, L & Padrela, L. (2022). Controlling the Polymorphism of Indomethacin with Poloxamer 407 in a Gas Antisolvent Crystallization Process. *ACS omega*, 7(48), pp. 43945–43957.
61. Merck. (2005). *Capsules, Oral suspension and Suppositories Indocin (indomethacin)*. Available at: http://www.accessdata.fda.gov/drugsatfda_docs/label/2007/016059s097,017814s040,018332s030lbl.pdf [Accessed: 10 August 2023].
62. Morita, T. S., Chen, Z., Higashi, K., Imamura, H., Moribe, K & Sumi, T. (2021). Unveiling the Interaction Potential Surface between Drug-Entrapped Polymeric Micelles Clarifying the High Drug Nanocarrier Efficiency. *Nano letters*, 21(3), pp. 1303-1310.
63. Moseson, D & Taylor, L. (2018). The application of temperature-composition phase diagrams for hot melt extrusion processing of amorphous solid dispersions to prevent residual crystallinity. *International Journal of Pharmaceutics*, 553(1-2), pp. 454-466.
64. Nair, A., Lakshman, Y., Anand, V., Sree, K., Bhat, K & Dengale, S. (2020). Overview of Extensively Employed Polymeric Carriers in Solid Dispersion Technology. *AAPS PharmSciTech*, 21(8), pp. 309.
65. Novakovic, D., Peltonen, L., Isomäki, A., Fraser-Miller, S., Nielsen, L., Laakkonen, T & Strachan, C. (2020). Surface Stabilization and Dissolution Rate Improvement of Amorphous Compacts with Thin Polymer Coatings: Can We Have It All? *Molecular Pharmaceutics*, 17(4), pp. 248-1260.
66. Nyamba, I., Jennotte, O., Sombié, C., Lechanteur, A., Sacre, P., Abdoulaye, D & Evrard, B. (2023). Preformulation study for the selection of a suitable polymer for the

- development of ellagic acid-based solid dispersion using hot-melt extrusion. *International Journal of Pharmaceutics*, 641, pp. 123088.
67. Pandi, P., Bulusu, R., Kommineni, N., Khan, W & Singh, M. (2020). Amorphous solid dispersions: An update for preparation, characterization, mechanism on bioavailability, stability, regulatory considerations and marketed products. *International Journal of Pharmaceutics*, 586, pp. 119560.
68. Pezzoli, R., Lyons, J.G., Gately, N., & Higginbotham, C.L. (2019). Stability studies of hot-melt extruded ternary solid dispersions of poorly-water soluble indomethacin with poly(vinyl pyrrolidone-co-vinyl acetate) and polyethylene oxide. *Journal of Drug Delivery Science and Technology*, 52, pp. 248-254.
69. Pina, M., Zhao, M., Pinto, J., Sousa, J & Craig, D. (2014). The influence of drug physical state on the dissolution enhancement of solid dispersions prepared via hot-melt extrusion: a case study using olanzapine. *Journal of Pharmaceutical Sciences*, 103(4), pp. 1214-1223.
70. Pires, P., Mascarenhas-Melo, F., Pedrosa, K., Lopes, D., Lopes, J., Macário-Soares, A & Paiva-Santos, A. (2023). Polymer-based biomaterials for pharmaceutical and biomedical applications: A focus on topical drug administration. *European Polymer Journal*, 187, pp. 111868.
71. Potter, C., Tian, Y., Walker, G., McCoy, C., Hornsby, P., Donnelly, C & Andrews, G. (2015). Novel Supercritical Carbon Dioxide Impregnation Technique for the Production of Amorphous Solid Drug Dispersions: A Comparison to Hot Melt Extrusion. *Molecular Pharmaceutics*, 12(5), pp. 1377–1390.
72. Salehi, N., Al-Gousous, J., Mudie, D., Amidon, G., Ziff, R & Amidon, G. (2020). Hierarchical Mass Transfer Analysis of Drug Particle Dissolution, Highlighting the Hydrodynamics, pH, Particle Size, and Buffer Effects for the Dissolution of Ionizable and Nonionizable Drugs in a Compendial Dissolution Vessel. *Molecular Pharmaceutics*, 17(10), pp. 3870-3884.
73. Samineni, R., Chimakurthy, J & KONIDALA, S. (2021). Emerging Role of Biopharmaceutical Classification and Biopharmaceutical Drug Disposition System in Dosage form Development: A Systematic Review. *Turkish Journal of Pharmaceutical Science*, 19(6), pp. 706-713.
74. Sangroniz, L., Wang, B., Su, Y., Liu, G., Cavallo, D., Wang, D & Müller, A. (2021). Fractionated crystallization in semicrystalline polymers. *Progress in Polymer Science*, 115, pp. 101376.
75. Sathisaran, I & Dalvi, S. (2018). Engineering Cocrystals of Poorly Water-Soluble Drugs to Enhance Dissolution in Aqueous Medium. *Pharmaceutics*, 10(3), pp. 108.

76. Schenkel, G. (2022). Trends and highlights in polymer processing 1938 to 1988. *International Polymer Processing*, 3(1), pp. 3-32.
77. Shen, P., Zhang, C., Hu, E., Gao, Y., Heng, W., Zhang, J & Heng, W. (2023). Switch between Cocrystal and Coamorphous Forms Depending on Thermal Modulation of Hot-Melt Extrusion. *Molecular Pharmaceutics*, 20(7), pp. 3412-3426.
78. Shi, Q., Chen, H., Wang, Y., Wang, R., Xu, J & Zhang, C. (2022). Amorphous Solid Dispersions: Role of the Polymer and Its Importance in Physical Stability and In Vitro Performance. *Pharmaceutics*, 14(8), pp. 1747.
79. Shi, Q., Li, F., Yeh, S., Wang, Y & Xin, J. (2020). Physical stability of amorphous pharmaceutical solids: Nucleation, crystal growth, phase separation and effects of the polymers. *International Journal of Pharmaceutics*, 590, pp. 119925.
80. Shukla, A., Nagi Reddy Dumpa, T. R., Ashour, E., Bandari, S & Repka, M. (2023). Influence of Poloxamer on the Dissolution and Stability of Hot-Melt Extrusion–Based Amorphous Solid Dispersions Using Design of Experiments. *Aaps Pharmscitech*, 24(5), pp. 107.
81. Simões, M., Nogueira, B., Tabanez, A., Fausto, R., Pinto, R & Simões, S. (2020). Enhanced solid-state stability of amorphous ibrutinib formulations prepared by hot-melt extrusion. *International Journal of Pharmaceutics*, 579, pp. 119156.
82. Simões, M., Pinto, R & Simões, S. (2019). Hot-melt extrusion in the pharmaceutical industry: toward filing a new drug application. *Drug Discovery Today*, 24(9), pp. 1749-1768.
83. Sinclair, W., Leane, M., Clarke, G., Dennis, A & Toby, M. A. (2011). Physical stability and recrystallization kinetics of amorphous ibipinabant drug product by fourier transform raman spectroscopy. *Journal of Pharmaceutical Sciences*, 100(11), pp. 4687–4699.
84. Singh, B., Sharma, C & Sharma, S. (2020). *Fundamentals of extrusion processing*. In: *Novel Food Processing*. New Delhi: New India Publishing Agency.
85. Singh, N., Singh, A & Singh, A. (2021). Solubility: An overview. *International Journal of Pharmaceutical Chemistry and Analysis*, 7(4), pp. 166-171.
86. Singla, P., Singh, O., Sharma, S., Betlem, K., Aswal, V., Peeters, M & Mahajan, R. (2019). Temperature-Dependent Solubilization of the Hydrophobic Antiepileptic Drug Lamotrigine in Different Pluronic Micelles—A Spectroscopic, Heat Transfer Method, Small-Angle Neutron Scattering, Dynamic Light Scattering, and in Vitro Release Study. *ACS Omega*, 4(6), pp. 11251–11262.
87. Solanki, N., Kathawala, M & Serajuddin, A. (2019). Effects of Surfactants on Itraconazole-Hydroxypropyl Methylcellulose Acetate Succinate Solid Dispersion

Prepared by Hot Melt Extrusion III: Tableting of Extrudates and Drug Release From Tablets. *Journal of Pharmaceutical Sciences*, 108(12), pp. 3859-3869.

88. Solanki, N., Tahsin, M., Shah, A & Serajuddin, A. (2018). Formulation of 3D printed tablet for rapid drug release by fused deposition modeling: screening polymers for drug release, drug-polymer miscibility and printability. *Journal of pharmaceutical sciences*, 107(1), pp. 390-401.
89. Srinivasan, P., Mashan, A., Adel, A., Almotairy, A., Bandari, S & Repka, M. (2023). Numerical simulation of five different screw configurations used during the preparation of hot-melt extruded Kollidon® and Soluplus® based amorphous solid dispersions containing indomethacin. *Journal of Drug Delivery Science and Technology*, 85, pp. 104561–104561.
90. Srinivasan, S., Elhassan, G., Janakiraman, A., Kayarohanam, S., Tathagata Dey, R., Jainaf Nachiya, U. N & Mohamed, J. (2023). PREPARATION AND CHARACTERIZATION OF ETORICOXIB TERNARY COMPLEX FOR THE ENHANCEMENT OF SOLUBILITY. *Journal of Pharmaceutical Negative Results*, 14(2), pp. 1703-1712.
91. Štukelj, J., Agopov, M., Yliruusi, J., Strachan, C & Svanbäck, S. (2020). Machine-Vision-Enabled Salt Dissolution Analysis. *Analytical Chemistry*, 92(14), pp. 9730-9738.
92. Suksiriworapong, J., Rungvimolsin, T., A-gomol, A., Junyaprasert, V & Chantasart, D. (2014). Development and Characterization of Lyophilized Diazepam-Loaded Polymeric Micelles. *AAPS PharmSciTech*, 15(1), pp. 52-64.
93. Sun, D & Lee, P. (2013). Evolution of Supersaturation of Amorphous Pharmaceuticals: The Effect of Rate of Supersaturation Generation. *Molecular Pharmaceutics*, 10(11), pp. 4330-4346.
94. Sun, D & Lee, P. (2015). Probing the mechanisms of drug release from amorphous solid dispersions in medium-soluble and medium-insoluble carriers. *Journal of Controlled Release*, 211, pp. 85-93.
95. Svärd, M., Ahuja, D & Rasmuson, Å. (2020). Calorimetric Determination of Cocrystal Thermodynamic Stability: Sulfamethazine–Salicylic Acid Case Study. *Crystal Growth & Design*, 20(7), pp. 4243-4251.
96. Tambe, S., Jain, D., Agarwal, Y & Amin, P. (2021). Hot-melt extrusion: Highlighting recent advances in pharmaceutical applications. *Journal of Drug Delivery Science & Technology*, 63, pp. 102452.
97. Thakur, P., Sheokand, S & Bansal, A. (2019). Factors Affecting Crystallization Kinetics of Fenofibrate and Its Implications for the Generation of Nanocrystalline Solid Dispersions via Spray Drying. *Crystal Growth & Design*, 19(8), pp. 4417-4428.

98. Tian, Y., Jacobs, E., Jones, D., McCoy, C., Wu, H & Andrews, G. (2020). The design and development of high drug loading amorphous solid dispersion for hot-melt extrusion platform. *International Journal of Pharmaceutics*, 586, pp. 119545.
99. Tran, P., Lee, B & Tran, T. (2021). Recent studies on the processes and formulation impacts in the development of solid dispersions by hot-melt extrusion. *European Journal of Pharmaceutics and Biopharmaceutics*, 164, pp. 13-19.
100. Tran, P., Pyo, Y., Kim, D., Lee, S., Kim, J & Park, J. (2019). Overview of the Manufacturing Methods of Solid Dispersion Technology for Improving the Solubility of Poorly Water-Soluble Drugs and Application to Anticancer Drugs. *Pharmaceutics*, 11(3), pp. 132.
101. Tran, T & Tran, P. (2020). Molecular Interactions in Solid Dispersions of Poorly Water-Soluble Drugs. *Pharmaceutics*, 12(8), pp. 745.
102. Tres, F., Treacher, K., Booth, J., Hughes, L., Wren, S., Aylott, J & Burley, J. (2016). Indomethacin-Kollidon VA64 Extrudates: A Mechanistic Study of pH-Dependent Controlled Release. *Molecular Pharmaceutics*, 13(3), pp. 1166-1175.
103. Ulbrich, K., Holá, K., Šubr, V., Bakandritsos, A., Tuček, J & Zbořil, R. (2016). Targeted Drug Delivery with Polymers and Magnetic Nanoparticles: Covalent and Noncovalent Approaches, Release Control, and Clinical Studies. *Chemical Reviews*, 116(9), pp. 5338-5431.
104. Van der Merwe, J., Steenekamp, J., Steyn, D & Hamman, J. (2020). The Role of Functional Excipients in Solid Oral Dosage Forms to Overcome Poor Drug Dissolution and Bioavailability. *Pharmaceutics*, 12(5), pp. 393.
105. Wang, B., Sun, X., Xiang, J., Guo, X., Cheng, Z. L & Tan, S. (2022). A critical review on granulation of pharmaceuticals and excipients: Principle, analysis and typical applications. *Powder Technology*, 401, pp. 117329.
106. Xavier, S. (2022). *Thermoplastic Polymer Composites: Processing, Properties, Performance, Applications and Recyclability*. Hoboken, NJ, United States: John Wiley & Sons.
107. Xu, S., Chen, Y., Gong, J & Wang, J. (2018). Interplay between Kinetics and Thermodynamics on the Probability Nucleation Rate of a Urea–Water Crystallization System. *Crystal Growth & Design*, 18(4), pp. 2305–2315.
108. Yu, D., Li, J., Wang, H., Pan, H., Li, T., Bu, T & Zhang, X. (2022). Role of polymers in the physical and chemical stability of amorphous solid dispersion: A case study of carbamazepine. *European Journal of Pharmaceutical Sciences*, 169, pp. 106086.
109. Yuan, X., Xiang, T.-X., Anderson, B & Munson, E. (2015). Hydrogen Bonding Interactions in Amorphous Indomethacin and Its Amorphous Solid Dispersions with

Poly(vinylpyrrolidone) and Poly(vinylpyrrolidone-co-vinyl acetate) Studied Using ¹³C Solid-State NMR. *Molecular Pharmaceutics*, 12(12), pp. 4518–4528.

110. Zhang, W., Zhang, C., He, Y., Duan, B., G, Y., & Ma, W. (2017). Factors affecting the dissolution of Indomethacin Solid Dispersions . *AAPS PharmSciTech*, 18(8), pp. 3258-3273.
111. Zhao, Y., Zhang, X., Xu, X & Zhang, S. (2020). Research progress in nucleation and supercooling induced by phase change materials. *Journal of Energy Storage*, 27, pp. 101156.
112. Zhuang, Y., Nooshin, S., Morgani, M., Xu, T., Martin, C., Patience, G & Abdellah, A. (2022). Experimental methods in chemical engineering: Reactive extrusion. *The Canadian Journal of Chemical Engineering*, 101(1), pp. 59-77.

Relevant Publications

D Hurley, CB Potter, GM Walker, CL Higginbotham

Investigation of ethylene oxide-co-propylene oxide for dissolution enhancement of hot-melt extruded solid dispersions

Journal of Pharmaceutical Sciences 107 (5), 1372-1382, 2018

D Hurley, D Carter, LYF Ng, M Davis, GM Walker, JG Lyons, CL Higginbotham

An investigation of the inter-molecular interaction, solid-state properties and dissolution properties of mixed copovidone hot-melt extruded solid dispersions

Journal of Drug Delivery Science and Technology 53, 101132, 2019

D Hurley, M Davis, GM Walker, JG Lyons, CL Higginbotham

The effect of cooling on the degree of crystallinity, solid-state properties, and dissolution rate of multi-component hot-melt extruded solid dispersions

Pharmaceutics 12 (3), 212, 2020